



Published in final edited form as:

Coord Chem Rev. 2018 November 1; 374: 314–344. doi:10.1016/j.ccr.2018.07.010.

Detection and identification of solids, surfaces, and solutions of uranium using vibrational spectroscopy

Grace Lu, Amanda J. Haes*, and Tori Z. Forbes*

Department of Chemistry, University of Iowa, Iowa City, IA 52242, United States

Abstract

The purpose of this review is to provide an overview of uranium speciation using vibrational spectroscopy methods including Raman and IR. Uranium is a naturally occurring, radioactive element that is utilized in the nuclear energy and national security sectors. Fundamental uranium chemistry is also an active area of investigation due to ongoing questions regarding the participation of *5f* orbitals in bonding, variation in oxidation states and coordination environments, and unique chemical and physical properties. Importantly, uranium speciation affects fate and transportation in the environment, influences bioavailability and toxicity to human health, controls separation processes for nuclear waste, and impacts isotopic partitioning and geochronological dating. This review article provides a thorough discussion of the vibrational modes for U(IV), U(V), and U(VI) and applications of infrared absorption and Raman scattering spectroscopies in the identification and detection of both naturally occurring and synthetic uranium species in solid and solution states. The vibrational frequencies of the uranyl moiety, including both symmetric and asymmetric stretches are sensitive to the coordinating ligands and used to identify individual species in water, organic solvents, and ionic liquids or on the surface of materials. Additionally, vibrational spectroscopy allows for the *in situ* detection and real-time monitoring of chemical reactions involving uranium. Finally, techniques to enhance uranium species signals with vibrational modes are discussed to expand the application of vibrational spectroscopy to biological, environmental, inorganic, and materials scientists and engineers.

Keywords

Uranium; Vibrational spectroscopy; Infrared; Raman

1. Introduction to uranium chemistry

Uranium, element number 92, is one of the most abundant radioactive metals and possesses a troubled history with regard to both its use in the energy and defense sectors and its impact on public health and environmental systems. The most abundant (99.3%) uranium isotope, ^{238}U , is a primordial radionuclide with a half-life of 4.7×10^9 years and is found in the earth crust at an average concentration of 2.7 ppm [1,2]. Other isotopes, such as ^{233}U , ^{234}U , ^{235}U ,

*Corresponding authors. amanda-haes@uiowa.edu (A.J. Haes), tori-forbes@uiowa.edu (T.Z. Forbes).

[†] Author contributions

The manuscript was written through contributions of all authors. All authors have given approval to the final version of the manuscript.

and ^{236}U , occur at concentrations below 1% of natural abundance although their specific activity is higher than that of ^{238}U . Due to its fissile nature, enriched uranium (3–5% ^{235}U) is widely used in nuclear reactors for power generation and higher levels (20–90% ^{235}U) are used for the development of nuclear weapons [2]. The enrichment process combined with mining and milling of natural uranium ore bodies generates radioactive waste. Additional waste is added after use in a nuclear reactor, where the solid product still contains 95% U that is now mixed with fission products and transuranic materials [3]. Characterizing the chemical nature of waste forms is important for reprocessing and/or long-term storage in a geologic repository so that impacts on the biosphere are minimized [4]. In addition, there are many sites around the world where abandoned uranium mines, tailing piles, or legacy waste are currently in need of remediation to reduce the risk to environmental systems or the public [5].

The complex chemistry of uranium dictates how the element behaves in natural waters, which will in-turn, impact transport processes and bioavailability. While uranium can exist in oxidation states between +3 and +6, the most common states in natural systems are +4 and +6 [6]. U(IV) is the dominate state in slightly oxidizing to anoxic conditions and typically forms insoluble (0.01 $\mu\text{g/L}$) hydrolysis and microbial mediated oxide products in natural waters [7,8]. These solids contain the U(IV) cation coordinated to 6–10 O atoms and possess interesting catalytic, semiconducting, and magnetic properties [9–11]. U(VI) exists in aerobic conditions and is relatively soluble in natural waters [8]. Bonding is quite unusual in U(VI) as it possesses strong, covalent bonds to two axial O atoms, creating the uranyl cation, $[\text{U}(\text{VI})\text{O}_2]^{2+}$ [12]. Additional bonding to the uranyl moiety by four, five, or six equatorial ligands forms an overall coordination geometry of square, pentagonal, or hexagonal bipyramidal about the metal center [12]. U(VI) is also considered a hard Lewis acid and prefers to bond to O and N functional groups thus forming a range of soluble complexes and mineral phases in natural waters [8]. Speciation influences the overall solubility of U, ranging from 1 $\mu\text{g U/L}$ for groundwater in equilibrium with vanadates to 120 mg U/L in the presence of carbonates and silicates [13]. Due to the complex chemistry of U(VI), important species for environmental systems can exist as soluble coordination complexes [8,14] and nanoclusters [15,16], colloids [17,18], amorphous precipitates [19,20], or surface adsorbed phases [21]. Pentavalent U(V) is often not mentioned in the discussion of environmental uranium chemistry because it is considered extremely unstable and readily disproportionates to U(IV) and U(VI) [22]; however, it has been observed as a stable phase on mica surfaces [23] and more recently been detected in a catalytic transformations of iron oxyhydroxide mineral phases [24–26].

Given the complexity of uranium chemistry in natural waters, it is important to develop tools to assess speciation, characterize solid phases, understand surface processes, and probe chemical mechanisms. Radiometric techniques, such as alpha spectrometry, quantify U in natural systems down to 0.22 mBq/L and provide isotopic ratios of the materials [27]. These methods, however, do not reveal chemical information on speciation or bonding. Powder and single X-ray diffraction techniques can detect and identify solid-state phases, but require milligram quantities of the material [28,29]. Higher-energy X-ray sources, such as those found at synchrotron facilities, overcome this limitation but require specialized instrumentation and dedicated staff support [30]. Mass spectrometry is more widely used

and provides quantitative analysis along with some speciation information [31,32]. Isotopic effects and complex matrices, however, lead to difficulties in data analysis. There are also a wide range of spectroscopic techniques that have been used to characterize uranium compounds and solutions, including fluorescence [33–35], X-ray photoelectron [36], X-ray absorption [18,37,38], and vibrational spectroscopy [39]. Each of these techniques provides different chemical information regarding the complexation, coordination environment, bonding, and photoelectric properties although some are limited to either solution or solid phase (Table 1).

One of the most versatile and wide-spread spectroscopic methods is based on measuring vibrational energies and encompasses both infrared (IR) absorption and Raman scattering. These complementary spectroscopic methods reveal information regarding bonding and local environment for compounds and species, including those for uranyl. While both methods rely on excitation of quantized vibrational-rotational energy levels in these samples, observed spectral features depend on unique selection rules. For infrared spectroscopy, a change in dipole moment must arise upon vibrational motion for the mode to be IR-active while a change in polarizability (i.e., distortion of the electron cloud) must occur similarly for a mode to be Raman-active. The asymmetric (ν_3) and symmetric (ν_1) uranyl stretches are the most probable and intense modes in IR and Raman spectra, respectively, and both are sensitive to coordinating ligands, local environment, and molecular geometries. These modes occur at different frequencies, however, because they require different amounts of energy to excite vibrational motion. Because water vibrational modes are silent or weak in Raman spectra, Raman spectroscopy is widely utilized for characterizing environmental and aqueous-phase uranyl samples, but the signals for uranyl are weak because of the probability of exciting the Raman-active modes is low. In comparison, water exhibits strong IR bands that interfere with uranyl detection from these samples unless attenuated total reflectance (ATR) cells are used. This approach works best for solid samples that can adhere to the ATR crystal so that the spectroscopic signal from water can be minimized. The signals are more intense in comparison to Raman spectral features but often exhibit a large background and/or features that overlap with other chemical species in the samples. Advanced vibrational spectroscopic methods have been developed for solution phases, solid materials, and surfaces [40,41]. Traditionally, one of the limitations of these methods was poor detection limits; but in more recent years, new technologies have been employed to enhance detection and provide additional chemical information.

The purpose of this review is to provide an overview of how uranium can be characterized using vibrational spectroscopy, including IR absorption and Raman scattering. Previous literature examinations focused on the detection and identification of uranium speciation using X-ray spectroscopy [42,43], time-resolved laser-induced fluorescence spectroscopy [44–46], and computational modeling [47]. An excellent review of IR vibrational frequencies of uranyl (VI) mineral compounds was also provided by Cejka in 1999, but the reported uses of vibrational spectroscopy for uranium chemistry has grown in number and significant advances in sample preparation and data analysis have increased in both breadth and depth; therefore, there is a critical need to provide an update on this important chemical technique [39]. We have also published a study investigating the best practices for collecting and analyzing Raman spectra in aqueous solutions, but determined that additional

information was lacking in regards to the analysis of solid state samples and surfaces [48]. Building on the previous work by Cejka [39], the current review focuses on how both IR and Raman spectroscopies are used to characterize solid state uranium compounds; identify U adsorbed on surfaces; and provide speciation information within aqueous solutions, organic solvents, and ionic liquids. In addition, we explore the latest advances in uranium detection and provide an analysis of future needs and unanswered questions.

2. Detection and identification of uranium using vibrational spectroscopy

Vibrational spectroscopy is used to elucidate uranium speciation because each species possesses a unique vibrational frequency, which is influenced by the valence number, bond length, coordination ligands, structure, and local environment. Correct analysis of these complex data is of utmost importance. Careful analysis requires an understanding of (1) appropriate spectral windows relevant for uranyl speciation determination, (2) implications of possible vibrational band overlap arising from multiple uranyl species, and (3) impacts of coordinating ligands and phase on vibrational band widths. In the following section, we provide an overview of the overall spectral characteristics of uranium in different valence states and summarize additional information on proper data analysis.

2.1. Vibrational spectroscopy of U(IV)

U(IV) solids have variable coordination numbers, and UAO bonds contain substantial ionic character, leading to smaller vibrational mode cross sections and less intense vibrational bands. UO_2 solid crystallizes in the fluorite $Fm\bar{3}m$ space group, and group theory predicts one IR and one Raman active mode [49]. With hyper-stoichiometric U(V) oxides, the fluorite lattice often distorts, leading to relatively lower symmetry structures and activation of more vibrational modes [49,50]. For instance, $\beta\text{-U}_4\text{O}_9$ forms in the $I\bar{4}3d$ space group with 7 crystallographically unique U and 14 O atoms [50]. Modeling suggests that modes consistent with UO_2 and phonon lattice vibrations could arise in Raman analysis thus increasing the number of possible vibrational modes observed in this structure type by a factor of four [49]. Vibrational band broadening may also occur with increasing disorder within the crystalline lattice [50]. Based upon solubility limitations and the weak vibrational bands, the use of vibrational spectra in U(IV) solutions is rather limited. Often the use of absorption spectroscopy is more conducive for confirming the presence of U(IV) whereas vibrational spectroscopy is appropriate for identifying other inorganic or organic anions with active bands [51].

2.2. Vibrational spectroscopy of U(VI)

In contrast to the tetravalent state, U(VI) forms the uranyl cation, $[\text{U(VI)O}_2^{2+}]$ and displays strong active vibrational bands associated with the covalent axial bonds. There are three fundamental modes of vibration for the uranyl moiety ($D_{\infty h}$): the symmetric stretch (ν_1), bend (ν_2), and antisymmetric stretch (ν_3) [39] (Fig. 1). The bending mode occurs in two mutually perpendicular planes making it degenerate. When the $D_{\infty h}$ symmetry is maintained, the ν_1 is Raman active, and ν_2 and ν_3 are IR active [39]. Symmetry lowering ($D_{\infty h} \rightarrow C_{\infty v}$, $C_{\infty v}$, C_s) occurs when the two axial bonds within the uranyl moiety are not equal in length or through significant bending ($>5^\circ$) of the linear dioxo bond [52,53].

Decreasing the symmetry of the uranyl moiety should result in the activation of all three fundamental modes in IR and Raman spectra.

The symmetric and asymmetric stretching modes are both informative and sensitive to coordinating ligands and structure (e.g., mono-, bi-, or tridentate chelation). This occurs because the uranyl bond is weakened by additional coordination in the equatorial plane [54]. Perturbation of the uranyl bond can be explained by either the presence of strong electron donating ligands occupying the equatorial coordination sites or destabilization from purely electrostatic interactions [55]. Weakening of the uranyl bond results in bond elongation, causing the uranyl vibrational frequency to red-shift from the widely-used comparative standard, the pentahydrate species ($\text{UO}_2(\text{H}_2\text{O})_5^{2+}$). The symmetric and asymmetric stretching bands for $\text{UO}_2(\text{H}_2\text{O})_5^{2+}$ is commonly observed at 870 and 962 cm^{-1} , respectively [48]. This leads to a typical spectral window for U(VI) compounds ranging from 900 to 750 cm^{-1} for Raman and 980–830 cm^{-1} for IR spectroscopy.

The Raman-active bands can be fit to a Gaussian function, and the full width at half-maximum (Γ) of these bands is typically between 13 and 15 cm^{-1} [48]. Vibrational band frequencies are observed for monomeric, dimeric, and trimeric hydrolysis products. For instance, a ~20–30 cm^{-1} shift in vibrational frequency of the symmetric stretch has been reported as oligomeric species are generated by hydrolysis [56]. This shift is also accompanied by slight broadening of the bands ($\Gamma = 5 \text{ cm}^{-1}$) due to the formation of these larger soluble clusters [48].

An example of Raman data analysis for speciation determination is demonstrated in Fig. 2. Here, Raman spectra of uranyl nitrate crystals (used as received from International Bio-Analytical Industries, Inc. Lot #55971) were collected using a 785 nm laser to reduce the effects of elastic scattering and fluorescence interference on the background in the uranyl window (950–700 cm^{-1}). Raw spectral data are shown in panel B. Next, inverse second derivative spectra are generated and plotted so that approximate vibrational band centers can be noted. Bands were considered significant if band widths were greater than 15 cm^{-1} and larger than 5% of the noise. As shown, four significant features were noted and were centered at 874, 865, 754, and 715 cm^{-1} . These vibrational band centers with $\pm 3 \text{ cm}^{-1}$ windows and 15–45 cm^{-1} widths were used for subsequent fitting using Lorentzian functions. In so doing, four bands were identified at 875 ($\nu_1 \text{ U=O}$; uranyl nitrate dihydrate) [57], 868 ($\nu_1 \text{ U=O}$; uranyl nitrate hexahydrate) [58], 754 ($\nu_3 (A_1)$, NO), and 714 ($\nu_5 (B_1)$, NO) cm^{-1} [59]. Note that the m_1 band for the dehydrate material is slightly blue-shifted compared to the original pentaqua uranyl species whereas the hexahydrate compound exhibits a 2 cm^{-1} red-shift compared to the same benchmark complex. The splitting of the band associated with the uranyl symmetric stretch, also allowed us to determine that the compound was composed of a biphasic mixture with differences in hydration state.

2.3. Vibrational spectroscopy of U(V)

While U(V) complexes are quite unstable, the presence of this moiety in solution or solid state can be detected using vibrational spectroscopy. Pentavalent uranium also forms the

uranyl cation, but the charge is reduced to $[\text{U}(\text{V})\text{O}_2]^+$. Additional coordination about the equatorial plane leads to a similar coordination environment as with U(VI) species. The major difference with the two valence states is the elongation of the $\text{U}(\text{V})=\text{O}$ bond to 1.808–1.916 Å and a red shift in the vibrational modes [60]. The oxo groups of the $\text{U}(\text{V})\text{O}_2^+$ species are more reactive than the hexavalent moiety and interact with other cations or actinyl groups [61]. This interaction should promote elongation of one of the uranyl bonds, resulting in lower molecular symmetry. The consequence of asymmetric uranyl bonds within the vibrational spectra is similar to what is reported for U(VI) species, where all three fundamental modes can be activated in both the IR and Raman spectra [39].

3. Chemical and structural elucidation of uranium solid-state compounds

Vibrational spectroscopy has been used for over 80 years to identify and understand the structural features of simple inorganic U salts and mineral phases [62]. This is particularly true for mineral phases, and we would be remiss if we did not acknowledge the amazing body of literature provided by Ray L. Frost, Jiri Cejka, and their research groups/colleagues. In the last 10 years, spectroscopic analysis of uranyl hybrid materials significantly expanded due to an interest in understanding the uranyl moiety bond strength and providing additional characterization to enhance the structural description of novel compounds. In the next section, we analyze the spectral signals for uranium compounds with extended topologies and mineral phases before exploring uranium coordination compounds and hybrid materials. In addition, we use a subset of well-characterized compounds to provide updated metrics for the analysis of bond lengths and predicted spectroscopic signals.

3.1. Mineral phases and inorganic uranium compounds with extended topologies

Some natural mineral specimens contain chemical and structural variations based upon the specific geologic conditions that influence vibrational band intensities and frequencies. To simplify the discussion of these compounds, we focus on the major bands associated with the uranyl cation, and the reader should refer to the primary literature to evaluate subtle spectral differences in these data. Relationships between vibrational band frequencies and bond lengths, which are based upon the empirical formula derived from Bartlett and Cooney [63] are discussed herein. We summarize the major vibrational modes within the text and provide detailed in Table 2. We would like to note that the values included in the tables are those directly reported in the literature and not our own interpretation. In addition, the Raman bands are emphasized in this section because of difficulties in identifying the ν_3 mode in IR spectra due to significant band overlap from interfering species. When possible, we obtained information on the asymmetric stretch and included those values in the tables.

3.1.1. Uranium oxide, peroxides, hydroxides, and halides—The most abundant and economically important uranium mineral is uraninite (UO_2). This phase is always partially oxidized in environmental systems, which leads to the formation of varying stoichiometries (UO_{2+x} , U_4O_9 , U_3O_7 , and U_3O_8) that occur independently or as a corrosion rind on solid materials [64]. For stoichiometric UO_2 with the defect-free fluorite structure, group theory predicts one strong Raman (T_{2g}) and one weak IR active band (340 cm^{-1} , T_{1u}). A narrow Raman band is located at 445 cm^{-1} , whereas a broad IR mode is centered at ~ 340

cm^{-1} and overlaps with another band at $\sim 470 \text{ cm}^{-1}$ [65–68]. A second weak band at 1150 cm^{-1} also appears in Raman spectra and was previously assigned by Livneh and Sterer as a second-order longitudinal optical (LO) phonon mode [69]. Hyperstoichiometric amounts of oxygen in uranium dioxide ($\text{UO}_{2.03}$) leads to the appearance of a broad asymmetric feature with a maximum centered at 560 cm^{-1} and shoulder at 630 cm^{-1} , corresponding to defect induced degenerate LO modes and anion sublattice distortions, respectively [49,70]. Increasing the O content leads to further broadening and a blue-shift of the T_{2g} band, a decrease in the LO band intensity, an increase in the intensity of the peak at 630 cm^{-1} , and changes in the relative intensity at 560 cm^{-1} [49].

Elorrieta et al. [49] utilized Raman spectroscopy to quantitatively characterize the hyperstoichiometric material by closely investigating the anion sublattice distortion at 630 cm^{-1} . The value for x within UO_{2+x} can be quantified using one of the following two equations using the intensities of the modes at 630 and 445 cm^{-1} (I_{630} and I_{445} , respectively):

$$\nu_{630} = 654 \pm 4 - (610 \pm 60)x, \text{ when } \frac{I_{630}}{I_{445}} < 0.24$$

$$\nu_{630} = 647 \pm 4 - (90 \pm 30)x, \text{ when } 0.27 < \frac{I_{630}}{I_{445}} < 0.24$$

It is important to note that these equations are valid for the 632.8 nm excitation wavelength because other excitation wavelengths may lead to selective resonant enhancements or high fluorescent backgrounds both of which prohibit quantitative analysis [49].

Partial oxidation to $\text{U(IV,V)}_3\text{O}_7$ (also reported as $\text{UO}_{2.3}$ or tetragonal UO_{2+x}) and $\text{U(V,VI)}_3\text{O}_8$ results in the appearance of new Raman bands that have been previously used to characterize corrosion of UO_2 fuel pellets [71]. Group theory for D_{4h} point symmetry predicts 18 phonon branches for the tetragonal U_3O_7 phase, with nine Raman active ($A_1^+ + 2 E_1^+ + 3 \Gamma^+$) and five infrared active (A_2^- and $2 \Gamma^-$) modes.[72] Only six of those modes ($A_{1g} + 2 B_{1g} + 3 E_g$) were observed experimentally for U_3O_7 and centered at 630 , 155 , and $\sim 470 \text{ cm}^{-1}$, respectively [72]. The ingrowth of the B_{1g} and E_g bands, therefore, are used to determine structural transformations from the cubic to tetragonal phase of UO_{2+x} . Formation of orthorhombic U_3O_8 results in the characteristic A_{2u} combination band at 750 cm^{-1} [73,74]. Other bands associated with U_3O_8 include the A_{1g} (335 cm^{-1}), A_{1g} (410 cm^{-1}), and the A_{1g} (475 cm^{-1}) stretching bands. Precise analysis of these bands during aging of fuel pellets provided growth rates of secondary alteration phases, formation of lattice defects, and inhomogeneities to due irradiation of the material [67,68,72,75–77].

Full oxidation to U(VI) leads to the formation of the uranyl moiety and related spectroscopic signals for the oxide phases. The simplest U(VI) oxide is UO_3 , which can form at least seven different crystalline forms depending on the identity of the starting material [78,79]. Of the seven polymorphs, $\gamma\text{-UO}_3$ is the most studied, with major Raman modes located at 767 ,

484, and 399 cm^{-1} [79]. DFT calculations combined with experimental results provide structural details of the gamma phase and indicate that there are two crystallographically unique U atoms [78,80]. U1 is observed in a square bipyramidal coordination geometry with a uranyl bond length of 1.87 Å. The coordination geometry of the U2 site is an unusual dodecahedron with axial bond lengths of 1.78 Å and an O=U=O bond angle of 174.6°. Using the relationship established by Barlett and Cooney [63], the calculated bond length associated with the Raman mode at 767 cm^{-1} is 1.85 Å, which agrees well with the reported values [80]. Other vibrational modes have not been specifically assigned, but likely arise from uranyl stretching modes. Diuranate compounds ($\text{X}_2\text{U}_2\text{O}_7$), particularly sodium and ammonium forms, are also important U(VI) oxides because they are precipitated as an intermediate product during the production of yellowcake and nuclear fuel pellets [81]. The main spectroscopic band associated with uranyl in $\text{Na}_2\text{U}_2\text{O}_7$ is located between 789 and 778 cm^{-1} , whereas the NH_4 form ($(\text{UO}_2(\text{OH})_{2-x}(\text{O})(\text{NH}_4)_x) \cdot y\text{H}_2\text{O}$) exhibits bands within a larger spectral window (841–804 cm^{-1}) due to hydrolysis and variability in hydration that occurs between synthetic batches [82,83]. Only one other U(VI) oxide phase, the rare mineral Vorlanite (Ca,U(VI)O_4), has been reported in the literature. The major band associated with the uranium cation is observed at 683 cm^{-1} , which corresponds to octahedrally coordinated U(VI) with a bond length of 2.33 Å [84].

Hydrolysis of uranium oxide materials occurs in the presence of water and leads to a range of uranyl oxyhydroxide phases in a complex matrix such as groundwater. Schoepite [$(\text{UO}_2)_8\text{O}_2(\text{OH})_{12}$] $\cdot 12\text{H}_2\text{O}$ occurs in solutions at near neutral pH and low ionic strength values [85]. The ν_1 mode for this phase occurs at 839 cm^{-1} with a distinct shoulder at 855 cm^{-1} and a weak band at 802 cm^{-1} [86]. With increasing ionic strength, other common uranyl oxyhydroxide minerals form, with the overall general formula of $\text{M}_n[(\text{UO}_2)_x\text{O}_y(\text{OH})_z](\text{H}_2\text{O})_m$, where $\text{M} = \text{K}^+, \text{Ca}^{2+}, \text{Pb}^{2+}, \text{Ba}^{2+}, \text{and Sr}^{2+}$ [85]. The spectroscopic envelope for most of the oxyhydroxide minerals are observed from 855 to 830 cm^{-1} , with a handful of weak modes appearing at lower wavenumbers [86,87]. Curite ($\text{Pb}_{3+x}(\text{H}_2\text{O})[(\text{UO}_2)_4\text{O}_{4+x}(\text{OH})_{3x}]_2$) and vandenbrandeite ($\text{Cu}[\text{UO}_2(\text{OH})_4]$) are notable exceptions because the uranyl bands are significantly red shifted to ~800–770 cm^{-1} [86,88,89]. This difference in vibrational frequency arises from structural variations within the mineral sheet topologies. The curite sheet topology is quite different than that of the other uranyl oxyhydroxides, such that it contains U1 in a distorted square bipyramid [90]. Vandenbrandeite is also unique as it contains Cu^{2+} cations bonded to oxo atoms of the neighboring uranyl pentagonal bipyramids [90,91]. In the case of curite, this leads to an elongation of the uranyl bonds (1.79(2)–1.89(2) Å), which induces a significant red-shift in the vibrational band compared to the other oxyhydroxide phase [86,90]. For vandenbrandeite, the uranyl bond distances are closer to the average value (1.77 Å), thus additional investigations are needed to clarify the perturbation of the uranyl bond [91].

The uranyl mineral, studtite, is the only naturally occurring peroxide-bearing phase and widely occurs as a secondary corrosion product of uraninite ores and nuclear fuel rods [92,93]. The material contains a chain topology that propagates through edge sharing peroxide bridges [94]. The Raman spectra contains a ν_1 uranyl band located at 831 cm^{-1} and a secondary ν_1 (O=O) stretching mode at 870 cm^{-1} [95]. Both studtite and the dehydrated form (metastudtite [$\text{UO}_2(\text{O}_2)(\text{H}_2\text{O})_2$]) have been identified as a secondary alteration phase

formed due to the alpha radiolysis of water using Raman spectroscopy as the main surface characterization technique [76,77,96,97].

While there are several uranyl halide phases reported in the literature, significant spectral data are only available for UO_2F_2 and UO_2Cl_2 . Structural features of the fluoride compound was first established by Zachariassen [98] and then refined with neutron diffraction by Atoji and McDermott [99]. The structure contains sheets of uranyl hexagonal bipyramids, with six edge sharing F atoms located in the equatorial plane and an experimental UAO bond length of 1.74(2) Å. Theoretical studies predict a Raman band at 915 cm^{-1} and a calculated bond length of 1.71 Å. Hydration of the uranyl fluoride compound induces a red shift in the m_1 mode to 867 cm^{-1} , which agrees well with the calculated bond length of 1.75 Å [100]. Bullock spectroscopically characterized UO_2Cl_2 , denoting the ν_1 at 871 cm^{-1} and ν_3 at 960 cm^{-1} [101]. The uranyl bond distance reported for the chloride compound is 1.70 Å, which is lower than expected based upon the spectroscopic signal (1.74 Å) [102].

3.1.2. Uranium compounds and minerals containing oxyanions—The chemical complexity of oxyanion-containing U(VI) compounds and mineral phases leads to a wide spectral envelope for the vibrational bands associated with the uranyl moiety. Fig. 3 provides the averaged ν_1 vibrational band frequencies (stars) as well as the range of values for the various oxyanion species. We have chosen to present these published results as box and whisker plots to emphasize the variation in values reported. In particular, these plots visually depict the distribution of results including the mean (x), median (middle vertical line), 25th and 75th quartiles (3rd and 1st vertical lines, respectively), as well as the minimum and maximum values (ends of error bars). Average values are observed between 840 and 800 cm^{-1} with ranges extending from 870 to 760 cm^{-1} . This large range likely arises because of the complex nature of the extended structural topologies and subtle variations in the coordination environment about the uranyl cation within different compounds and mineral phases. Complexity is enhanced from symmetry lowering within the solid state compounds upon activating the vibrational and splitting degenerate modes. Despite this, there are subtle trends that can be observed. For instance, sul-fate tends to red shift the vibrational bands less significantly than other oxyanions, and selenate exhibits the largest range of vibrational frequencies (865–788 cm^{-1}).

Similarities within structural topology can also be used to understand trends in uranyl vibrational frequencies. Uranyl phosphates, which are a well-studied group of compounds due to their relative abundance as a secondary mineral phase in geologic systems and waste products [103,104], contain the two major 2-D structural topologies autunite or phosphoruranylite sheets [12]. The autunite sheet contains uranyl square bipyramids that share vertices to phosphate tetrahedral and account for 17+ different compounds. Within these compounds, the autunite sheet is retained while the identity of the charge balancing cations varies [105,106]. Phosphoruranylite sheets, which are slightly more complex, contain U(VI) with different coordination environments (square, pentagonal, and hexagonal bipyramids) leading to chain structures linked into 2-D sheets through phosphate tetrahedral [107]. This topology accounts for 11 different compounds with variability in the interstitial charge balancing cations and phosphate tetrahedra orientation. While these two classes of

uranyl phosphates contain similar chemical components, both their structural complexity and vibrational spectra are unique.

A first look at the Raman spectra for the autunite family of minerals reveals a major band between 837 and 825 cm^{-1} that was previously identified as the uranyl moiety [108–110]. Ranking the vibrational band centroid (cm^{-1}) by cation identity from largest to smallest reveals the trend $\text{Mg(II)} > \text{Ca(II)} > \text{Al(III)} > \text{Cu(II)}$. Further investigation of the interactions between these interstitial cations and the uranyl oxo atoms can provide additional insight in the relative shift in the ν_1 band (Fig. 4). For instance, Mg(II) cations interact more with interstitial water molecules present in the interlayer region of saleeite than with uranyl unit because the distances between the uranyl oxo and the Mg cation is 4.12 and 4.14 Å (Fig. 4b) [111]. The large interatomic distance suggests no significant interaction with the uranyl bond. Replacing Mg(II) with a larger cation (Ca(II) in autunite) leads to a shorter interatomic distance (3.28 Å) between divalent cations and the uranyl oxo atoms. The uranyl symmetric stretch for autunite (830 cm^{-1}) is red-shifted from that observed in saleeite (837 cm^{-1}), suggesting a longer, weaker uranyl bond (Fig. 4c). As the sheet topology is identical between autunite and saleeite, the additional interaction between the interstitial cation likely influences the uranyl bond. Structural characterization of sabugalite has not been reported, but the spectral data suggests that Al(III) exhibits increased electrostatic interactions with the uranyl oxo atoms and a longer uranyl bond length. Inclusion of Cu(II) cations (torbernite) is unique because the d^{10} transition metal can form 4+2 Jahn-Teller distortions that often involve uranyl oxo groups. Thus, the distance between the uranyl oxo and Cu(II) is shorter (2.55 Å) than with other cations, and the ν_1 vibration mode red-shifts (825 cm^{-1}) accordingly (Fig. 4d) [112].

A closer evaluation of the vibrational features and employment of fitting techniques reveals multiple bands in uranyl phosphate minerals that cannot be linked to crystallographically unique U atoms within the lattice. Furthermore, spectral lineshapes varied significantly when evaluating the Raman spectra. To highlight these differences, we obtained raw spectral data for meta-autunite and phosphouranylite from the RRUFF project [113] and utilized Origin software to fit the ν_1 spectral bands. Two and three independently collected spectra were collected for phosphouranylite and autunite, respectively (Fig. 5). Striking similarities and differences are noted for each compound upon normalizing these spectra to the band at $\sim 840 \text{ cm}^{-1}$ to correct for differences in detector efficiency, laser powers, and excitation geometries. First, meta-autunite contains one crystallographically unique U atom, but spectral analysis identifies at least two bands within the uranyl spectral envelope [105,114]. In addition, significant spectral variation is observed in three spectra evaluated from the database.

By comparison, phosphouranylite spectra are much more similar. First, the spectra for phosphouranylite possess at least two unique vibrational features – a primary mode centered at $\sim 840 \text{ cm}^{-1}$ and a shoulder at $\sim 820 \text{ cm}^{-1}$. Slight differences are noticed when making spectrum to spectrum comparison. These are highlighted in Fig. 6 where previously discussed second derivative spectral analysis was performed. In both spectra, three significant vibrational features are identified and are centered at 844/839, 820/815, and 775 cm^{-1} . This compound possesses three crystallographically unique U atoms with distinct

coordination geometries, and the spectral fitting also finds three bands within the complexes [107]. While clear sample to sample variations are evident, difficulties also arise from lack of spectral analysis so the ν_1 uranyl symmetric stretch for uranyl solid-state materials can be identified. This is highlighted again by the phosphuranylite system, where Driscoll et al. [109] found the major vibrational band associated with the ν_1 stretching vibration to be centered at 801 cm^{-1} , whereas Frost et al. [115] and Faulques et al. [108] reported bands from 845 to 768 or at 827 cm^{-1} , respectively. Driscoll et al. [109] and Faulques et al. [108] did not attempt to fit the bands associated with the uranyl symmetric stretch, but Frost [115] identified four bands within the spectral envelop of interest and the bands exhibited variable peak widths (6 – 49 cm^{-1}). Moving forward, additional investigations are necessary to identify the nature and variability of the bands that arise from solid-state uranyl compounds.

Vibrational analysis provides additional information regarding the unusual coordination environment of uranium within inorganic or mineral phases. In rare cases, a uranyl oxo atom can bond to a neighboring uranyl through the equatorial plane [116]. Historically, this is described as a cation-cation interaction and was previously shown to perturb the uranyl bond [116,117]. Cation-cation interactions cause the uranyl bond engaged in this interaction to weaken and the ν_1 band to red shift. Xiao et al. [118] reported Raman spectra of the two uranyl tungstate compounds, $\text{Cs}_4[(\text{UO}_2)_4(\text{WO}_5)\text{W}_2\text{O}_8]\text{O}_2$ and $\text{Cs}_4[(\text{UO}_2)_7(\text{WO}_5)_3\text{O}_3]$. These compounds contain cation-cation interactions in four of the seven crystallographically unique U(VI) polyhedra. Substantial elongation of the uranyl bonds (1.805 – 1.821 \AA) is observed with $\text{Cs}_4[(\text{UO}_2)_4(\text{WO}_5)\text{W}_2\text{O}_8]\text{O}_2$ while there is more variability (1.76 – 1.99 \AA) for $\text{Cs}_4[(\text{UO}_2)_7(\text{WO}_5)_3\text{O}_3]$. Concurrently, the Raman spectra reveal two uranyl vibrational modes [118]. The first is located at 828 cm^{-1} for unperturbed uranyl bonds and a red shifted mode between ~ 780 and 760 cm^{-1} for the uranyl oxo bonds engaged in cation-cation interactions. In addition, the ν_3 mode is activated because cation-cation interactions break the $D_{\infty h}$ symmetry. Features are weak, but can be observed between 832 and 815 cm^{-1} .

The oxidation state of the inorganic uranium compounds and minerals can be confirmed using Raman spectroscopy. While pentavalent uranium is quite rare in natural settings, hydrothermal reactions conditions in geologic or synthetic systems can result in the formation of mixed valence compounds [119–123]. X-ray diffraction data provides information on elongated bond lengths and reduced bond valence sums that would be indicative of U(V)O_2^+ . This oxidation state change is confirmed using Raman spectroscopy via a reduced ν_1 vibrational mode energy. The presence of U(V) within inorganic compounds and mineral phases has been suggested twice and in both instances, inconclusively. Wyartite ($\text{CaU(V)(U(VI)O}_2)_2(\text{CO}_3)\text{O}_4(\text{OH})(\text{H}_2\text{O})_7$) was characterized using Raman spectroscopy by Frost [124]. Vibrational features were observed between 850 and 830 cm^{-1} , which are consistent with U(VI), while no bands were observed in the U(V) region (800 – 750 cm^{-1}). In a second case, $\text{K}_3(\text{U}_3\text{O}_6)(\text{Si}_2\text{O}_7)$ and $\text{Rb}_3(\text{U}_3\text{O}_6)(\text{Ge}_2\text{O}_7)$ phases were synthesized under hydrothermal conditions [122]. The presence of U(V) was confirmed using XPS, XAS, and magnetic susceptibility; however, the U(V) spectral window was silent upon Raman spectroscopy analysis. These initially conflicting results can be understood by considering the covalency and Raman cross section of the uranyl moiety. Specifically, the U—O bonds within this compound give rise to a distorted octahedron,

which potentially limits the covalency of the uranyl moiety thus decreasing the probability of observing this mode.

3.2. U(VI) coordination compounds and hybrid materials

Vibrational spectroscopy has been an important characterization tool for uranyl coordination compounds since the earliest reported spectra of uranyl salts by Conn in 1938 [62]. The evaluation of these simple uranyl coordination compounds using vibrational spectroscopy gave rise to our initial understanding of the uranyl cation and the covalent nature of these bonds. Over the last 10 years, instrument availability and improvements led to widespread use of these methods as characterization tools for more complex uranyl hybrid materials. With increasing use, large data sets for both coordination compounds and uranyl organic materials are available, which provides additional insights into the uranyl bond. In this section, we again focus on the use of Raman spectroscopy because of the difficult interpretation of the IR-active asymmetric stretching mode given the overlap with the fingerprint region of most organic molecules. Additional details can be found in Table 3.

Average symmetric stretching mode and vibrational frequency ranges for simple coordination complexes and more complex uranyl organic compounds are provided in Fig. 7. Uranyl coordination complexes exhibit more discrete vibrational frequencies compared to the larger spectral ranges observed for complex species containing peroxides and phosphonates. This is understandable as the coordination spheres within these two types of ligands are chemically complex and change dramatically by forming diverse extended lattices. O-donating ligands such as ketones, carboxylates, and alcohols are also diverse as multiple coordination geometries and topologies can form (see Table 2).

Several additional trends are noted within uranyl coordination compounds and hybrid materials. First, the coordination compounds $(\text{UO}_2)\text{L}_x$ ($X = 3, 4, \text{ or } 5$) show that the symmetric mode increases as follows: $\text{NO}_3 < \text{CH}_3\text{COO} < \text{SCN} < \text{Cl}, \text{Br} < \text{CO}_3 < \text{O}_2 < \text{OH}$. Nguyen Trung et al. [14] reported a similar trend for solution phase species. A notable exception is that solution phase $\text{UO}_2(\text{CH}_3\text{COO})_3$ exhibits a band at 843 cm^{-1} , which is lower in energy than the soluble tetrahalides (UO_2Cl_4 (854 cm^{-1})) [14]. The opposite is true for solid phases.

Differences between the solution and solid-state spectra are likely related to crystallization effects as well as intermolecular interactions between neighboring cations with the uranyl oxo atoms. Careful evaluation of the uranyl tetrachloro system, which has been thoroughly characterized in solution and in 18 solid-state coordination compounds, provides us with an excellent platform to understand these effects. Schnaars and Wilson [125] systematically studied $[\text{UO}_2\text{Cl}_4]^{2-}$ complex crystallized with the tetraphenylphosphonium/tetraphenylarsonium cation and various solvent molecules. The ν_1 mode was shown to be independent of solvent composition and tetraphenylarsonium cation presence. Crystal packing of the $[\text{PPh}_4]_2\text{UO}_2\text{Cl}_4$ compound induced the largest impact on this vibrational frequency. Two polymorphs formed with either a triclinic ($P-1$) cell (838 cm^{-1}) or a monoclinic form (823 cm^{-1}). Schnaars and Wilson [125] hypothesized that the 15 cm^{-1} difference in the symmetric stretching band arose from either 1) additional hydrogen bonding to the uranyl oxo in the monoclinic form or 2) subtle differences in the UACl bond

lengths that would lead to an increased electrostatic effect and uranyl bond destabilization. Qu et al. demonstrated similar effects by crystallizing the uranyl tetrachloro species with imidazolium cations [126]. An 8 cm^{-1} difference was observed between $[\text{Emim}]_2\text{UO}_2\text{Cl}_4$ (Emim = 1-ethyl-3-methyl-imidazolium; 827 cm^{-1}) and $[\text{Emmim}]_2\text{UO}_2\text{Cl}_4$ (Emmim = 1-ethyl-2,3-dimethylimidazolium; 835 cm^{-1}). Hydrogen bonding interactions between uranyl oxo atoms and the charged imidazolium group were used to describe these vibrational frequency variations. Hydrogen bonding interactions were disrupted upon methyl group substitution at the N1 position for Emmim⁺. Consistent with Raman spectral features in general, this suggests that hydrogen bonding interactions and other intermolecular forces can influence the ν_1 frequency from solid-state samples.

Equatorial ligand composition also influences the ν_1 frequency because of variations in the electron-donating capabilities of the ligand and the coordination environment. The uranyl nitrate system, which has several different substitutions, provides an excellent system to discuss these differences. The ν_1 mode for $\text{X}[(\text{UO}_2)(\text{NO}_3)_3]$ X = K, Cs, Rb, NH_4 , Et_4N ranges from 880 to 870 cm^{-1} with an average value of 875 cm^{-1} [101,127,128]. Substitution of a nitrate group for two water molecules in the trans position occurs in case of uranyl nitrate hexahydrate $[(\text{UO}_2)(\text{NO}_3)_2(\text{H}_2\text{O})_2]\cdot 6\text{H}_2\text{O}$ and the dihydrate form, resulting in a slight decrease in the symmetric stretching vibrational frequency (876 – 865 cm^{-1}) [57,58,129]. Ligands that provide sigma donation (PPh₃O or diamide ligands- $\text{Et}_2\text{N}(\text{C}=\text{O})(\text{CH}_2)_n(\text{C}=\text{O})\text{NEt}_2$, cyclic amides) form $[(\text{UO}_2)(\text{NO}_3)_2(\text{L})_2]$ species, which also cause the vibrational frequency to decrease in energy [130]. Ligand position likely influences the extent of vibrational energy change. For instance, when the nitrate groups of diamide ligands are in the *trans* position, the ν_1 frequency is observed between 860 and 854 cm^{-1} [130]. Complexes that contain the nitrate ligands in the *cis*-conformation exhibit modes centered at 846 and 841 cm^{-1} . Similar trends are observed for cyclic amides where all three compounds contain nitrate ligands in the *trans* position and ν_1 bands for uranyl between 856 and 850 cm^{-1} [130].

Hydrolysis of the U(VI) cation leads to the formation of larger oligomers and variations in the symmetric stretching mode. When hydrolysis occurs,olation or oxolation reactions result in the formation of bridged hydroxo or oxo groups [131]. These bridging groups provide additional electron donation to the metal centers, which further lowers the vibrational mode energy and causes the vibrational feature to broaden 20 – 30 cm^{-1} [14,132]. The uranyl nitrate and citrate systems provide excellent platforms for demonstrating this. The $[(\text{UO}_2)(\text{NO}_3)_2(\text{H}_2\text{O})_2]$ complex exhibits a vibrational frequency between 876 and 865 cm^{-1} and hydrolysis to the dimeric form $[(\text{UO}_2)_2(\text{OH})_2(\text{NO}_3)_4]^{2-}$ causing this mode to red shift to 853 cm^{-1} in solid state spectra [58]. Similar trends in m_1 are observed for the uranyl citrate system. The 2:2 U: citrate dimer occurs at 825 cm^{-1} in the solid state while the trimeric 3:2 and 3:3 U: citrate species are observed at 800 and 790 cm^{-1} , respectively [16].

Overlapping vibrational modes increase the difficulty of spectral interpretation for coordination compounds and hybrid materials, particularly in the presence of some organic ligands or peroxide molecules. Spectral features from chelating ligands were specifically noted for the citrate [16], malate [133], pyromellitate [134], benzenedicarboxylate [135], and hydrobenzoate [136] systems. Similarly, uranyl peroxide spectra contain overlapping modes

from uranyl and peroxide stretches. The peroxide mode frequency depends on the coordination to uranyl polyhedra and ranges from 904 to 822 cm^{-1} [137,138]. In the case of $\text{LiK}_3[(\text{UO}_2)_4(\text{O}_2)_2(\text{C}_{10}\text{H}_{12}\text{O}_8\text{N}_2)_2(\text{H}_2\text{O})_2] \cdot 18 \text{H}_2\text{O}$, two partially resolved vibrational features are located near 830 cm^{-1} [139]. Speciation assignment of these bands was achieved using both isotopic labeling and DFT calculations. These techniques were highlighted in the case of uranyl triperoxide $(\text{UO}_2(\text{O}_2)_3)^{4-}$ complexes where the ν_1 mode was observed between 738 and 677 cm^{-1} [140]. Empirical band predictions based upon bond distances do not accurately predict vibrational frequency, indicating a need for additional computational approaches. Quantum considerations that were developed by Vallet et al. [141] and utilized by Dembowski [138] for the peroxide system provided better agreement between the predicted (717 cm^{-1}) and experimental (710 cm^{-1}) values.

3.3. Spectroscopy as predictive tools for solid state bonds

Many spectroscopic investigations of solid-state materials focus on vibrational mode frequencies, but additional information is available from established semi-empirical relationships. The vibrational frequency can be calculated using Hooke's law, and as a result, depends on bond lengths and force constants. Force constants provide an initial estimation of bond strength to understand the influence of the equatorial ligands on the uranyl bond [39]. Accumulated empirical vibrational spectra also allow for the estimation of vibrational frequency based on bond lengths and coordinating ligands. This section provides both the background for these relationships and an updated analysis based upon the larger data-set provided in Tables 2 and 3.

Empirical equations can be derived from experimentally observed vibrational frequencies, which are then used to calculate force constants [142,143]. For example, the vibrational frequency for a chemical bond can be modeled using Hooke's law, and the relationship between vibrational frequency ($\bar{\nu}_{\text{vib}}$) and force constant (k_F) can be derived as follows:

$$\bar{\nu}_{\text{vib}} = \frac{1}{2\pi c} \sqrt{\frac{k_F}{\mu}} \quad (1)$$

where $\bar{\nu}_{\text{vib}}$, k_F , μ and c are the vibrational frequency (cm^{-1}), force constant (N/m), reduced mass (kg), and speed of light in a vacuum, respectively. The force constant can be represented using the following equations [101,144]:

$$4\pi^2 c^2 \bar{\nu}_1^2 = \frac{k_F + k_{12}}{m_O} \quad (2)$$

$$4\pi^2 c^2 \bar{\nu}_3^2 = \left(1 + \frac{2m_O}{m_U}\right) \frac{k_F + k_{12}}{m_O} \quad (3)$$

$$4\pi^2c^2\bar{\nu}_2^2 = \left(1 + \frac{2m_O}{m_U}\right)\left(\frac{2}{m_O}\right)\left(\frac{k_\delta}{r^2}\right) \quad (4)$$

where $\bar{\nu}_1$ is the symmetric stretching frequency, $\bar{\nu}_3$ is the asymmetric stretching frequency, $\bar{\nu}_2$ is the bending frequency, m_O is the atomic weight of oxygen, m_U is the atomic weight of uranium, k_{12} is the stretching interaction constant (dynes/cm), k_δ is the bending force constant, and r is the uranyl bond length.

Force constants for uranyl compounds have been reported since the early 1960s and are now again gaining traction to quickly assess relative bond strength. McGlynn et al. [145] and Bartlett and Cooney [63] first reported a range of force constants for uranyl compounds and more recently, Schnaars and Wilson [125,146] utilized force constants within uranyl tetrachloride complexes to understand slight differences in bond strength. Force constants have also been used to evaluate subtle differences in intermolecular interactions within carboxylate complexes and to assess the impact of charge-assisted hydrogen bonding within uranyl glycine compounds [147]. Previously, the lowest k_f value for isolated uranyl complexes was reported for $K_3UO_2F_5$ at 6.03 mdyn/Å [63], although a majority of the values were observed between 6.4 and 7.5 mdyn/Å. Lower values were observed for extended compounds with the U(VI) cation in octahedral coordination. Expanding this to our current work reveals similar trends with a majority of compounds exhibiting force constants in the same region, even within non-aqueous compounds. One benefit in utilizing force constants is that these can provide relative bond strengths for a particular set of ligands. If we order the $[(UO_2)L_x]$ $X = 3, 4, 5$ complex from largest to smallest force constants, which are $NO_3 > CH_3COO > Cl, SCN > Br > CO_3 > OH$, then trends in Raman vibrational frequencies are understood as these are directly related. A decrease in k_f by 0.18 is observed when $[(UO_2)(NO_3)_2L]$ forms upon ligand substitution. It is important to note that the k_{12} is always a small (−0.1 to −0.25) negative value that does not change significantly upon ligand substitution.

When k_{12} is small with respect to k_F , the relationship between the symmetric stretching and asymmetric stretching modes is $\nu_1 = 0.939 \cdot \nu_3$ [101]. As a first approximation for predicting the symmetric mode frequency, this works reasonably well. The k_{12} is always non-zero so additional formulas have been postulated for both solid state and solution samples. The empirical results for solid state species are $\nu_1 = 0.89 \cdot \nu_3 + 30.8$ (cm^{-1}) [148], $0.89 \cdot \nu_3 + 21$ (cm^{-1}) [145], or $0.912 \nu_3 - 1.04$ (cm^{-1}) while the empirical result in aqueous solution is $\nu_1 = 0.795 \cdot \nu_3 + 107$ (cm^{-1}) [149]. Cejka previously noted that these relationships are likely influenced by structural details (hydrogen bonding, crystalline packing) and character of the ligands on the equatorial plane thereby warranting further study on these relationships [39].

By focusing on the well-characterized $[UO_2Cl_4]^{2-}$ system, a comparison among the three empirical results for UO_2^{2+} symmetric stretching feature predictions can be made. Using the equation from Bartlett and Cooney [63] ($\nu_1 = 0.89 \cdot \nu_3 + 30.8$ (cm^{-1})) results in an average difference of 11.2 cm^{-1} between the predicted and experimentally determined ν_1

frequencies. In comparison, the predicted and experimental values differ by ~ 3.2 and ~ 3.1 cm^{-1} when utilizing the McGlynn et al. [145] ($\nu_1 = 0.89 \cdot \nu_3 + 21$ (cm^{-1})) or Bagnall and Wakerley [150] ($\nu_1 = 0.912 \cdot \nu_3 - 1.04$ (cm^{-1})) relationships, respectively. The largest differences were observed with the densely packed solids, $\text{Rb}_2\text{UO}_2\text{Cl}_4 \cdot 2\text{H}_2\text{O}$ and $\text{Cs}_2\text{UO}_2\text{Cl}_4$ using the Bagnall and Wakerley [150] and McGlynn et al. [145] equations where average differences were 11.8 and 8.7 cm^{-1} , respectively.

To investigate if more specialized empirical relationships improve predictions of the vibrational modes that are observed experimentally, least squares regression and well characterized compounds are used. First, ν_1 and ν_3 frequencies are plotted for uranyl tetrachloride compounds (Fig. 8). Data from densely packed solids and less resolved compounds with crown ether molecules are excluded from the analysis. Least-squares regression produced an identical relationship reported by McGlynn et al. [145] demonstrating that data segregation of specialized compounds does not lead to predictive improvements.

Similar analysis was performed by plotting all spectral data observed for uranyl carbonate and nitrate coordination complexes and hybrid materials. The empirical relationship established by McGlynn et al. [145] provided the most accurate predictions for the ν_1 mode with an average difference from experimental values of 7.8 cm^{-1} . Additional data analysis for the uranyl peroxide system and compounds synthesized in non-aqueous conditions reveals differences between predicted and experimentally observed values. Smaller differences could arise from crystallization effects as well as hydrogen bonding and cation-oxo interactions that perturb the uranyl bond within the solid-state compound.

If the force constant is known, then the bond length of uranyl bond (\AA) can be estimated. The relationship between the bond length (r) obtained from crystallographic measurements and the force constant (mdyn/\AA) is as follows: $r = 1.17 \cdot k_F^{-1/3} + 1.08$ [143]. This relationship has been utilized extensively for mineralogical samples with variable degrees of success. For coordination compounds, the relationship tends to underestimate the bond distance by an average of 0.07 \AA , which is significant for the relatively inflexible uranyl bond.

Vibrational frequencies for aqueous uranyl species can also be estimated by considering the coordinating ligands on the equatorial plane of the complex. Previously, an empirical equation: ν_1 (cm^{-1}) = $-A \cdot n + 870$ cm^{-1} was derived where A (cm^{-1}) is defined as the characteristic coefficient (related to the vibrational frequency difference before (870 cm^{-1}) and after uranyl coordination by a select ligand), and n is the number of ligands [151,152]. The characteristic coefficient (A) (cm^{-1}), depends on the bond strength between equatorially bound ligands to the U(VI) metal center and the length of uranyl bond. As a result, the uranyl symmetric stretching frequency decreases, and the characteristic coefficient (A (cm^{-1})) for that ligand increases. The bond strength between uranyl and coordinating ligands typically depends on bond strength as follows:

$\text{OH}^- > \text{CO}_3^{2-} > \text{C}_2\text{O}_4^{2-} > \text{F}^- > \text{SO}_4^{2-}$, $\text{CH}_3\text{CO}_2^- > \text{Cl}^- > \text{Br}^-, \text{NO}_3^-$ [55,152–155]. This series

indicates that when OH^- coordinates with uranyl, the vibrational frequency of uranyl ($\bar{\nu}_1$) is lowest in energy, and complexes containing Br^- or NO_3^- are nearly degenerate at 870 cm^{-1} .

4. Chemical identification and dynamic studies of soluble uranyl species

(UO_2^{2+})

Vibrational spectroscopy is a powerful technique to monitor uranyl speciation in aqueous solutions, organic solvents, and ionic liquids. Signature bands can be observed for specific UO_2^{2+} complexes, which can be monitored to determine synthetic processes, determine equilibrium, or understand solvation of the uranyl cation. The importance of IR and Raman spectroscopies within uranyl solutions is highlighted in different chemical systems and solvents. Given the use of these techniques in chemistry, materials, and geoscience, the characterization of soluble uranyl species in aqueous solutions, organic solvents, and ionic liquids using vibrational spectroscopy are reported and discussed in the following sections. We specifically focus on U(VI) in this section because vibrational spectroscopy is not generally used for U(IV) detection due to the insoluble nature of these complexes and its weak spectral features.

4.1. Uranyl species in aqueous solutions

Relative abundance of each uranyl species in aqueous solution depends on the formation constant for the complex, kinetics of the system, concentrations of U(VI) and ligand, and solution pH. The pH affects the amount of hydroxide ion present in water and the amount of hydrolysis that the U(VI) metal cation will undergo to form oligomeric species. In aqueous solutions, the most soluble inorganic uranyl species contain carbonate, nitrate, and/or sulfate as inner coordination sphere ligands [156–159]. In addition, small organic molecules with O- or N-donors can also bind strongly to the uranyl cation and form soluble complexes in solution. The uranyl species in aqueous solution are now discussed in detail below and Table 4 summarizes these vibrational details.

The solvated uranyl molecule is the simplest complex observed in aqueous solutions and can be observed in the presence of weakly binding anions such as nitrate and perchlorate. Both X-ray scattering experiments and computational studies have determined that the pentaaqua complex is the dominant species under these conditions. The symmetric and asymmetric bands for the $[(\text{UO}_2)(\text{H}_2\text{O})_5]^{2+}$ complex is located at 870 and 962 cm^{-1} , respectively. These values generally serve as a baseline to indicate the stabilization or destabilization of the uranyl bond upon coordination to other ligands in the equatorial plane.

As indicated above, the influence of nitrate and perchlorate anions in uranyl solutions is minimal, but there is evidence that under high anion concentration in solution, complexes can form, which impact vibrational band width. Formation of the $[\text{UO}_2(\text{NO}_3)]^+$ complex results in a simple spectra with a band centered at $\sim 870\text{ cm}^{-1}$ [160]. When the nitrate to uranyl ratio increases, the formation of nitrate species causes the valence electron from NO_3^{2-} to shift to UO_2^{2+} . This causes the width of the vibrational band to increase, but the

position remains constant [161]. Similarly, the vibrational frequency of uranyl perchlorate is degenerate with the uranyl pentahydrate species; thus the vibrational frequency of the ν_1 band is observed at 870 cm^{-1} . These bands also exhibit similar full width at half maxima (FWHM, Γ). These spectral similarities are reasonable given that the perchlorate ligands in this system do not undergo inner sphere coordination with the uranyl cation in solution [162].

In the presence of weakly complexing ligands, hydrolysis of the uranyl cation is also commonly observed in aqueous solutions, and molecular speciation depends heavily on pH. Olation and oxolation reactions result in the formation monomers, dimers, and trimers, which increase the difficulty of spectral interpretation [131]. Consequently, knowing accurate vibrational frequencies of these species facilitates species identification. From pH 2.88–3.46, uranyl dimers, $[(\text{UO}_2)_2(\text{OH})_2]^{2+}$, exhibit characteristic symmetric stretching frequencies centered at $853\text{--}851\text{ cm}^{-1}$ [56,163], and the asymmetric stretch appears in IR spectra at 943 cm^{-1} [164]. At pH 4, the symmetric and asymmetric stretching modes of the trimer uranyl species, $(\text{UO}_2)_3(\text{OH})_5^+$, are centered at 836 [56] and 923 cm^{-1} , respectively [164]. Finally, other uranyl hydrolysis species including $(\text{UO}_2)_3(\text{OH})_8^{2-}$, $(\text{UO}_2)_3(\text{OH})_{10}^{4-}$, $(\text{UO}_2)_3(\text{OH})_{11}^{5-}$, and $\text{UO}_2(\text{OH})_4^{2-}$ [151] are detected in solution with pH ranging from 5.63 to 14.96 [132]. The long-term stability of these hydrolysis products in aqueous solutions depends on uranyl concentration and the presence of other complexing ligands in solution.

Carbonate species are naturally abundant complexing ligands that can impart control over the presence of hydrolysis products in solution. Soluble uranyl carbonate complexes are important in environmental systems because of the equilibrium between carbonate anions and dissolved carbon dioxide in natural waters as well as the presence of widespread carbonate minerals and rock formations [165]. The two most soluble forms of carbonate species are $\text{UO}_2(\text{CO}_3)_2^{2-}$ and $\text{UO}_2(\text{CO}_3)_3^{4-}$, which readily occur at neutral to basic pH values [13]. Their symmetric stretching vibrational frequencies are located at 832 and 812 cm^{-1} , respectively [14,152,166,167]. In addition, the IR-active asymmetric stretching vibrational frequencies for $\text{UO}_2(\text{CO}_3)_3^{4-}$ is centered at 885 cm^{-1} [168]. At near neutral pH conditions, there is an equilibrium between uranyl carbonate species and hydrolysis products in solution that can easily be monitored using vibrational spectroscopy. Lu et al. [48] analyzed the spectra of aqueous solution containing $\text{UO}_2^{2+}_{(\text{aq})}$ and $105\text{ mM Na}_2\text{CO}_3$ at pH 3, 6, and 11 and compared these results to the expected equilibrium diagram (Fig. 9). The solution at pH 3 was predicted to contain free UO_2^{2+} cation as well as a small amount of the $(\text{UO}_2)_2(\text{OH})_{(\text{aq})}^{3+}$ phase, and this was confirmed with the bands at 871 and 859 cm^{-1} that were observed in the Raman spectra [48]. Under alkaline conditions, the only signal observed in Raman spectra was located at 814 cm^{-1} , which corresponds to the only equilibrium diagram predicted species, $\text{UO}_2(\text{CO}_3)_3^{4-}$. The diagram also predicted the formation of a $\text{Na}_2\text{U}_2\text{O}_7$ solid precipitate, but this did not form until 12 days after sample preparation. Similar slow

kinetics were observed under near neutral conditions, as hydrolysis products $(\text{UO}_2)_2(\text{OH})_2^{2+}$ and $(\text{UO}_2)_3(\text{OH})_5^+$ along with $\text{UO}_2(\text{CO}_3)_2^{2-}$ and $\text{UO}_2(\text{CO}_3)_3^{4-}$ were observed in spectra. The equilibrium diagram indicated that hydrolysis products should not be present in the solution under these conditions and indeed the spectral signals associated with the hydroxide phases were absent after 12 days of aging the sample.

Alpha radiolysis of carbonate-rich water can result in the formation of peroxide and stable peroxocarbonate species that have importance in the corrosion of spent nuclear fuel [169,170]. Peroxide forms in aqueous solution due to the alpha-radiolysis of water and precipitates to the previously described studtite phase at low pH conditions. In higher pH solutions, mixed peroxocarbonato species $[\text{UO}_2(\text{O}_2)_x(\text{CO}_3)_y]^{2-2x-2y}$ forms with x:y = 1:2, 2:0, and 0:3 complexes present depending on the solution pH values [171]. Raman spectroscopy can be used to differentiate these complexes as the symmetric stretching bands for $(\text{UO}_2(\text{O}_2)(\text{CO}_3)_2^{4-})$, $(\text{UO}_2(\text{CO}_3)_3^{4-})$, and $(\text{UO}_2(\text{O}_2)_2^{2-})$ are centered at 769, 811, and 848 cm^{-1} , respectively [171]. The uranyl peroxocarbonato complex is not stable in solution for long periods of time and decomposes to the uranyl tricarbonato species under alkaline conditions or elevated temperatures (Fig. 10). Kim et al. monitored this decomposition reaction using Raman spectroscopy and determined the activation energy of the reaction to be 7.144×10^3 J/mol [169].

Uranyl halide complexes form in high ionic strength salt solutions, which is hypothesized to impact the uranyl symmetric stretching mode energy via electrostatic interactions between the U(VI) cation and halide anions. Monomeric $\text{UO}_2\text{X}_n^{2-n}$ (X = F⁻, Cl⁻, and Br⁻; n = 1, 2, 3, 4) complexes have been previously characterized in aqueous solutions by Nyugen-Trung et al. [14]. The conditions needed to form these complexes vary, and the UO_2F^+ , UO_2Cl^+ , and UO_2Br^+ species form when the ligand to U(VI) ratio is 1, 300, and 500, respectively. The impact of halide ligands on the uranyl symmetric stretching mode decreases by 12, 4, and 0 cm^{-1} (from the $\text{UO}_2(\text{H}_2\text{O})_5^{2+}$ complex) when the uranyl cation is coordinated by four fluoride, chloride, and bromide anions, respectively [152,172]. Vallet et al. utilized quantum chemical methods to probe the nature of the uranyl halide interaction and concluded that electrostatics alone could sufficiently cause bond destabilization, which is influenced by ligand electronegativity [141]. This result corresponds to spectroscopic trends where the more electronegative F⁻ anion influences the band position more than the Cl⁻ anion.

Pure uranyl peroxide species can also be observed in solution and exhibit complex speciation with the formation of large, fullerene-type nanoclusters under alkaline conditions [173]. While monomeric $(\text{UO}_2)(\text{H}_2\text{O})_2(\text{O}_2)_2^{2-}$, $(\text{UO}_2)(\text{H}_2\text{O})(\text{OOH})(\text{O}_2)_2^{3-}$, and $(\text{UO}_2)(\text{OOH})(\text{O}_2)_2^{3-}$ as well as dimeric $(\text{UO}_2)_2(\mu^2-\text{O}_2)(\text{O}_2)_4^{6-}$ uranyl peroxide complexes are expected to be present in basic systems, larger nanoclusters containing 24–60 uranyl peroxide units have also been identified as stable species in aqueous solutions [137,174]. Raman spectroscopy has been used as a tool to explore the presence of these uranyl peroxide species in solution, and the signals identified in the spectra include bands between 900 and

750 cm^{-1} . The peroxide symmetric stretching mode has been identified in the range between 850 and 820 cm^{-1} and the band located between 820 and 750 cm^{-1} has been previously assigned to the symmetric stretching mode for the uranyl cation for solutions containing U_{24} and U_{60} clusters at concentrations of 45 or 85 mg/mL [137]. In addition, a third band can be observed in solution at 878 cm^{-1} that is absent in the solid state spectra. McGrail et al. postulated that this band could be associated with the peroxy stretching mode when there are a limited number of coordinating counter cations present in the solution [137].

Larger uranyl peroxide nanoclusters can also be formed in the presence of oxyanions with phosphate, pyrophosphate, and phosphonate anions yielding a maximum number of characterized clusters [175–178]. The stability of the U_{20}P_6 cluster, which contains phosphate anions, was evaluated using NMR, SAXS, and Raman spectroscopy [178]. The solid state crystalline material was redissolved in aqueous solution, and the original solution revealed vibrational bands at 805 and 836 cm^{-1} that were assigned to the uranyl symmetric stretch and the peroxide stretch, respectively. These bands blue-shifted to 808 and 847 cm^{-1} after aging the solution for 48 h, which suggested that the original U_{20}P_6 cluster transformed to the widely observed U_{24} species [178].

The uranyl cation forms complexes with a wide range of oxyanions in aqueous solution, but only a handful of these have been systematically evaluated in solution. Some anions, particularly phosphate and vanadate, form solid compounds with low solubilities (10^{-7} to 10^{-9} M for uranyl phosphate and vanadates) [20,179,180]; thus, low concentrations in solution limit spectral characterization. Silicate forms a rather weak uranyl complex, and $\text{UO}_2(\text{SiO}(\text{OH})_3)^+$ is the only major species observed between the narrow pH regime from 5 to 6.5. Due to the limited range of this uranyl silicate species, there has not been spectral characterization reported in the literature. Uranyl sulfate species including UO_2SO_4 , $\text{UO}_2(\text{SO}_4)_2^{2-}$, and $\text{UO}_2(\text{SO}_4)_3^{4-}$ are soluble and have been identified at 861, 852, and 841 cm^{-1} in Raman spectra [14,152,181,182], and 956, 950, and 945 cm^{-1} in IR spectra, respectively [183]. Ligand binding in the uranyl sulfate complexes vary as UO_2SO_4 is considered in the mono-dentate structure, while $\text{UO}_2(\text{SO}_4)_2^{2-}$ is bidentate as indicated from EXAFS measurements [184]. Differences in chelation can also result in changes within active modes of the sulfate.

Carboxylate ligands including acetate [152,185], citrate [186], glycolate [187], lactate [187], malate [187], oxalate [152,188], succinate [185], tartrate [187] and tricarboxylate [187] ions, readily form complexes with the uranyl cation and are important species in natural and biological systems. Hexavalent uranium is a hard Lewis acid that prefers hard O-donors; thus, carboxylate complexes are stable in water and have formation constants ($\log K$) that range between 2 and 16 [189–192]. The overall coordination geometry of these species were previously studied using density functional theory (DFT) calculations, which predicted that both mono- and bi-dentate coordination structures are possible but depend on ligand stereochemistry [185]. Organic acids contain a hydroxyl group adjacent to a carbonyl carbon, such as in the case of citrate ($\text{C}_6\text{H}_5\text{O}_7^{3-}$), glycolate ($\text{C}_2\text{H}_4\text{O}_3^-$), lactate ($\text{C}_3\text{H}_5\text{O}_3^-$).

malate ($C_4H_6O_5^-$), and tartrate ($C_4H_4O_6^{2-}$), coordinate with uranyl via one oxygen from both the carboxyl and alcohol groups [187]. Uranyl complexation to these molecules is pH dependent in solution because of the need to deprotonate the carboxylate before binding can occur. This was demonstrated in the uranyl acetate system where U(VI) ligand complexes do not form at pH 2.5, even up to a ratio of acetate to uranyl of 20 because the pK_a of acetic acid is 4.75 [152]. The pK_a of the alcohol group is generally much higher so binding to the uranyl cation can occur in the protonated form. The observed asymmetric stretching IR bands and calculated symmetric stretching Raman bands (in parenthesis) [149] are 921 (840), 932.8 (849), 930.2 (847), 916.2 (835), and 918.4 (837) for uranyl citrate ($C_6H_5O_7^{3-}$), glycolate ($C_2H_4O_3^-$), lactate ($C_3H_5O_3^-$), malate ($C_4H_6O_5^-$), and tartrate ($C_4H_4O_6^{2-}$), respectively [168,187].

Spectral interpretation of the uranyl carboxylate system can be complex due to the variability in chelation and activation of modes upon complexation to the U(VI) cation. Simple uranyl acetate species include $UO_2(CH_3COO)^+$, $UO_2(CH_3COO)_2$, and $UO_2(CH_3COO)_3^-$ with identified symmetric stretches at 861, 852, and 843 cm^{-1} and asymmetric stretches at 949, 939, and 924 cm^{-1} , respectively [185]. Initial investigation of the vibrational frequencies of the uranyl symmetric stretches for $UO_2(CH_3COO)_2$ and $UO_2(CH_3COO)_3^-$ were assigned to bands centered at 841 and 823 cm^{-1} vs. 852 and 843 cm^{-1} , respectively [153]. This assignment discrepancy is likely attributed to overlapping vibrational bands from various uranyl species and (the lack of) band deconvolution used during spectral analysis. This also occurred for succinic acid, which also chelates to the uranyl cation through mono- or bidentate coordination modes and displays multiple vibrational frequencies in ATRIR spectra (950, 938, and 925 cm^{-1}) [185].

Assignments of uranyl citrate species were also difficult to interpret due to the presence of overlapping bands combined with the formation of stable hydrolysis products in solution. Uranyl citrate species are highly soluble and used to improve U removal from soils and enhance phytoremediation strategies [193,194]. NMR studies from Nunes et al. [195] defined several well-defined species within this system with U(VI):ligand ratios of 2:2, 3:3, and 3:2. Raman studies found multiple bands centered at 852, 812, and 797 cm^{-1} that were initially assigned to the 2:2, 3:3, and 3:2 complexes [186]. More recent studies determined that the band at 812 cm^{-1} was associated with the activation of a citrate vibrational mode that is only observed upon complexation to the uranyl cation. Current assignments for the uranyl symmetric stretches of $(UO_2)_2(C_6H_5O_7)_2^{2-}$, $(UO_2)_3(C_6H_5O_7)_3^{3-}$, $(UO_2)_3(C_6H_5O_7)_2$ are located at 825, 800, and 790 cm^{-1} (Fig. 11), [16] and asymmetric stretches at 919, 891, and 888 cm^{-1} , respectively [186].

Much of this section has focused on well-defined systems, but the speciation of U(VI) in the presence of complex organic biomolecules, like fulvic and humic acids, are vitally important for understanding the fate and transport of U in natural systems. Humic and fulvic acids represent families of organic acids that vary in acidity, polymerization, and functional groups. These organic biomolecules can mobilize natural uranium and enhance the transport

within subsurface systems.[196] Vibrational spectroscopy is an important tool for developing an enhanced understanding of U(VI) speciation in these systems as demonstrated by Stuedtner et al. [197]. In this study, ATR FT-IR was paired with geochemical modeling to identify binary and ternary U(VI) humate (HA) complexes. Under N₂ gas, the uranyl cation binds with humic acid to form two soluble species (UO₂(HA) ($\nu_3 = 925 \text{ cm}^{-1}$) and (UO₂(OH)(HA)($\nu_3 = 913 \text{ cm}^{-1}$)) and one solid phase ($\nu_3 = 932 \text{ cm}^{-1}$). In the presence of CO₂, a ternary complex (UO₂)(CO₃)₂HA ($\nu_3 = 892 \text{ cm}^{-1}$) is expected to form and dominate under alkaline conditions [197]. Additional studies are necessary to provide details on the exact speciation in the presence of organic acids and explore other biomolecules relevant for environmental transport and human health.

4.2. Uranyl species in ionic liquids

Ionic liquids have been explored as novel solvents for uranyl extraction from aqueous solution, and vibrational spectroscopy is the primary characterization tool for assessing dominant uranyl species. Pasilis et al. explored the 1-ethyl-3-methylimidazolium bis(trifluoromethylsulfonyl)imide ([EMIM][Tf₂N]) system and observed that the addition of uranyl perchlorate resulted in the formation of a symmetric stretch mode at 884 cm^{-1} , which is attributed to the hydrated uranyl perchlorate complex [198]. Addition of tetrabutylammonium nitrate to this system resulted in the displacement of water and perchlorate ligands thereby forming two uranyl nitrate species (UO₂(NO₃)₂, and UO₂(NO₃)₃⁻) with Raman vibrational frequencies centered at 869 and 865 cm^{-1} , respectively.

Hopkins et al. investigated the ionic liquid, aluminum chloride-1-ethyl-3-methylimidazolium chloride (AlCl₃-EMIC) and determined that the major species was the uranyl chloride complex (UO₂Cl₄²⁻) [199]. The vibrational frequency of this species in the ionic liquid is located at 838 cm^{-1} , which is similar to the solid state vibrational frequency for Cs₂UO₂Cl₄ that is centered at 836 cm^{-1} [200]. As a comparison, the vibrational frequency for UO₂Cl₄²⁻ is located at 854 cm^{-1} in aqueous solution [152]. This suggests that the environment around the UO₂Cl₄²⁻ complex in ionic liquids may be similar to that of the densely-packed cesium uranyl chloride salt lattice. More recent studies by Krishna et al., confirmed that the tetrachloro species is present in 1-butyl-3-methylimidazolium bis(trifluoromethylsulfonyl)imide (C(4)mimNTf (2)) ionic liquid and found that these complexes underwent facile and favorable electrochemical reduction [201,202].

If the ionic liquid contains strongly complexing functional groups, then additional complexes must be considered when describing the chemical complexity within these systems. For example, the addition of uranyl perchlorate in 1-butyl-3-methylimidazolium nonafluorobutanesulfonate (BMINfO) results in the displacement of the perchlorate anions by the sulfonate group in BMINfO. This results in a red-shift of the uranyl symmetric stretch from 880 [162,203] to 871 cm^{-1} [204]. Other ionic liquids, such as those containing dicyanamide [205], have the ability to complex with the uranyl cation as evidenced by crystallization studies. Additional experiments are necessary to determine the vibrational bands present in these solvents and the identity of other uranyl species that form in ionic liquids with O- and N-donor groups.

4.3. Uranyl species in polar organic solvents

While there is a large body of literature on the use of vibrational spectra to determine aqueous uranyl species, much less is known about speciation of uranium in polar organic solvents. One major difference between non-aqueous and aqueous solutions is that many organic solvent molecules do not inhabit the inner sphere coordination of the uranyl cation [206,207]. The most prominent differences in vibrational mode frequency are observed in diethyl ether (C_2H_5O). The vibrational frequency (ν_3) of $UO_2(NO_3)_2 \cdot 2(C_2H_5O)_{(s)}$ is centered at 940 cm^{-1} in the solid phase, and $[UO_2(NO_3)_2]$ dissolved in C_2H_5O exhibits an identical vibration frequency [207]. This same vibrational frequency is observed for $[UO_2(NO_3)_2]$ dissolved in other organic solvents including methanol, butanol, iso-butanol, acetone, and methyl ethyl ketone [207]. As such, the inner sphere coordination for this species is unlikely. Additional studies are necessary to explore solvents with ligands that may complex via inner sphere coordination with the uranium, including pyridine, DMSO, and THF.

4.4. Using vibrational spectroscopy to provide thermodynamics of solution-phase species

As the previous sections highlight, vibrational spectroscopy is a powerful tool for developing speciation models and stability constants in uranyl systems. Analyzing either the band intensity or areas associated with the ν_1 or ν_3 band for the uranyl species present in solution provides information regarding the concentration of the various complexes. Typically, this is done by assuming that the cross section is the same across similar species. This was demonstrated *vide supra* with the uranyl carbonate system [48], but advanced chemometric methods can also be used for quantifying relative amounts of various species in more complicated systems. Chemometrics [155] successfully facilitated the identification and quantification of oligomeric uranyl species ($U_{\text{total}} = 0.1\text{ M}$) present in solutions with pH ranging from 1.55 to 4.20 using both Raman and FT-IR spectroscopies. The multivariate method partial least squares (PLS2) was employed and revealed the relative abundance of $(UO_2)_2(OH)_2^{2+}$ and $(UO_2)_3(OH)_5^+$ in aqueous systems. Importantly, this approach eliminated the possibility that the previously reported uranyl species $(UO_2)_2OH^{3+}$ existed under these conditions.

Linear free energy relationships can also be developed to determine stability constants for U(VI) complexes. The relationship between the overall stability constant ($\log \beta$) and the shift in the Raman vibrational frequency was highlighted in the study by Nguyen-Trung et al. [14]. Plotting these values lead to straight lines that can be used to estimate the stability constant for mononuclear U(VI) complexes with the following equations:

$$\log \beta_1(UO_2)L = -0.52 \Delta \nu_1 - 1.61 \quad (5)$$

$$\log \beta_2(UO_2)L_2 = -0.50 \Delta \nu_1 - 4.10 \quad (6)$$

$$\log\beta_3(UO_2)L_3 = -0.46 \Delta v_1 - 5.68 \quad (7)$$

It must be noted that a complete understanding and identification of species present in solution are necessary to effectively utilize these equations. In addition, Nguyen-Trung noted that there are significant variations in spectral interpretation and large uncertainties (as much as two log units for β) for the stability constants published in the literature [14]. This suggests the need for additional studies to further explore these relationships.

5. Surface speciation studied by IR and Raman spectroscopies

Uranium adsorption onto surfaces has implications for environmental transport modeling, remediation strategies, and radio-chemical separations that can be further understood using vibrational spectroscopy [208–211]. Both U(IV) and U(VI) readily hydrolyzes in aqueous solution, which also promotes their adsorption onto mineral surfaces [212,213]. This is important for modeling uranium transport in natural waters, but also has importance in Mn hydroxide precipitation steps during radiochemical separations protocols [214,215]. In addition, U(VI) species readily interacts with organic matter associated with soil particles [209] and adsorbs to the organic ligands present in separation columns [216]. Vibrational spectra can provide chemical insight via band frequencies and bandwidths, both of which that aid in the characterization of uranyl surface species and local environmental conditions. Much of the work involving the characterization of uranyl sorption onto surfaces has been performed with IR spectroscopy; therefore, much of this section will include the assessment of the asymmetric stretching vibrational mode.

5.1. Uranyl adsorption onto oxide surfaces

The vibrational frequencies of uranyl species adsorbed to oxide and oxyhydroxide surfaces have been rigorously reported in the literature. For instance, uranyl adsorption to hematite (α -Fe₂O₃) [214,217–219], maghemite (γ -Fe₂O₃) [220], ferrihydrite (Fe₂O₃·0.5H₂O) [221,222], smectite [223], hydrous titania (TiO₂·nH₂O) [224], hydrous zirconia (ZrO₂·nH₂O) [224], and hydrous silica gel (SiO₂·nH₂O) has been explored using vibrational spectroscopy [224]. Variations in vibrational frequency are observed from adsorbed uranyl species indicating the presence of multiple binding structures and/or species that depend on the oxide mineral identify (Fig. 12). For instance, the ν_3 asymmetric mode for uranium species adsorbed to maghemite and ferrihydrite surfaces are centered at 912 and 903 cm⁻¹, respectively [220,221]. The vibrational band of uranyl adsorbed to ferrihydrite is red-shifted compared to that to maghemite surfaces indicating stronger interactions between uranium and ferrihydrite. This is further supported as uranyl desorbs less from ferrihydrite versus maghemite [220]. Outer sphere coordination mode was postulated for uranyl on the surface of maghemite from the asymmetric stretching (ν_3) modes whereas a bridging bidentate inner sphere coordination is predicted for ferrihydrite. An inner sphere complex is also predicted for SiO₂ and Al₂O₃, but the Raman modes are blue-shifted from spectral features collected from iron oxide surfaces, suggesting a weak interaction with the oxide surface [224–226].

Vibrational spectroscopy is a powerful technique for observing changes in uranyl speciation from environmental perturbations, including pH and carbonate concentration variations. Under acidic conditions, adsorption of uranium to a solid is generally reduced. This occurs because the positively charged major uranyl cation in solution, $U(VI)O_2^{2+}$, is repelled by the positively charged metal oxide surface [228]. Increasing pH leads to the formation of hydrolysis products, such as $(UO_2)_3(OH)_5^+$; but in the presence of carbonate, both $(UO_2)_2CO_3(OH)_3^-$ and $UO_2(CO_3)_3^{4-}$ complexes form [8,229]. Changes in uranyl speciation subsequently and significantly influence surface adsorption energetics while surface complex identity is less impacted if adsorption occurs. For instance, the adsorption capacity of uranyl on hematite is maximized when the pH is above 6.2 [227]. The asymmetric stretching band of the uranyl cation, however, remains at 906 cm^{-1} while the intensity increases upon adsorption to the mineral surface. In the presence of carbonate, adsorption capacity decreases in the same pH range, suggesting the formation of free $(UO_2)_2CO_3(OH)_3^-$ and $UO_2(CO_3)_3^{4-}$ complexes [214]. The vibrational frequencies of uranyl adsorbed to ferrihydrite are observed at 889 cm^{-1} , suggesting the formation of ternary uranyl carbonate complexes. Vibrational spectroscopy has explored the interaction between ferrihydrite surfaces and uranyl carbonate complexes and revealed a red-shift in the asymmetric stretch from 902 to 881 cm^{-1} [222].

5.2. Identification of insoluble aqueous species on solid-state surfaces

In some cases, examining surface chemical composition provides information on low abundance, insoluble species, whose detectability in solution is near the detection limit of vibrational spectroscopy [230]. For instance, uranyl phosphate complexes with a formula of $(UO_2)_3(PO_4)_2 \cdot 4H_2O$ form in solution with pH ranging from 1.5 to 9 [230]. These species remain stable at dilute concentrations because of their low solubility in water [179]. Experimentally, phosphate species can be investigated by detecting adsorbed species to SiO_2 crystals using ATR FT-IR spectroscopy [230]. Species detected using this method were $\equiv SiO_2 - UO_2PO_4^{3-}$ and possessed a vibrational frequency at 919 cm^{-1} , which is identical to that for $(UO_2)_3(PO_4)_2 \cdot 6H_2O_{(s)}$. In addition, Raman bands for the solid-phase uranyl complexes $[UO_2(PO_4)]^-$ ($\nu_1 = 840\text{ cm}^{-1}$) and $[UO_2(PO_4)(H_2O)_4]^-$ ($\nu_1 = 841\text{ cm}^{-1}$) [231] are similar to calculated vibrational frequencies, both of which are predicted to be centered at 837 cm^{-1} [149].

5.3. Monitoring uranium redox using vibrational spectroscopy

U(IV) redox processes that occur on mineral surfaces can also be explored using vibrational spectroscopy. In some cases, the reduction of U(VI) was monitored to explore the retention of uranium on mineral surfaces. For example, Wersin et al. investigated uranyl adsorption to sulfide bearing minerals including (PbS) and pyrite (FeS_2) using Raman spectroscopy and monitored the redox promoted generation of the surface precipitate $U_3O_8_{(s)}$ [232]. Oxidation and corrosion of spent nuclear fuel is a significant area of study, and Raman spectroscopy is a powerful tool for identifying fuel alteration under repository conditions. Bonales et al.

reported spent nuclear fuel oxidizes into U_3O_8 upon exposure to air or into uranyl carbonates and silicates if exposed to groundwater from Sierra Albarrana (Spain) [71,233]. Schmeide et al. explored the redox behavior of uranyl on silicate rock (diorite) surfaces under anoxic conditions and found that uranyl carbonate species reduced the affinity of U(VI) to mineral surfaces and stabilized soluble high valence species in solution [234]. In a final example, Traboulsi et al. used Raman spectroscopy to explore alpha radiolysis of water and oxidation of solid UO_2 to form uranyl peroxide species [66,235].

5.4. Changes in Raman bandwidths on solid state surfaces

Vibrational mode bandwidths are important components when evaluating and reporting the uranium speciation upon adsorption. Increases in bandwidth upon adsorption arise from the formation of multiple uranyl species, varying uranyl orientations, and/or activation of multiple vibrational modes all of which can overlap spectrally [214]. For example, the bandwidth (FWHM) of a ν_1 Raman mode for an adsorbed species is $\sim 57\text{ cm}^{-1}$, which is broader [224] than a variety of uranium species in solution (FWHM = $13\text{--}20\text{ cm}^{-1}$) [48]. Multiple uranyl species can arise from original surface speciation or change upon adsorption with or without coordinated ligand displacement [221,224,236–238]. Inner-sphere coordination increases the vibrational mode band width to a greater extent than outer-sphere coordination. This is because the binding strength of the ligands to the uranyl cation influences the exact nature of these interaction and vibrational mode perturbations [237]. Additional broadening can be caused by bond contraction on the surface, crystallite size, temperature, pressure, and crystallinity. While some of these properties only minimally impact vibrational linewidths, it is important to note that these can induce slight variations.

5.5. Spectral signals collected on functionalized solid materials

Radiochemical separations often rely on surface-driven adsorption processes, and vibrational spectroscopy methods can be used in conjunction with other techniques to provide insight into chemical binding and resulting surface speciation. In addition to the previously discussed oxide materials, both functionalized solids including silica and polymers have been used for uranium extraction. Huynh et al. reported 250 mg U(VI) uptake per g of a sorbent composed of amine functionalized mesoporous silica (SBA-15). Both IR ($\nu_3 = 909\text{ cm}^{-1}$) and Raman ($\nu_1 = 827\text{ cm}^{-1}$) spectroscopies suggested inner sphere coordination with the surface amines of the sorbent [239]. Amidoxime-containing materials have been shown to selectively uptake U(VI). Vibrational spectroscopy has helped identify surface speciation in these systems [236]. For instance, polyacrylonitrile polymers are easily functionalized with amidoxime groups, which makes these types of materials of particular interest for extracting U(VI) from sea water. The coordination geometry of uranium adsorbed to amidoxime have been studied using extended x-ray absorption fine structure (EXAFS) [240], X-ray absorption near-edge structure (XANES) [241], density function theory (DFT) [242,243], as well as Raman and IR spectroscopy [242,244–246]. DFT studies suggested that uranyl coordinated with amidoxime groups form tridentate or η^2 – coordination structures [243]. This provided support with respect to the high extraction efficiency of amidoximated materials for uranyl; however, Abney et al., utilized EXAFS to explore the coordination and concluded that cooperative binding from multiple sites was a more likely

binding mechanism [240]. Future studies utilizing vibrational spectroscopy could provide additional insight into the coordination of the U(VI) on amidoxime surfaces.

6. Challenges, opportunities, and vision

This review has highlighted the importance of how vibrational spectroscopy can provide insight into uranium chemistry and speciation, but there is an opportunity for the development of new methodologies and techniques that can lead to additional advancements in characterization and detection. Current limitations include deconvolution of overlapping vibrational bands in the narrow uranyl spectral window [152] and the relatively low signals from vibrational modes compared to signal collected using other methods, such as fluorescence spectroscopy [247]. Spectral deconvolution techniques can overcome the limitation of unresolved spectral features, and additional computational assessment can provide supporting information on vibrational band assignments and questions related to electronic structure of the uranium cation. Furthermore, uranyl detectability can be improved by introducing nanomaterials to enhance vibrational band intensities. As a result, the application of vibrational spectroscopy for uranium speciation analysis and detection can be widened compared to current capabilities. In the next sections, we highlight the current challenges and present opportunities for overcoming these limitations.

6.1. Uranium detection in complex aqueous matrices

Complex samples, such as those found in environmental and biological systems, can significantly hamper the analysis of vibrational spectra. Matrix effects pose challenges in that detection (signal to noise) limits are higher than in simple systems, and increased diversity of uranium species present in a sample increases the possibility that vibrational bands overlap in a spectrum. Many times, resulting spectra are analyzed by reporting the center (i.e., centroid) of a broad uranyl feature, but these broad spectral bands likely do not correspond to any one uranyl species present in a sample. One way to overcome this challenge is to determine the relative abundance of each uranyl species from spectral analysis and compare these to a model generated from known thermodynamic constants [157,248–250]. Dargent et al. evaluated solutions containing 10 mM uranyl and chloride concentrations ranging from 0.3 to 12 M using Raman spectroscopy, and the spectral features were fit using pseudo-Voigt functions (a combination of Gaussian and Lorentzian functions) to obtain the equilibrium constants [172]. Lu et al. developed a step-by-step process for Raman scattering peak analysis using Gaussian function fitting (Fig. 13). This approach facilitated the accurate extraction of uranyl speciation from uranyl solutions prepared in the presence of the commonly observed ligands including CO_3^{2-} , NO_3^- , and SO_4^{2-} as well as a function of pH [48]. Using this approach, the spectral fitting procedure resulted in accurate relative abundance predictions for species from equilibrium diagrams and also provided speciation predictions from samples that were not at equilibrium. As a result, vibrational spectroscopy coupled with careful analysis could provide realistic details regarding the complex and dynamic speciation of uranyl in samples.

Additional studies are necessary to confirm previously reported speciation modeling and can be enhanced by pairing vibrational spectroscopy with other techniques. Lucks et al.

employed chemometric analysis to reaffirm speciation for the uranyl acetate and succinate systems. An iterative transformation factor analysis on ATR-FTIR spectra confirmed the assignments originally delineated by Ahrlund [251], but a new 1:3 U:succinate complex was detected that alters the speciation diagram within the system. This study also highlights a problem in using vibrational spectroscopy to analyze uranyl species. That is, there can be discrepancies between speciation determined from experimental spectra analysis and thermodynamic predictions [48,155,252]. To overcome these limitations, vibrational spectroscopy will need to be paired with experimental measurement techniques, such as potentiometry, X-ray spectroscopy, time-resolved fluorescence spectroscopy, and computational analysis. This will be particularly important as the complexity of the system increases to provide real-world analysis of environmental and biological matrices.

6.2. In situ detection and monitoring of intermediate and metastable uranium compounds

In situ detection of uranium can be successfully achieved using Raman microscopy. As such, changes in uranyl spectral features can be used to identify intermediate and metastable uranyl species. In addition, the combination of Raman microscopy with other instrumental techniques including XPS, X-ray crystallography, and EXAFS can be used to identify metastable uranium compounds. For example, uranium peroxide species undergo thermal decomposition that can be monitored using Raman ($\lambda_{\text{ex}} = 488 \text{ nm}$), IR, and NMR spectroscopies [254]. Spectral changes indicated that uranium is transformed from $\text{UO}(\text{UO}_2(\text{O}_2)(\text{H}_2\text{O})_2 \cdot 2\text{H}_2\text{O})$ into UO_3 as temperature increases from 30 to 500 °C (Fig. 14). The vibrational frequency of $\text{UO}_4 \text{H}_2\text{O}$, for instance, is centered at 818 cm^{-1} when the temperature is between 25 and 50 °C. As the temperature increases beyond 120 °C, a new Raman band appears at 748 cm^{-1} . This vibrational band continues to broaden as temperature increases and red-shifts from 748 to 707 cm^{-1} as $\text{UO}_{3x}(\text{OH})_{2x} \cdot z\text{H}_2\text{O}$ forms. The vibrational bandwidth of the feature at 707 cm^{-1} is wider than the original band at 818 cm^{-1} as the crystalline structure is converted into an amorphous form [254]. As such, vibrational spectroscopy is a powerful tool for tracking the properties of uranyl species.

The dynamic uranium speciation after irradiation by alpha-radiation can also be monitored using Raman spectroscopy. For instance, the transformation of uranium (IV) dioxide ($\text{UO}_{2(\text{s})}$) into uranium peroxide occurs in the presence of water and oxygen [76]. The growth of studtite $\text{UO}(\text{UO}_2(\text{O}_2)(\text{H}_2\text{O})_2 \cdot 2\text{H}_2\text{O})$ and metaschoepite ($\text{UO}_2 \cdot 2\text{H}_2\text{O}$) are observed at $820/870$ and 840 cm^{-1} , respectively. These species form upon hydrogen peroxide generation from water irradiation in the presence of oxygen. $\text{UO}(\text{UO}_2(\text{O}_2)(\text{H}_2\text{O})_2 \cdot 2\text{H}_2\text{O})$, the product of irradiated UO_2 , is similar to the products that form after UO_2 is dissolved in hydrogen peroxide, water, and oxygen. The time-dependent *in situ* formation of $\text{UO}_2\text{O}_2 \cdot 4\text{H}_2\text{O}$ and $\text{UO}_3 \cdot 2\text{H}_2\text{O}$ was monitored using Raman spectroscopy ($\lambda_{\text{ex}} = 632.8 \text{ nm}$) without affecting reaction process [76]. Furthermore, oxidation of UO_2 solid to polycrystalline U_3O_8 occurs at 300 K in the presence of water (Fig. 15) [67]. This reaction was monitored successfully and confirmed using Raman spectroscopy ($\lambda_{\text{ex}} = 488$ and 785 nm). The valency of uranium was confirmed using XPS. Raman bands for U_3O_8 were observed at 756 cm^{-1} (combination band of $340 (\text{A}_{1g})$ and $405 \text{ cm}^{-1} (\text{A}_{1g})$). Speciation assignments were validated from the oxidation state of surface and bulk UO_2 [67].

6.3. Extending vibrational spectroscopy to evaluate newly discovered uranium species

Vibrational spectroscopy assists in the *in situ* identification of solid uranium samples because the observed features in vibrational spectra including vibrational frequencies, FWHM, and relative signal intensities provide information related to the coordination environment, crystallinity, and relative abundance of each uranium species. For example, vibrational frequencies for uranium shift from 445 to 870 cm^{-1} when the valence number of uranium increases from 4+ to 6+ [66,152]. As a result, vibrational spectroscopy is capable of verifying the identity of known synthesized products [255–257] and newly discovered uranium species such as U (II) [258,259]. Additional Raman spectroscopy measurements were reported for characterizing one-dimensional uranium polymers [255], complex uranyl copper hybrid compounds [257], and uranyl sulfide species $[(\text{UO}_2)\text{S}_4]^{6-}$ [256]. These results support that coordination and structural changes from mono- to bi-dentate or transformations variations in coordination bonds between uranyl and ligands such as from U—O to U—S bond formation in the equatorial plane of uranyl can be monitored successfully using vibrational spectroscopy.

6.4. Use of advanced Raman spectroscopy techniques (resonance Raman and SERS)

Inherently, Raman scattering is an inefficient process, which limits the detectability of molecules. As a result, both resonance Raman spectroscopy, a method where excitation energies are similar in energy to electronic transitions in a molecule are utilized, and surface-enhanced Raman scattering (SERS), a method whereby Raman signals can be increased by 6–8 orders of magnitude via interactions with metallic nanostructures, are useful for detecting uranium species. Resonance Raman spectroscopy was applied to develop Raman excitation profiles (REPs) for uranyl nitrate [260,261], acetate [262], chloride [263] and formate [260] in dimethyl sulfoxide (DMSO). As shown in Fig. 16, DMSO is utilized as both the solvent and internal standard. The obtained vibrational frequencies of these uranyl species include ground and excited state resonance Raman features. Vibrational frequencies of excited state species are much more sensitive to changes in the number of ligands and surrounding environment compared to species in their ground state. For instance, the probability of observing uranyl nitrate in an excited state increases as the number of ligands increases from 2 ($\text{UO}_2(\text{NO}_3)_2$) to 3 ($\text{RbUO}_2(\text{NO}_3)_3$). This causes the vibrational frequency to blue-shift from 703 to 740 cm^{-1} ($\nu_1 = 37 \text{ cm}^{-1}$) [260,261,263]. As a comparison, the vibrational frequencies of ground state species red-shift by 1 cm^{-1} , that is, from 835 to 834 cm^{-1} ($\nu_1 = -1 \text{ cm}^{-1}$) when the number of coordinating ligands increase from 2 to 3. Vibrational frequencies obtained from resonance Raman spectroscopy are sensitive to changes in coordination number; therefore, this technique is an alternative approach for characterizing uranyl species.

While vibrational spectroscopy is a powerful method for detecting uranium, detection limits do not provide information on trace levels of uranium. To improve the detectability of uranium using vibrational spectroscopy, plasmonic nanomaterials can be used to enhance vibrational band signals thus lowering detection limits. To date, surface enhanced Raman scattering (SERS) is the most widely used technique for this purpose. For instance, the detection of uranium was exploited with different SERS substrates including both silver and gold nanostructures. Silver nanomaterials, in general, provide larger signal enhancements

versus gold due to the inherent metal permittivity [265]. In addition, native oxide layers that form on silver promote the adsorption of uranyl via oxophilic interactions [237,266,267]. This was confirmed from SERS spectra where a UAO symmetric stretch was observed at 730 and 710–700 cm^{-1} on silver [266] and silver doped sol-gel substrates [267], respectively.

Uranyl was successfully detected down to 85 nM when silver doped sol-gel materials were used. Gold nanomaterials exhibit superior chemical stability versus silver and have also been employed for uranyl detection [237,268,269]. Because gold lacks a native oxide layer, gold nanomaterials must be functionalized with molecules that coordinate to uranyl for SERS detection. In general, this strategy improves uranyl detectability on both silver and gold nanomaterials [268–271]. For instance, N-(2-mercaptopropionyl)glycine (MPG) was assembled onto silver SERS substrates because both amide and carboxyl groups can coordinate with uranyl. By doing this, a SERS signal was observed at $\sim 840 \text{ cm}^{-1}$, and a detection limit of 5 nM was achieved [270].

Gold nanomaterials can be modified with many different terminal functional groups. For instance, carboxylate terminated alkanethiols were selected to modify gold nanostars for uranyl detection. The carboxylate groups coordinated to uranyl and caused the vibrational frequency of uranyl to be centered at $\sim 840\text{--}830 \text{ cm}^{-1}$. Quantitative SERS detection of uranyl was also achieved using gold nanomaterials [269]. Here, (aminomethyl) phosphonic acids facilitated interactions between uranyl and gold [268] through phosphate-uranyl coordination. This resulted in a vibrational mode centered at 830 cm^{-1} and selective uranyl detection from a 10 mM NaHCO_3 and humic acid solution.

To improve the robustness of SERS detection for uranyl, nano-materials can be dispersed onto supports. For instance, silver nanoparticles were deposited onto reduced graphene oxide nanosheets to form SERS substrates [272]. This led to efficient uranyl adsorption via electrostatic interactions between the cationic uranyl species and anionic oxide groups on graphene oxide. SERS signals for uranyl acetates were shown to red-shift from 838 (Fig. 15A) to 714 cm^{-1} (Fig. 17B) from a pH 5 solution upon adsorption to the substrate, respectively. These vibrational frequency changes indicate that charge transfer from graphene oxide to uranyl occurs once uranyl adsorbs to silver. This approach showed that uranyl detection was reproducible, and detection limits down to 10 nM were demonstrated. Accordingly, applying SERS for the identification and quantification of uranyl is a promising avenue for uranyl detection opportunities.

6.5. Conclusions and outlook

In summary, both infrared and Raman spectroscopies are powerful techniques for the detection and identification of uranium species. Importantly, unique vibrational frequencies generally correlate to specific uranyl coordination environments providing a robust method for identification of solid compounds, solution complexes, and surface species. Additionally, vibrational frequencies for uranyl species in both solid and solution phases can be used to estimate force constants, bond lengths, and/or coordinating ligand composition. Vibrational frequencies for uranyl species adsorbed on mineral surfaces and sorbents were summarized as were those for aqueous uranyl species. Vibrational spectroscopy is highly suitable for the

in situ detection of uranium species; however, overlapping bands can result in poorly assigned uranyl species found in samples. This can limit uranyl detectability because Raman spectral cross sections are small. In cases where significant signals are detected, spectral deconvolution techniques can be employed as can nanomaterials so that Raman signals are further enhanced.

Continued development of instrumentation and data analysis procedures will lead to improvements in the identification, detectability and understanding of uranium species using vibrational spectroscopy. These tools will provide more robust methods for the detection of uranium in the environment, provide new opportunities for nuclear forensics applications, and provide a better understanding of separations processes. The development of these techniques for uranium can also then be translated to other actinides (Np, Pu, Am) that are relevant within the nuclear fuel cycle. A detailed evaluation of how the spectral bands change along the 5f-series can also provide additional information on electronic structure and bonding within this complex family of elements.

Acknowledgments

Funding sources

T.Z.F. acknowledges support from the U.S. Department of Energy, Basic Energy Sciences, Heavy Elements Chemistry Division grant (DE-SC0013980) regarding the sections associated with the solid-state uranium compounds and minerals. A. J. H. was supported by the National Institute of Environmental Health Sciences of the U.S. National Institutes of Health under award number R01ES027145.

References

- [1]. Lide DR, in: CRC Handbook of Chemistry and Physics, Taylor & Francis Group, Boca Raton, FL, 2008.
- [2]. Choppin G, Liljenzin J-O, Rydberg J, Ekberg C, Radiochemistry and Nuclear Chemistry, fourth ed., Academic Press, Oxford, 2013.
- [3]. Bruno J, Ewing RC, Elements 2 (2006) 343–349.
- [4]. Macfarlane AM, Ewing RC, in: Uncertainty Underground, MIT Press, Cambridge, MA, 2006.
- [5]. Abdelouas A, Elements 2 (2006) 335–341.
- [6]. Morss LR, Edelstein N, Fuger J, Katz JJ, in: The Chemistry of the Actinide and Transactinide Elements, Springer-Verlag Publishing, Berlin, Germany, 2011.
- [7]. Shvareva TY, Fein JB, Navrotsky A, Ind. Eng. Chem. Res 51 (2012) 607–613.
- [8]. Murphy WM, Shock EL, Environmental aqueous geochemistry of actinides, in: Burns PC, Finch R (Eds.), Uranium: Mineralogy, Geochemistry and the Environment, The Mineralogical Society of America, Washington DC, 1999, pp. 221–254.
- [9]. Meek T, Hu M, Haire MJ, in: Waste Magement 2001 Symposium, Tucson, AZ, 2000.
- [10]. Aksenov VL, Frauenheim T, Sikora V, Magnetic structure and lattice deformation in UO₂, in: Geuertin RP, Suski W, Zolnierok Z (Eds.), Crystalline Electric Field Effects in f-Electron Magnetism, Springer, Boston, MA, 1982, pp. 525–531.
- [11]. Dai S, Burleigh MC, Haire MJ, Myer E, Zhang Z, Konduru MV, Overbury SH, in: Waste Management 2001 Symposium, Tucson, AZ, 2000.
- [12]. Burns PC, Can. Mineral 43 (2005) 1839–1894.
- [13]. Elless MP, Lee SY, Water Air, Soil Pollut 107 (1998) 147–162.
- [14]. Nguyen-Trung C, Begun GM, Palmer DA, Inorg. Chem 31 (1992) 5280–5287.
- [15]. Sadergaski LR, Stoxen W, Hixon AE, Environ. Sci. Technol 52 (2018) 3304–3311. [PubMed: 29436227]

- [16]. Basile M, Unruh DK, Gojdas K, Flores E, Streicher L, Forbes TZ, Chem. Commun 51 (2015) 5306–5309.
- [17]. Priyadarshini N, Sampath M, Kumar S, Mudali UK, Natarajan R, J. Radioanal. Nucl. Chem 298 (2013) 1923–1931.
- [18]. Denecke MA, Coord. Chem. Rev 250 (2006) 730–754.
- [19]. Gorman-Lewis D, Skanthakumar S, Jensen MP, Mekki S, Nagy KL, Soderholm L, Chem. Geol 253 (2008) 136–140.
- [20]. Kanematsu M, Perdrial N, Um W, Chorover J, O'Day PA, Environ. Sci. Technol 48 (2014) 6097–6106. [PubMed: 24754743]
- [21]. Geckeis H, Lutzenkirchen J, Polly R, Rabung T, Schmidt M, Chem. Rev 113 (2013) 1016–1062. [PubMed: 23363455]
- [22]. Renshaw JC, Butchins LJC, Livens FR, May I, Charnock JM, Lloyd JR, Environ. Sci. Technol 39 (2005) 5657–5660. [PubMed: 16124300]
- [23]. Ilton ES, Haiduc A, Cahill CL, Felmy AR, Inorg. Chem 44 (2005) 2986–2988. [PubMed: 15847396]
- [24]. Ilton ES, Boily JF, Buck EC, Skomurski FN, Rosso KM, Cahill CL, Bargar JR, Felmy AR, Environ. Sci. Technol 44 (2010) 170–176. [PubMed: 20039748]
- [25]. Boland DD, Collins RN, Payne TE, Waite TD, Environ. Sci. Technol 45 (2011) 1327–1333. [PubMed: 21210678]
- [26]. Nico PS, Stewart BD, Fendorf S, Environ. Sci. Technol 43 (2009) 7391–7396. [PubMed: 19848151]
- [27]. Jia G, Belli M, Sansone U, Rosamilia S, Ocone R, Gaudino S, J. Radioanal. Nucl. Chem 253 (2002) 395–406.
- [28]. Klug HP, Alexander LE, X-ray Diffraction Procedures: For polycrystalline and amorphous materials, John Wiley & Sons Inc, New York, 1974.
- [29]. Clegg W, Crystal Structure Determination, Oxford University Press, Oxford, 1998.
- [30]. Shi WQ, Yuan LY, Wang CZ, Wang L, Mei L, Xiao CL, Zhang L, Li ZJ, Zhao YL, Chai ZF, Adv. Mater 26 (2014) 7807–7848. [PubMed: 25169914]
- [31]. De Laeter J, Mass Spectrom. Rev 29 (2010) 845–859. [PubMed: 19877268]
- [32]. Santos JS, Teixeira LSG, dos Santos WNL, Lemos VA, Godoy JM, Ferreira SLC, Anal. Chim. Acta 674 (2010) 143–156. [PubMed: 20678624]
- [33]. Whitkop PG, Anal. Chem 54 (1982) 2475–2477.
- [34]. Geipel G, Coord. Chem. Rev 250 (2006) 844–854.
- [35]. Natrajan L, Coord. Chem. Rev 256 (2012) 1583–1603.
- [36]. Drot R, Roques J, Simoni E, Comptes Rendus Chimie 10 (2007) 1078–1091.
- [37]. Den Auwer C, Simoni E, Conradson S, Madic C, Eur. J. Inorg. Chem (2003) 3843–3859.
- [38]. Szabo Z, Toraishi T, Vallet V, Grenthe I, Coord. Chem. Rev 250 (2006) 784–815.
- [39]. Cejka J, Infrared spectroscopy and thermal analysis of the uranyl minerals, in: Burns PC, Finch RJ (Eds.), Uranium: Mineralogy, Geochemistry, and the Environment, Mineralogical Society of America, Washington D.C., 1999, pp. 521–622.
- [40]. Stuart B, Kirk-Othmer Encyclopedia of Chemical Technology, John Wiley and Sons, New York, 2015.
- [41]. Kiefer W, Buback M, Hoffmann GG, Korte E-H, Roseler A, Lentz E, Gerwert K, Leipertz A, Spiekermann M, Special techniques and applications, in: Schrader B (Ed.), Infrared and Raman Spectroscopy: Methods and applications, John Wiley and Sons, New York, 1995, pp. 465–694.
- [42]. Nitsche H, J. Alloys Compd 223 (1995) 274–279.
- [43]. Sutton SR, Rivers ML, Bajt S, Jones K, Smith JV, Nucl. Instrum. Methods Phys. Res., Sect. A 347 (1994) 412–416.
- [44]. Bernhard G, Geipel G, Adv. Trace Anal (2010) 127–147.
- [45]. Arnold T, Grossmann K, Baumann N, Anal. Bioanal. Chem 396 (2010) 1641–1653. [PubMed: 20091156]
- [46]. Meinrath G, J. Radioanal. Nucl. Chem 224 (1997) 119–126.

- [47]. Wang D, van Gunsteren WF, Chai Z, Chem. Soc. Rev 41 (2012) 5836–5865. [PubMed: 22777520]
- [48]. Lu G, Forbes TZ, Haes AJ, Anal. Chem 88 (2016) 773–780. [PubMed: 26607279]
- [49]. Elorrieta JM, Bonales LJ, Rodriguez-Villagra N, Baonza VG, Cobos J, PCCP 18 (2016) 28209–28216. [PubMed: 27722274]
- [50]. Desgranges L, Baldinozzi G, Simon P, Guimbretiere G, Canizares A, J. Raman Spectro 43 (2012) 455–458.
- [51]. Aoyagi N, Watanabe M, Kirishima A, Sato N, Kimura T, J. Radioanal. Nucl. Chem 303 (2015) 1095–1098.
- [52]. Lu E, Cooper OJ, McMaster J, Tuna F, McInnes EJJ, Lewis W, Blake AJ, Liddle ST, Angew. Chem.-Int. Ed 53 (2014) 6696–6700.
- [53]. Hayton TW, Dalton Trans 47 (2018).
- [54]. Di Pietro P, Kerridge A, Inorg. Chem 55 (2016) 573–583. [PubMed: 26700790]
- [55]. Tsushima S, Dalton Trans 40 (2011) 6732–6737. [PubMed: 21611649]
- [56]. Toth LM, Begun GM, J. Phys. Chem 85 (1981) 547–549.
- [57]. Khulbe PK, Tripathi R, Bist HD, J. Phys. Chem. Solids 53 (1992) 639–650.
- [58]. Faulques E, Russo RE, Perry DL, Spectrochim. Acta A-Mol. Biomol. Spectro 50 (1994) 757–763.
- [59]. Irish DE, Walrafen GE, J. Chem. Phys 46 (1967) 378–384.
- [60]. Graves CR, Kiplinger JL, Chem. Commun 2009 (2009) 3831–3853.
- [61]. Arnold PL, Love JB, Patel D, Coord. Chem. Rev 253 (2009) 1973–1978.
- [62]. Conn GKT, Wu CK, Trans. Faraday Soc 34 (1938) 1483–1491.
- [63]. Bartlett JR, Cooney RP, J. Mol. Struct 193 (1989) 295–300.
- [64]. Finch R, Ewing RC, J. Nucl. Mater 190 (1992) 133–156.
- [65]. Kim J-G, Park Y-S, Ha Y-K, Song K, J. Nucl. Sci. Tech 46 (2009) 1188–1192.
- [66]. Traboulsi A, Vandenborre J, Blain G, Humbert B, Haddad F, Fattahi M, J. Nucl. Mater 467 (2015) 832–839.
- [67]. Senanayake SD, Rousseau R, Colegrave D, Idriss H, J. Nucl. Mater 342 (2005) 179–187.
- [68]. Maslova OA, Guimbretiere G, Ammar MR, Desgranges L, Jegou C, Canizares A, Simon P, Mater. Charact 129 (2017) 260–269.
- [69]. Livneh T, Sterer E, Phys. Rev. B 73 (2006) 095118.
- [70]. Rousseau G, Degranges L, Charlot F, Millot N, Niepce JC, Pijolat J, Faldivieso F, Baldinozzi G, Berar JF, J. Nucl. Mater 355 (2006) 10–20.
- [71]. Bonales LJ, Elorrieta JM, Menor-Salvan C, Cobos J, MRS Adv 1 (2016) 4157–4162.
- [72]. He HM, Shoesmith D, PCCP 12 (2010) 8108–8117. [PubMed: 20532290]
- [73]. Butler IS, Allen GC, Tuan NA, Appl. Spectrosc 42 (1988) 901.
- [74]. Palacios ML, Taylor SH, Appl. Spectrosc 53 (2000) 1665.
- [75]. Manara D, Renker B, J. Nucl. Mater 321 (2003) 233–237.
- [76]. Canizares A, Guimbretiere G, Tobon YA, Raimboux N, Omnee R, Perdicakis M, Muzeau B, Leoni E, Alam MS, Mendes E, Simon D, Matzen G, Corbel C, Barthe MF, Simon P, J. Raman Spectrosc 43 (2012) 1492–1497.
- [77]. Guimbretiere G, Desgranges L, Jegou C, Canizares A, Simon P, Caraballo R, Raimboux N, Barthe MF, Ammar MR, Maslova OA, Duval F, Omnee R, IEEE Trans. Nucl. Sci 61 (2014) 2045–2051.
- [78]. Brincat NA, Parker SC, Molinari M, Allen GC, Storr MT, Inorg. Chem 53 (2014) 12253–12264. [PubMed: 25405569]
- [79]. Sweet LE, Blake TA, Henager CH, Hu SY, Johnson TJ, Meier DE, Peper SM, Schwantes JM, J. Radioanal. Nucl. Chem 296 (2013) 105–110.
- [80]. Loopstra BO, Taylor JC, Waugh AB, J. Solid State Chem 20 (1977) 9–19.
- [81]. Janov J, Vilkaitis VK, Alfredson PG, J. Nucl. Mater 44 (1972), 161–+.

- [82]. Berlizov A, Ho DML, Nicholl A, Fanghanel T, Mayer K, J. Radioanal. Nucl. Chem 307 (2016) 285–295.
- [83]. Stuart WI, Miller DJ, J. Inorg. Nucl. Chem 35 (1973) 2109–2111.
- [84]. Galuskin EV, Armbruster T, Galuskin IO, Lazic B, Winiarski A, Gazeev VM, Dzierzanowski P, Zadov AE, Pertsev NN, Wrzalik R, Gurbanov AG, Janeczek J, Am. Mineral 96 (2011) 188–196.
- [85]. Finch R, Murakami T, Systematics and paragenesis of uranium minerals, in: Burns PC, Finch R (Eds.), Uranium: Mineralogy, Geochemistry and the Environment, Mineralogical Society of America, Washington DC, 1999, pp. 91–166.
- [86]. Frost RL, Cejka J, Weier ML, J. Raman Spectrosc. 38 (2007) 460–466.
- [87]. Biswas S, Steudtner R, Schmidt M, McKenna C, Vintro LL, Twamley B, Baker RJ, Dalton Trans 45 (2016) 6383–6393. [PubMed: 27028717]
- [88]. Frost RL, Cejka J, Ayoko GA, Weier ML, Polyhedron 26 (2007) 3724–3730.
- [89]. Botto IL, Barone VL, Sanchez MA, J. Mater. Sci 37 (2002) 177–183.
- [90]. Li YP, Burns PC, Can. Mineral 38 (2000) 727–735.
- [91]. Rosenzweig A, Ryan RR, Cryst. Struct. Comm 6 (1977) 53–56.
- [92]. Armstrong CR, Nyman M, Shvareva T, Sigmon GE, Burns PC, Navrotsky A, Proc. Natl. Acad. Sci. U.S.A 109 (2012) 1874–1877. [PubMed: 22308442]
- [93]. Hanson B, McNamara B, Buck E, Friese J, Jenson E, Krupka K, Arey B, Radiochim. Acta 93 (2005) 159–168.
- [94]. Burns PC, Hughes KA, Am. Mineral 88 (2003) 1165–1168.
- [95]. Mallon C, Walshe A, Forster RJ, Keyes TE, Baker RJ, Inorg. Chem 51 (2012) 8509–8515. [PubMed: 22813353]
- [96]. Sundin S, Dahlgren B, Roth O, Jonsson M, J. Nucl. Mater 443 (2013) 291–297.
- [97]. Magnin M, Jegou C, Caraballo R, Broudic V, Tribet M, Peugeot S, Talip Z, J. Nucl. Mater 462 (2015) 230–241.
- [98]. Zachariasen WH, Acta Crystallogr 7 (1954) 795.
- [99]. Atoji M, McDermott MJ, Acta Cryst. B-Struct. Cryst. Cryst. Chem., B 26 (1970) 1540–.
- [100]. Kirkegaard MC, Langford J, Steill J, Anderson B, Miskowicz A, J. Chem. Phys 146 (2017).
- [101]. Bullock JI, J. Chem. Soc. A Inorg. Phys. Theor (1969) 781–1000.
- [102]. Taylor JC, Wilson PW, Acta Cryst. B Struct. Cryst. Cryst. Chem 30 (1974) 169–175.
- [103]. Baker RJ, Coord. Chem. Rev 266 (2014) 123–136.
- [104]. Reynolds JG, Cooke GA, Page JS, Warrant RW, J. Radioanal. Nucl. Chem 316 (2018) 289–299.
- [105]. Locock AJ, Burns PC, Duke MJM, Flynn TM, Can. Mineral 42 (2004) 973–996.
- [106]. Locock AJ, Burns PC, Flynn TM, Can. Mineral 42 (2004) 1699–1718.
- [107]. Demartin F, Diella V, Donzelli S, Gramaccioli CM, Pilati T, Acta Crystallogr., B 47 (1991) 439–446.
- [108]. Faulques E, Kalashnyk N, Massuyeau F, Perry DL, RSC Adv 5 (2015) 71219–71227.
- [109]. Driscoll RJP, Wolverson D, Mitchels JM, Skelton JM, Parker SC, Molinari M, Khan I, Geeson D, Allen GC, RSC Adv 4 (2014) 59137–59149.
- [110]. Frost RL, Weier ML, Martens WN, Klopprogge JT, Kristof J, J. Raman Spectros 36 (2005) 797–805.
- [111]. Dal Bo F, Hatert F, Mees F, Philippo S, Baijot M, Fontaine F, Eur. J. Mineral 28 (2016) 663–675.
- [112]. Locock AJ, Burns PC, Can. Mineral 41 (2003) 489–502.
- [113]. Lafuente B, Downs RT, Yang H, Sone N, The power of databases: the RRUFF project, in: Armbruster T, Danisi RM (Eds.), Highlights in Mineralogical Crystallography, W. De Gruyter, Berlin, Germany, 2015, pp. 1–30.
- [114]. Locock AJ, Burns PC, Am. Mineral 88 (2003) 240–244.
- [115]. Frost RL, Cejka J, Ayoko G, J. Raman Spectros 39 (2008) 495–502.
- [116]. Tecmer P, Hong SW, Boguslawski K, PCCP 18 (2016) 18305–18311. [PubMed: 27335229]
- [117]. Balboni E, Burns PC, J. Solid State Chem 213 (2014) 1–8.

- [118]. Xiao B, Schlenz H, Dellen J, Bosbach D, Suleimanov EV, Alekseev EV, *Cryst. Growth Des* 15 (2015) 3775–3784.
- [119]. Nguyen QB, Chen CL, Chiang YW, Lii KH, *Inorg. Chem* 51 (2012) 3879–3882. [PubMed: 22390822]
- [120]. Belai N, Frisch M, Ilton ES, Ravel B, Cahill CL, *Inorg. Chem* 47 (2008) 10135–10140. [PubMed: 18842038]
- [121]. Chen CS, Lee SF, Lii KH, *J. Am. Chem. Soc* 127 (2005) 12208–12209. [PubMed: 16131183]
- [122]. Lin CH, Chen CS, Shiryaev AA, Zubavichus YV, Lii KH, *Inorg. Chem* 47 (2008) 4445–4447. [PubMed: 18447328]
- [123]. Hawthorne FC, Finch RJ, Ewing RC, *Can. Mineral* 44 (2006) 1379–1385.
- [124]. Frost RL, Henry DA, Erickson K, *J. Raman Spectros* 35 (2004) 255–260.
- [125]. Schnaars DD, Wilson RE, *Inorg. Chem* 53 (2014) 11036–11045. [PubMed: 25299307]
- [126]. Qu F, Zhu QQ, Liu CL, *Cryst. Growth Des* 14 (2014) 6421–6432.
- [127]. Ohwada K, Fujisawa G, *Spectrochim. Acta A-Mol. Biomol. Spectros* 51 (1995) 309–318.
- [128]. Caville C, *J. Raman Spectros* 6 (1977) 235–237.
- [129]. Khulbe PK, Agarwal A, Raghuvanshi GS, Bist HD, Hashimoto H, Kitagawa T, Little TS, Durig JR, *J. Raman Spectros* 20 (1989) 283–290.
- [130]. Wahu S, Berthet JC, Thuery P, Guillaumont D, Ephritikhine M, Guillot R, Cote G, Bresson C, *Eur. J. Inorg. Chem* (2012) 3747–3763.
- [131]. Knope KE, Soderholm L, *Chem. Rev* 113 (2013) 944–994. [PubMed: 23101477]
- [132]. Nguyen-Trung C, Palmer DA, Begun GM, Peiffert C, Mesmer RE, *J. Solution Chem* 29 (2000) 101–129.
- [133]. Unruh DK, Gojdas K, Flores E, Libo A, Forbes TZ, *Inorg. Chem* 52 (2013) 10191–10198. [PubMed: 23957694]
- [134]. Zhang YJ, Bhadbhade M, Karatchevtseva I, Price JR, Liu H, Zhang ZM, Kong LG, Cejka J, Lu K, Lumpkin GR, *J. Solid State Chem* 226 (2015) 42–49.
- [135]. Zhang YJ, Clegg JK, Lu K, Lumpkin GR, Tran TT, Aharonovich I, Scales N, Li F, *Chemistryselect* 1 (2016) 7–12.
- [136]. Zhang YJ, Karatchevtseva I, Bhadbhade M, Tran TT, Aharonovich I, Fanna DJ, Shepherd ND, Lu K, Li F, Lumpkin GR, *J. Solid State Chem* 234 (2016) 22–28.
- [137]. McGrail BT, Sigmon GE, Jouffret LJ, Andrews CR, Burns PC, *Inorg. Chem* 53 (2014) 1562–1569. [PubMed: 24422479]
- [138]. Dembowski M, Bernales V, Qiu JE, Hickam S, Gaspar G, Gagliardi L, Burns PC, *Inorg. Chem* 56 (2017) 1574–1580. [PubMed: 28075121]
- [139]. Qiu J, Vlasisavljevich B, Jouffret L, Nguyen K, Szymanowski JES, Gagliardi L, Burns PC, *Inorg. Chem* 54 (2015) 4445–4455. [PubMed: 25868048]
- [140]. Falaise C, Nyman M, *Chem. -Eur. J* 22 (2016) 14678–14687. [PubMed: 27539640]
- [141]. Vallet V, Wahlgren U, Grenthe I, *J. Phys. Chem. A* 116 (2012) 12373–12380. [PubMed: 23151258]
- [142]. Roy RS, *J. Phys. B: Atom. Mol. Phys* 1 (1968) 445.
- [143]. Jones LH, *Spectrochim. Acta* (1959) 409–411.
- [144]. Wentink T, Jr., *J. Chem. Phys* 30 (1959) 105–115.
- [145]. McGlynn SP, Smith JK, Neely WC, *J. Chem. Phys* 35 (1961) 105–116.
- [146]. Schnaars DD, Wilson RE, *Inorg. Chem* 52 (2013) 14138–14147. [PubMed: 24256199]
- [147]. de Groot J, Cassell B, Basile M, Fetrow T, Forbes TZ, *Eur. J. Inorg. Chem* (2017) 1938–1946.
- [148]. Bullock JI, *J. Inorg. Nucl. Chem* 29 (1967) 2257–2264.
- [149]. Gál M, Goggin PL, Mink J, *J. Mol. Struct* 114 (1984) 459–462.
- [150]. Bagnall KW, Wakerley MW, *J. Inorg. Nucl. Chem* 37 (1975) 329–330.
- [151]. Maya L, Begun GM, *J. Inorg. Nucl. Chem* 43 (1981) 2827–2832.
- [152]. Nguyen Trung C, Begun GM, Palmer DA, *Inorg. Chem* 31 (1992) 5280–5287.
- [153]. Quilès F, Burneau A, *Vib. Spectrosc* 18 (1998) 61–75.

- [154]. Quilès F, Nguyen-Trung C, Carteret C, Humbert B, *Inorg. Chem* 50 (2011) 2811–2823. [PubMed: 21355568]
- [155]. Quiles F, Burneau A, *Vib. Spectrosc* 23 (2000) 231–241.
- [156]. Bachmaf S, Planer-Friedrich B, Merkel BJ, *Radiochim. Acta* 96 (2008) 359–366.
- [157]. Bernhard G, Geipel G, Brendler V, Nitsche H, *J. Alloys Compd* 271–273 (1998) 201–205.
- [158]. Kumar A, Rout S, Ghosh M, Singhal RK, Ravi PM, *SpringerPlus* 2 (2013) 1–7. [PubMed: 23419944]
- [159]. Rout S, Ravi PM, Kumar A, Tripathi RM, *J. Radioanal. Nucl. Chem* 303 (2015) 2193–2203.
- [160]. Bryan SA, Levitskaia TG, Johnsen AM, Orton CR, Peterson JM, *Radiochim. Acta* 99 (2011) 563–571.
- [161]. Minc S, Kecki Z, *Rocz. Chem* 32 (1958) 1427–1429.
- [162]. Brooker MH, Huang CH, Sylwestrowicz J, *J. Inorg. Nucl. Chem* 42 (1980) 1431–1440.
- [163]. Fujii T, Fujiwara K, Yamana H, Moriyama H, *J. Alloys Compd* 323–324 (2001) 859–863.
- [164]. Tsushima S, Rossberg A, Ikeda A, Mueller K, Scheinost AC, *Inorg. Chem* 46 (2007) 10819–10826. [PubMed: 17994731]
- [165]. Clark DL, Hobart DE, Neu MP, *Chem. Rev* 95 (1995) 25–48.
- [166]. Allen PG, Bucher JJ, Clark DL, Edelstein NM, Ekberg SA, Gohdes JW, Hudson EA, Kaltsoyannis N, Lukens WW, et al., *Inorg. Chem* 34 (1995) 4797–4807.
- [167]. De Jong WA, Apra E, Windus TL, Nichols JA, Harrison RJ, Gutowski KE, Dixon DA, *J. Phys. Chem. A* 109 (2005) 11568–11577. [PubMed: 16354049]
- [168]. Aoyama T, Aida M, Fujii Y, Okamoto M, *J. Phys. Chem* 93 (1989) 2666–2668.
- [169]. Kim KW, Lee KY, Chung DY, Lee EH, Moon JK, Shin DW, *J. Hazard. Mater* 233 (2012) 213–218. [PubMed: 22831997]
- [170]. Sunder S, Miller NH, Shoesmith DW, *Corros. Sci* 46 (2004) 1095–1111.
- [171]. Kim K-W, Jung E-C, Lee K-Y, Cho H-R, Lee E-H, Chung D-Y, *J. Phys. Chem. A* 116 (2012) 12024–12031. [PubMed: 23181400]
- [172]. Dargent M, Dubessy J, Truche L, Bazarkina EF, Nguyen-Trung C, Robert P, *Eur. J. Mineral* 25 (2013) 765–775.
- [173]. Burns PC, Nyman M, *Dalton Trans* (2018).
- [174]. Miro P, Vlasisavljevich B, Gil A, Burns PC, Nyman M, Bo C, *Chem. Eur. J* 22 (2016) 8571–8578. [PubMed: 27165671]
- [175]. Qiu J, Dembowski M, Szymanowski JES, Toh WC, Burns PC, *Inorg. Chem* 55 (2016) 7061–7067. [PubMed: 27355615]
- [176]. Qiu J, Dong SN, Szymanowski JES, Dobrowolska M, Burns PC, *Inorg. Chem* 56 (2017) 3738–3741. [PubMed: 28332833]
- [177]. Qiu J, Spano TL, Dembowski M, Kokot AM, Szymanowski JES, Burns PC, *Inorg. Chem* 56 (2017) 1874–1880. [PubMed: 28134511]
- [178]. Dembowski M, Colla CA, Yu P, Qiu J, Szymanowski JES, Casey WH, Burns PC, *Inorg. Chem* 56 (2017) 9602–9608. [PubMed: 28783329]
- [179]. Nipruk OV, Chernorukov NG, Pykhova YP, Godovanova NS, Eremina AA, *Radiochemistry* 53 (2011) 483–490.
- [180]. Hala J, Miyamoto H, *J. Phys. Chem. Ref. Data* 36 (2007) 1417–1736.
- [181]. Burneau A, Tazi M, Bouzat G, *Talanta* 39 (1992) 743–748. [PubMed: 18965445]
- [182]. Vercouter T, Vitorge P, Amekraz B, Moulin C, *Inorg. Chem* 47 (2008) 2180–2189. [PubMed: 18278865]
- [183]. Gál M, Goggin PL, Mink J, *Spectrochim. Acta A: Mol. Spectrosc* 48 (1992) 121–132.
- [184]. Hennig C, Schmeide K, Brendler V, Moll H, Tsushima S, Scheinost AC, *AIP Conf. Proc* 882 (2007) 262–264.
- [185]. Lucks C, Rossberg A, Tsushima S, Foerstendorf H, Scheinost AC, Bernhard G, *Inorg. Chem* 51 (2012) 12288–12300. [PubMed: 23110741]
- [186]. Pasilis SP, Pemberton JE, *Inorg. Chem* 42 (2003) 6793–6800. [PubMed: 14552631]

- [187]. Kakihana M, Nagumo T, Okamoto M, Kakihana H, J. Phys. Chem 91 (1987) 6128–6136.
- [188]. Basile M, Unruh DK, Flores E, Johns A, Forbes TZ, Dalton Trans 44 (2015) 2597–2605. [PubMed: 25372632]
- [189]. Rawat N, Bhattacharyya A, Tomar BS, Ghanty TK, Manchanda VK, Thermochim. Acta 518 (2011) 111–118.
- [190]. Crea F, Foti C, Sammartano S, Talanta 75 (2008) 775–785. [PubMed: 18585146]
- [191]. Berto S, Crea F, Daniele PG, De Stefano C, Prenesti E, Sammartano S, Anal. Chim 96 (2006) 399–420.
- [192]. Ramamoorthy S, Balakrishnan MS, Santappa M, J. Inorg. Nucl. Chem 33 (1971) 2713–2716.
- [193]. Ebbs SD, Brady DJ, Kochian LV, J. Exp. Bot 49 (1998) 1183–1190.
- [194]. Dodge CJ, Francis AJ, Radiochim. Acta 91 (2003) 525–532.
- [195]. Nunes MT, Gil VMS, Inorg. Chim. Acta 129 (1987) 283–287.
- [196]. Yang Y, Saiers JE, Xu N, Minasian SG, Tyliczszak T, Kozimor SA, Shuh DK, Barnett MO, Environ. Sci. Technol 46 (2012) 5931–5938. [PubMed: 22533547]
- [197]. Steudtner R, Muller K, Schmeide K, Sachs S, Bernhard G, Dalton Trans 40 (2011).
- [198]. Pasilis SP, Blumenfeld A, Inorg. Chem 50 (2011) 8302–8307. [PubMed: 21786806]
- [199]. Hopkins TA, Berg JM, Costa DA, Smith WH, Dewey HJ, Inorg. Chem 40 (2001) 1820–1825. [PubMed: 11312737]
- [200]. Flint CD, Tanner PA, J. Chem. Soc., Faraday Trans 2 (74) (1978) 2210–2217.
- [201]. Krishna GM, Suneesh AS, Kumaresan R, Venkatesan KA, Antony MP, J. Electroanal. Chem 795 (2017) 51–58.
- [202]. Krishna GM, Suneesh AS, Kumaresan R, Venkatesan KA, Antony MP, Chemistryselect 2 (2017) 8706–8715.
- [203]. Crandall HW, J. Chem. Phys 17 (1949) 602–606.
- [204]. Mizuoka K, Ikeda Y, Prog. Nucl. Energy 47 (2005) 426–433.
- [205]. Kelley SP, Rogers RD, Inorg. Chem 54 (2015) 10323–10334. [PubMed: 26479078]
- [206]. Jeowska-Trzebiatowska B, Chmielowska M, J. Inorg. Nucl. Chem 20 (1961) 106–116.
- [207]. Volod'ko LV, Sevchenko AN, Turetskaya EA, J. Appl. Spectros 6 (1967) 250–252.
- [208]. Yu SJ, Wang XX, Tan XL, Wang XK, Inorg. Chem. Front 2 (2015) 593–612.
- [209]. Cumberland SA, Douglas G, Grice K, Moreau JW, Earth-Sci. Rev 159 (2016) 160–185.
- [210]. Miller AW, Rodriguez DR, Honeyman BD, Environ. Sci. Technol 44 (2010) 7996–8007. [PubMed: 20942399]
- [211]. Rosenberg E, Pinson G, Tsosie R, Tutu H, Cukrowska E, Johnson Matthey Technol. Rev 60 (2016) 59–77.
- [212]. Mckinley JP, Zachara JM, Smith SC, Turner GD, Clay Clay Miner 43 (1995) 586–598.
- [213]. Waite TD, Davis JA, Payne TE, Waychunas GA, Xu N, Geochim. Cosmochim. Acta 58 (1994) 5465–5478.
- [214]. Ho CH, Miller NH, J. Colloid Interface Sci 110 (1986) 165–171.
- [215]. Lomenech C, Simoni E, Drot R, Ehrhardt JJ, Mielczarski J, J. Colloid Interface Sci 261 (2003) 221–232. [PubMed: 16256526]
- [216]. Baghdadi S, Bouvier-Capely C, Ritt A, Peroux A, Fevrier L, Rebiere F, Agarande M, Cote G, Talanta 144 (2015) 875–882. [PubMed: 26452903]
- [217]. Bargar JR, Reitmeyer R, Davis JA, Environ. Sci. Technol 33 (1999) 2481–2484.
- [218]. Lefèvre G, Noinville S, Fédoroff M, J. Colloid Interface Sci 296 (2006) 608–613. [PubMed: 16203012]
- [219]. Liger E, Charlet L, Van Cappellen P, Geochim. Cosmochim. Acta 63 (1999) 2939–2955.
- [220]. Foerstendorf H, Jordan N, Heim K, J. Colloid Interface Sci 416 (2014) 133–138. [PubMed: 24370412]
- [221]. Foerstendorf H, Heim K, Rossberg A, J. Colloid Interface Sci 377 (2012) 299–306. [PubMed: 22498368]

- [222]. Wazne M, Korfiatis GP, Meng X, Environ. Sci. Technol 37 (2003) 3619–3624. [PubMed: 12953874]
- [223]. Morris DE, Chisholm-Brause CJ, Barr ME, Conradson SD, Eller PG, Geochim. Cosmochim. Acta 58 (1994) 3613–3623.
- [224]. Maya L, Radiochim. Acta 31 (1982) 147–151.
- [225]. Guckel K, Rossberg A, Brendler V, Foerstendorf H, Chem. Geol 326 (2012) 27–35.
- [226]. Muller K, Foerstendorf H, Brendler V, Rossberg A, Stolze K, Groschel A, Chem. Geol 357 (2013) 75–84.
- [227]. Ho CH, Doern DC, Can. J. Chem 63 (1985) 1100–1104.
- [228]. Li D, Kaplan DI, J. Hazard. Mater 243 (2012) 1–18. [PubMed: 23141377]
- [229]. Choppin G, J. Radioanal. Nucl. Chem 273 (2007) 695–703.
- [230]. Comarmond MJ, Steudtner R, Stockmann M, Heim K, Müller K, Brendler V, Payne TE, Foerstendorf H, Environ. Sci. Technol 50 (2016) 11610–11618. [PubMed: 27754663]
- [231]. Jackson VE, Gutowski KE, Dixon DA, J. Phys. Chem. A 117 (2013) 8939–8957. [PubMed: 23905705]
- [232]. Wersin P, Hochella MF, Persson P, Redden G, Leckie JO, Harris DW, Geochim. Cosmochim. Acta 58 (1994) 2829–2843.
- [233]. Bonales LJ, Menor-Salvan C, Cobos J, J. Nucl. Mater 462 (2015) 296–303.
- [234]. Schmeide K, Gurtler S, Muller K, Steudtner R, Joseph C, Bok F, Brendler V, Appl. Geochem 49 (2014) 116–125.
- [235]. Traboulsi A, Vandenborre J, Blain G, Humbert B, Barbet J, Fattahi M, J. Phys. Chem. C 118 (2014) 1071–1080.
- [236]. Hirotsu T, Takagi N, Sakane K, Katoh S, Sugasaka K, Shikoku Kogyo Gijutsu Shikensho Kenkyu Hokoku (1988) 49–71.
- [237]. Tsushima S, Nagasaki S, Tanaka S, Suzuki A, J. Phys. Chem. B 102 (1998) 9029–9032.
- [238]. Jaffrezic-Renault N, Andrade-Martins H, J. Radioanal. Chem 55 (1980) 307–316.
- [239]. Huynh J, Palacio R, Safizadeh F, Lefevre G, Descostes M, Eloy L, Guignard N, Rousseau J, Royer S, Tertre E, Batonneau-Gener I, ACS Appl. Mater. Interfaces 9 (2017) 15672–15684. [PubMed: 28406007]
- [240]. Abney CW, Mayes RT, Piechowicz M, Lin Z, Bryantsev VS, Veith GM, Dai S, Lin W, Energy Environ. Sci 9 (2016) 448–453.
- [241]. Zhang L, Zhou J, Zhang J, Su J, Zhang S, Chen N, Jia Y, Li J, Wang Y, Wang J-Q, J. Synch. Rad 23 (2016) 758–768.
- [242]. Yang CT, Pei SQ, Chen BH, Ye LN, Yu HZ, Hu S, Dalton Trans 45 (2016) 3120–3129. [PubMed: 26777881]
- [243]. Zhang LJ, Qie MY, Su J, Zhang S, Zhou J, Li J, Wang Y, Yang ST, Wang SA, Li JY, Wu GZ, Wang JQ, J. Synch. Rad 25 (2018) 514–522.
- [244]. Endrizzi F, Melchior A, Tolazzi M, Rao L, Dalton Trans 44 (2015) 13835–13844. [PubMed: 25928044]
- [245]. Guo X, Xiong X-G, Li C, Gong H, Huai P, Hu J, Jin C, Huang L, Wu G, Inorg. Chim. Acta 441 (2016) 117–125.
- [246]. Piechowicz M, Abney CW, Zhou X, Thacker NC, Li Z, Lin W, Ind. Eng. Chem. Res 55 (2016) 4170–4178.
- [247]. Drobot B, Bauer A, Steudtner R, Tsushima S, Bok F, Patzschke M, Raff J, Brendler V, Anal. Chem 88 (2016) 3548–3555. [PubMed: 26977534]
- [248]. Guillaumont R (Ed.), Update on the Chemical Thermodynamics of Uranium, Neptunium, Plutonium, Americium and Technetium, 2003.
- [249]. Fuger J, Lemire RJ, Muller AB, Nguyen-Trung Cregu C, Konings RJM, Wanner H, Grenthe I, Chemical Thermodynamics of Uranium, North Holland, Amsterdam, 1992.
- [250]. Unsworth ER, Jones P, Hill SJ, J. Environ. Mon 4 (2002) 528–532.
- [251]. Ahrland S, Acta Chem. Scand 5 (1951) 199–219.

- [252]. Müller K, Brendler V, Foerstendorf H, *Inorg. Chem* 47 (2008) 10127–10134. [PubMed: 18831578]
- [253]. Kalashnyk N, Perry DL, Massuyeau F, Faulques E, *J. Phys. Chem. C* 122 (2018) 7410–7420.
- [254]. Thomas R, Rivenet M, Berrier E, de Waele I, Arab M, Amaraggi D, Morel B, Abraham F, *J. Nucl. Mater* 483 (2017) 149–157.
- [255]. Shepherd ND, Zhang Y, Karatchevtseva I, Price JR, Kong L, Scales N, Lumpkin GR, *Polyhedron* 113 (2016) 88–95.
- [256]. Ward MD, Klingsporn JM, Ibers JA, *Inorg. Chem* 52 (2013) 10220–10222. [PubMed: 24004070]
- [257]. Cole E, Flores E, Basile M, Jayasinghe A, de Groot J, Unruh DK, Forbes TZ, *Polyhedron* 114 (2016) 378–384.
- [258]. La Pierre HS, Scheurer A, Heinemann FW, Hieringer W, Meyer K, *Angew. Chem. Int. Ed* 53 (2014) 7158–7162.
- [259]. MacDonald MR, Fieser ME, Bates JE, Ziller JW, Furche F, Evans WJ, *J. Am. Chem. Soc* 135 (2013) 13310–13313. [PubMed: 23984753]
- [260]. Ohwada K, Takahashi A, Fujisawa G, *Appl. Spectrosc* 49 (1995) 216–219.
- [261]. Ohwada K, *Spectrochim. Acta A Mol. Biomol. Spectros* 53A (1997) 501–507.
- [262]. Soga T, Ohwada K, *Spectrochim. Acta A Mol. Biomol. Spectros* 55A (1999) 1337–1345.
- [263]. Soga T, *Spectrochim. Acta A Mol. Biomol. Spectros* 57 (2001) 1767–1780.
- [264]. Soga T, *Spectrochim. Acta A Mol. Biomol. Spectros* 56 (2000) 79–89.
- [265]. Radziuk D, Moehwald H, *Nanoscale* 6 (2014) 6115–6126. [PubMed: 24788867]
- [266]. Dai S, Lee Y-H, Young JP, *Appl. Spectrosc* 50 (1996) 536–537.
- [267]. Bao L, Mahurin SM, Haire RG, Dai S, *Anal. Chem* 75 (2003) 6614–6620. [PubMed: 16465717]
- [268]. Ruan C, Luo W, Wang W, Gu B, *Anal. Chim. Acta* 605 (2007) 80–86. [PubMed: 18022414]
- [269]. Lu G, Forbes TZ, Haes AJ, *Analyst* 141 (2016) 5137–5143. [PubMed: 27326897]
- [270]. Teiten B, Burneau A, *J. Raman Spectrosc* 28 (1997) 879–884.
- [271]. Burneau A, Teiten B, *Vib. Spectrosc* 21 (1999) 97–109.
- [272]. Dutta S, Ray C, Sarkar S, Pradhan M, Negishi Y, Pal T, *ACS Appl. Mater. Interfaces* 5 (2013) 8724–8732. [PubMed: 23947790]
- [273]. Frost RL, Dickfos MJ, Cejka J, *J. Raman Spectros* 39 (2008) 1158–1161.
- [274]. Plasil J, Skoda R, Cejka J, Bourgoin V, Boulliard JC, *Eur. J. Mineral* 28 (2016) 959–967.
- [275]. Olds TA, Plasil J, Kampf AR, Skoda R, Burns PC, Cejka J, Bourgoin V, Boulliard JC, *Eur. J. Mineral* 29 (2017) 129–141.
- [276]. Ok KM, O'Hare D, *J. Solid State Chem* 180 (2007) 446–452.
- [277]. Frost RL, Erickson KL, Weier ML, Carmody O, Cejka J, *J. Mol. Struct* 737 (2005) 173–181.
- [278]. Amayri S, Reich T, Arnold T, Geipel G, Bernhard G, *J. Solid State Chem* 178 (2005) 567–577.
- [279]. Cejka J, Sejkora J, Plasil J, Bahfenne S, Palmer SJ, Frost RL, *J. Raman Spectros* 41 (2010) 459–464.
- [280]. Anderson A, Chieh C, Irish DE, Tong JPK, *Can. J. Chem.-Rev. Can. Chim* 58 (1980) 1651–1658.
- [281]. Plasil J, Cejka J, Sejkora J, Skacha P, Golias V, Jarka P, Laufek F, Jehlicka J, Nemeč I, Strnad L, *Mineral. Mag* 74 (2010) 97–110.
- [282]. Frost RL, Cejka J, *J. Raman Spectros* 40 (2009) 1096–1103.
- [283]. Frost RL, Cejka J, *J. Ram. Spectros* 38 (2007) 1488–1493.
- [284]. Kalashnyk N, Perry DL, Massuyeau F, Faulques E, *J. Phys. D-Appl. Phys* 50 (2017) 9.
- [285]. Frost RL, Cejka J, Ayokol GA, Dickfos MJ, *J. Raman Spectros* 38 (2007) 1609–1614.
- [286]. Frost RL, Dickfos MJ, Cejka J, *J. Raman Spectros* 39 (2008) 582–586.
- [287]. Frost RL, Cejka J, Ayoko GA, Dickfos MJ, *J. Raman Spectros* 39 (2008) 374–379.
- [288]. Frost RL, Weier ML, Cejka J, Ayoko GA, *Spectrochim. Acta A-Mol. Biomol. Spectros* 65 (2006) 529–534.
- [289]. Vlcek V, Cejka J, Cisarova I, Golias V, Plasil J, *J. Mol. Struct* 936 (2009) 75–79.

- [290]. Faulques E, Russo RE, Perry DL, Spectrochim. Acta A-Mol. Biomol. Spectros 49 (1993) 975–983.
- [291]. Jouffret LJ, Wylie EM, Burns PC, Anorg Z. Allg. Chem 638 (2012) 1796–1803.
- [292]. Frost RL, Carmody O, Erickson KL, Weier ML, Henry DO, Cejka J, J. Mol. Struct 733 (2005) 203–210.
- [293]. Frost RL, Cejka J, Weier ML, Martens WN, Ayoko GA, J. Raman Spectros 38 (2007) 398–409.
- [294]. Cejka J, Frost RL, Sejkora J, Keeffe EC, J. Raman Spectros 40 (2009) 1464–1468.
- [295]. Frost RL, Cejka J, Bostrom T, Weier M, Martens W, Spectrochim. Acta A-Mol. Biomol. Spectros 67 (2007) 1220–1227.
- [296]. Frost RL, Cejka J, Ayokol GA, Weier ML, J. Raman Spectros 38 (2007) 1311–1319.
- [297]. Frost RL, Erickson KL, Cejka J, Reddy BJ, Spectrochim. Acta A-Mol. Biomol. Spectros 61 (2005) 2702–2707.
- [298]. Frost RL, Plasil J, Cejka J, Sejkora J, Keeffe EC, Bahfenne S, J. Raman Spectros 40 (2009) 1816–1821.
- [299]. Plasil J, Kasatkin AV, Skoda R, Novak M, Kallistova A, Dusek M, Skala R, Fejfarova K, Cejka J, Meisser N, Goethals H, Machovic V, Lapcak L, Mineral. Mag 77 (2013) 429–441.
- [300]. Plasil J, Hauser J, Petricek V, Meisser N, Mills SJ, Skoda R, Fejfarova K, Cejka J, Sejkora J, Hlousek J, Johannet JM, Machovic V, Lapcak L, Mineral. Mag 76 (2012) 2837–2860.
- [301]. Plasil J, Kampf AR, Kasatkin AV, Marty J, Skoda R, Silva S, Cejka J, Mineral. Mag 77 (2013) 2975–2988.
- [302]. Plasil J, Kampf AR, Kasatkin AV, Marty J, J. Geosci 59 (2014) 145–158.
- [303]. Plasil J, Hlousek J, Veselovsky F, Fejfarova K, Dusek M, Skoda R, Novak M, Cejka J, Sejkora J, Ondrus P, Am. Mineral 97 (2012) 447–454.
- [304]. Plasil J, Meisser N, Cejka J, Can. Mineral 54 (2016) 5–20.
- [305]. Kampf AR, Sejkora J, Witzke T, Plasil J, Cejka J, Nash BP, Marty J, J. Geosci 62 (2017) 107–120.
- [306]. Kampf AR, Plasil J, Kasatkin AV, Marty J, Cejka J, Lapcak L, Mineral. Mag 81 (2017) 273–285.
- [307]. Frost RL, Cejka J, Spectrochim. Acta -Mol. Biomol. Spectros 71 (2009) 1959–1963.
- [308]. Frost RL, Weier ML, Reddy BJ, Cejka J, J. Raman Spectros 37 (2006) 816–821.
- [309]. Frost RL, Cejka J, Keeffe EC, Dickfos MJ, J. Raman Spectros 39 (2008) 1413–1418.
- [310]. Frost RL, Cejka J, Scholz R, Lopez A, Theiss FL, Xi YF, Spectrochim. Acta A-Mol. Biomol. Spectrosc 117 (2014) 473–477. [PubMed: 24018173]
- [311]. Frost RL, Cejka J, Dickfos MJ, J. Raman Spectros 40 (2009) 476–480.
- [312]. Frost RL, Cejka J, Dickfos MJ, J. Raman Spectros 40 (2009) 355–359.
- [313]. Plasil J, Dusek M, Novak M, Cejka J, Cisarova I, Skoda R, Am. Mineral 96 (2011) 983–991.
- [314]. Tanner PA, Mak TCW, Inorg. Chem 38 (1999) 6024–6031. [PubMed: 11671309]
- [315]. Clavier N, Cretaz F, Szenknect S, Mesbah A, Poinssot C, Descostes M, Dacheux N, Spectrochim. Acta A-Mol. Biomol. Spectros 156 (2016) 143–150.
- [316]. Yagoubi S, Renard C, Abraham F, Obbade S, J. Solid State Chem 200 (2013) 13–21.
- [317]. Cejka J, Sejkora J, Scholz R, Lopez A, Xi YF, Frost RL, J. Mol. Struct 1068 (2014) 14–19.
- [318]. Cretaz F, Szenknect S, Clavier N, Vitorge P, Mesbah A, Descostes M, Poinssot C, Dacheux N, J. Nucl. Mater 442 (2013) 195–207.
- [319]. Frost RL, Cejka J, Ayoko GA, Weier M, Spectrochim. Acta A-Mol. Biomol. Spectros 66 (2007) 979–984.
- [320]. Frost RL, Cejka J, Weier M, Spectrochim. Acta A-Mol. Biomol. Spectros 65 (2006) 797–801.
- [321]. Frost RL, Cejka J, Weier M, Martens WN, J. Raman Spectros 37 (2006) 879–891.
- [322]. Frost RL, Cejka J, Weier M, Ayoko GA, J. Raman Spectros 37 (2006) 1362–1367.
- [323]. Frost RL, Cejka J, J. Raman Spectros 40 (2009) 591–594.
- [324]. Sejkora J, Cejka J, Hlousek J, Novak M, Srein V, Can. Mineral 42 (2004) 963–972.
- [325]. Armstrong CR, Nash KL, Griffiths PR, Clark SB, Am. Mineral 96 (2011) 417–422.

- [326]. Frost RL, Cejka J, Dickfos MJ, Spectrochim. Acta A-Mol. Biomol. Spectros 71 (2009) 1799–1803.
- [327]. Cejka J, Sejkora J, Frost RL, Keeffe EC, J. Raman Spectros 40 (2009) 1521–1526.
- [328]. Cejka J, Sejkora J, Frost RL, Keeffe EC, J. Raman Spectros 40 (2009) 1786–1790.
- [329]. Yu N, Kegler P, Klepov VV, Dellen J, Schlenz H, Langer EM, Bosbach D, Alekseev EV, Dalton Trans 44 (2015) 20735–20744. [PubMed: 26567703]
- [330]. Plasil J, Sejkora J, Cejka J, Novak M, Vinals J, Ondrus P, Veselovsky F, Skacha P, Jehlicka J, Golias V, Hlousek J, Can. Mineral 48 (2010) 335–350.
- [331]. Frost RL, Weier ML, Cejka J, Klopogge JT, J. Raman Spectros 37 (2006) 585–590.
- [332]. Colmenero F, Bonales LJ, Cobos J, Timon V, J. Solid State Chem 253 (2017) 249–257.
- [333]. Frost RL, Cejka J, Weier ML, Martens W, Klopogge JT, Spectrochim. Acta A-Mol. Biomol. Spectros 64 (2006) 308–315.
- [334]. Frost RL, Cejka J, Weier ML, Martens W, Spectrochim. Acta A-Mol. Biomol. Spectros 63 (2006) 305–312.
- [335]. Lehmann S, Geipel G, Foerstendorf H, Bernhard G, J. Radioanal. Nucl. Chem 275 (2008) 633–642.
- [336]. Frost RL, Cejka J, Weier ML, Martens W, J. Raman Spectros 37 (2006) 538–551.
- [337]. Frost RL, Cejka J, Weier ML, Martens WN, J. Mol. Struct 788 (2006) 115–125.
- [338]. Wall NA, Clark SB, McHale JL, Chem. Geol 274 (2010) 149–157.
- [339]. Ling J, Albrecht-Schmitt TE, Inorg. Chem 46 (2007) 346–347. [PubMed: 17279803]
- [340]. Bray TH, Beitz JV, Bean AC, Yu YQ, Albrecht-Schmitt TE, Inorg. Chem 45 (2006) 8251–8257. [PubMed: 16999424]
- [341]. Sykora RE, Albrecht-Schmitt TE, Inorg. Chem 42 (2003) 2179–2181. [PubMed: 12665344]
- [342]. Sykora RE, McDaniel SM, Wells DM, Albrecht-Schmitt TE, Inorg. Chem 41 (2002) 5126–5132. [PubMed: 12354046]
- [343]. Almond PM, Albrecht-Schmitt TE, Inorg. Chem 41 (2002) 5495–5501. [PubMed: 12377045]
- [344]. Frost RL, Cejka J, Weier M, Ayoko GA, Spectrochim. Acta A-Mol. Biomol. Spectros 65 (2006) 571–574.
- [345]. Frost RL, Cejka J, Dickfos MJ, J. Raman Spectros 40 (2009) 38–41.
- [346]. Gaunt AJ, May I, Copping R, Bhatt AI, Collison D, Fox OD, Holman KT, Pope MT, Dalton Trans (2003) 3009–3014.
- [347]. Frost RL, Cejka J, Weier ML, Martens W, Henry DA, Vib. Spectrosc 39 (2005) 131–138.
- [348]. Plasil J, Veselovsky F, Hlousek J, Skoda R, Novak M, Sejkora J, Cejka J, Skacha P, Kasatkin AV, Am. Mineral 99 (2014) 625–632.
- [349]. Zhang YJ, Bhadbhade M, Price JR, Karatchevtseva I, Kong LG, Scales N, Lumpkin GR, Li F, Polyhedron 92 (2015) 99–104.
- [350]. Bhattacharjee CR, Roy AKD, Polyhedron 16 (1997) 4205–4208.
- [351]. Qiu J, Ling J, Sieradzki C, Nguyen K, Wylie EM, Szymanowski JES, Burns PC, Inorg. Chem 53 (2014) 12084–12091. [PubMed: 25350361]
- [352]. Renier O, Falaise C, Neal H, Kozma K, Nyman M, Angew. Chem.-Int. Ed 55 (2016) 13480–13484.
- [353]. Grant DJ, Weng ZH, Jouffret LJ, Burns PC, Gagliardi L, Inorg. Chem 51 (2012) 7801–7809. [PubMed: 22765850]
- [354]. Danis JA, Lin MR, Scott BL, Eichhorn BW, Runde WH, Inorg. Chem 40 (2001) 3389–3394. [PubMed: 11421684]
- [355]. Shchelokov RN, Tsivadze AY, Orlova IM, Podnebesnova GV, Inorg. Nucl. Chem. Lett 13 (1977) 375–383.
- [356]. Shchelokov RN, Tsivadze AY, Orlova IM, Podnebesnova GV, Inorg. Nucl. Chem. Lett 13 (1977) 367–374.
- [357]. Clark DL, Conradson SD, Donohoe RJ, Keogh DW, Morris DE, Palmer PD, Rogers RD, Tait CD, Inorg. Chem 38 (1999) 1456–1466.
- [358]. Crawford MJ, Mayer P, Inorg. Chem 44 (2005) 8481–8485. [PubMed: 16270987]

- [359]. Koshino N, Harada M, Nogami M, Morita Y, Kikuchi T, Ikeda Y, *Inorg. Chim. Acta* 358 (2005) 1857–1864.
- [360]. Surbella RG, Ducati LC, Autschbach J, Deifel NP, Cahill CL, *Inorg. Chem* 57 (2018) 2455–2471. [PubMed: 29436836]
- [361]. Rowland CE, Kanatzidis MG, Soderholm L, *Inorg. Chem* 51 (2012) (1804) 11798–11801. [PubMed: 23072277]
- [362]. Nuzzo S, Twamley B, Platts JA, Baker RJ, *Inorg. Chem* 57 (2018) 3699–3712. [PubMed: 29542918]
- [363]. Masci B, Thuery P, *Polyhedron* 24 (2005) 229–237.
- [364]. Jayasinghe AS, Payne MK, Forbes TZ, *J. Solid State Chem* 254 (2017) 25–31.
- [365]. Klepov VV, Serezhkina LB, Serezhkin VN, Alekseev EV, *J. Solid State Chem* 244 (2016) 100–107.
- [366]. Carter KP, Kalaj M, Cahill CL, *Eur. J. Inorg. Chem* (2016) 126–137.
- [367]. Zhang YJ, Karatchevtseva I, Price JR, Aharonovich I, Kadi F, Lumpkin GR, Li F, *RSC Adv* 5 (2015) 33249–33253.
- [368]. Basile M, Unruh DK, Streicher L, Forbes TZ, *Cryst. Growth Des* 17 (2017) 5330–5341.
- [369]. Wang LH, Shang R, Zheng Z, Liu CL, Wang ZM, *Cryst. Growth Des* 13 (2013) 2597–2606.
- [370]. Henry N, Lagrenee M, Loiseau T, Clavier N, Dacheux N, Abraham F, *Inorg. Chem. Commun* 14 (2011) 429–432.
- [371]. Kalaj M, Carter KP, Cahill CL, *Acta Cryst. B-Struct. Sci. Cryst. Eng. Mater* 73 (2017) 234–239. [PubMed: 28362287]
- [372]. Carter KP, Kalaj M, Kerridge A, Ridenour JA, Cahill CL, *Inorg. Chem* 57 (2018) 2714–2723. [PubMed: 29436823]
- [373]. Carter KP, Kalaj M, Surbella RG, Ducati LC, Autschbach J, Cahill CL, *Chem.- Eur. J* 23 (2017) 15355–15369. [PubMed: 28707416]
- [374]. Umeda K, Zukerman-Schpector J, Isolani PC, *Polyhedron* 25 (2006) 2447–2451.
- [375]. Tellez-Sara CA, Arissawa M, Gomez-Lara J, Mondragon MA, *Polyhedron* 19 (2000) 2353–2360.
- [376]. Tellez CA, Lara JG, *J. Braz. Chem. Soc* 7 (1996) 505–511.
- [377]. Tellez C, Gomez J, Mondragon MA, Castano VM, Mena G, *Vib. Spectrosc* 9 (1995) 279–285.
- [378]. Tellez C, Lara JG, *Spectrochim. Acta A-Mol. Biomol. Spectros* 51 (1995) 395–404.
- [379]. Tellez CA, Lara JG, *Spectrosc. Lett* 27 (1994) 209–223.
- [380]. Goncalves NS, Deoliveira LFC, Santos PS, *Spectrochim. Acta A-Mol. Biomol. Spectros* 50 (1994) 263–269.
- [381]. Pedrick EA, Schultz JW, Wu G, Mirica LM, Hayton TW, *Inorg. Chem* 55 (2016) 5693–5701. [PubMed: 27177203]
- [382]. Weng ZH, Zhang ZH, Olds T, Sterniczuk M, Burns PC, *Inorg. Chem* 53 (2014) 7993–7998. [PubMed: 25029287]
- [383]. Cantos PM, Jouffret LJ, Wilson RE, Burns PC, Cahill CL, *Inorg. Chem* 52 (2013) 9487–9495. [PubMed: 23909845]
- [384]. Weng ZH, Wang SA, Ling J, Morrison JM, Burns PC, *Inorg. Chem* 51 (2012) 7185–7191. [PubMed: 22686331]
- [385]. Mihalcea I, Henry N, Clavier N, Dacheux N, Loiseau T, *Inorg. Chem* 50 (2011) 6243–6249. [PubMed: 21634393]
- [386]. Alexandropoulos DI, Mazarakioti EC, Corrales SA, Bryant JT, Gasparov LV, Lampropoulos C, Stamatatos TC, *Inorg. Chem. Commun* 78 (2017) 13–16.
- [387]. Bernstein KJ, Do-Thanh CL, Penchoff DA, Cramer SA, Murdock CR, Lu Z, Harrison RJ, Camden JP, Jenkins DM, *Inorg. Chim. Acta* 421 (2014) 374–379.
- [388]. Steinhauser G, Giester G, Wagner C, Weinberger P, Zachhuber B, Ramer G, Villa M, Lendl B, *Inorg. Chem* 51 (2012) 6739–6745. [PubMed: 22651244]
- [389]. Hardwick HC, Royal DS, Helliwell M, Pope SJA, Ashton L, Goodacre R, Sharrad CA, *Dalton Trans* 40 (2011) 5939–5952. [PubMed: 21526261]

- [390]. Nour EM, Alnaimi IS, Alem NA, J. Phys. Chem. Solids 53 (1992) 197–201.
- [391]. Sarsfield MJ, Steele H, Helliwell M, Teat SJ, Dalton Trans (2003) 3443–3449.
- [392]. Burns CJ, Clark DL, Donohoe RJ, Duval PB, Scott BL, Tait CD, Inorg. Chem 39 (2000) 5464–5468. [PubMed: 11154561]
- [393]. Nelson AGD, Rak Z, Abrecht-Schmitt TE, Becker U, Ewing RC, Inorg. Chem 53 (2014) 2787–2796. [PubMed: 24524249]
- [394]. Hao YC, Murphy GL, Bosbach D, Modo G, Albrecht-Schmitt TE, Alekseev EV, Inorg. Chem 56 (2017) 9311–9320. [PubMed: 28718634]
- [395]. Zheng T, Gao Y, Chen LH, Juan DW, Chai ZF, Albrecht-Schmitt TE, Wang S, Inorg. Chim. Acta 435 (2015) 131–136.
- [396]. Zheng T, Gao Y, Chen LH, Liu ZY, Juan DW, Chai ZF, Albrecht-Schmitt TE, Wang S, Dalton Trans 44 (2015) 18158–18166. [PubMed: 26419426]
- [397]. Yu YQ, Zhan W, Albrecht-Schmitt TE, Inorg. Chem 47 (2008) 9050–9054. [PubMed: 18722419]
- [398]. Crawford MJ, Ellern A, Karaghiosoff K, Martin F, Mayer P, Inorg. Chem 49 (2010) 2674–2683. [PubMed: 20141179]
- [399]. John GH, May I, Sarsfield MJ, Steele HM, Collison D, Helliwell M, McKinney JD, Dalton Trans (2004) 734–740. [PubMed: 15252493]

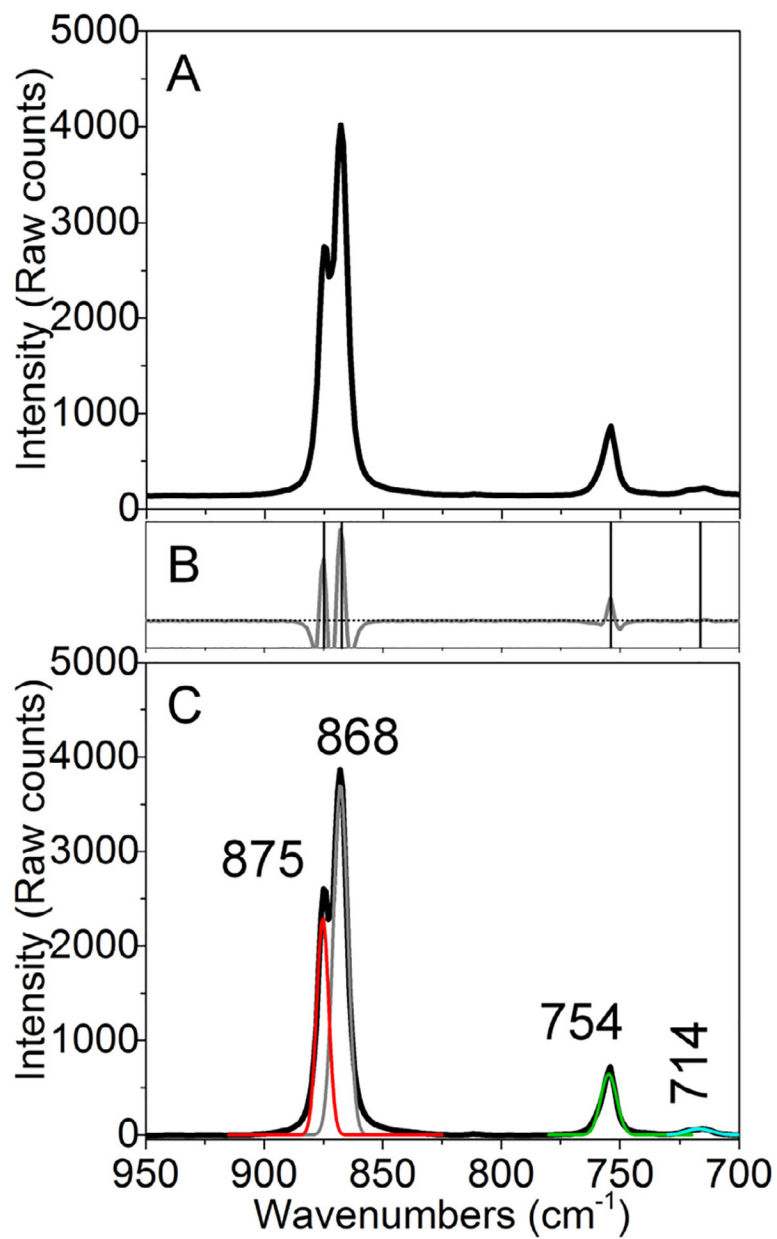


Fig. 2. Raman analysis of the uranyl window for uranyl nitrate (solid) including (A) raw, (B) - second derivative and barcode, and (C) analyzed Raman data.

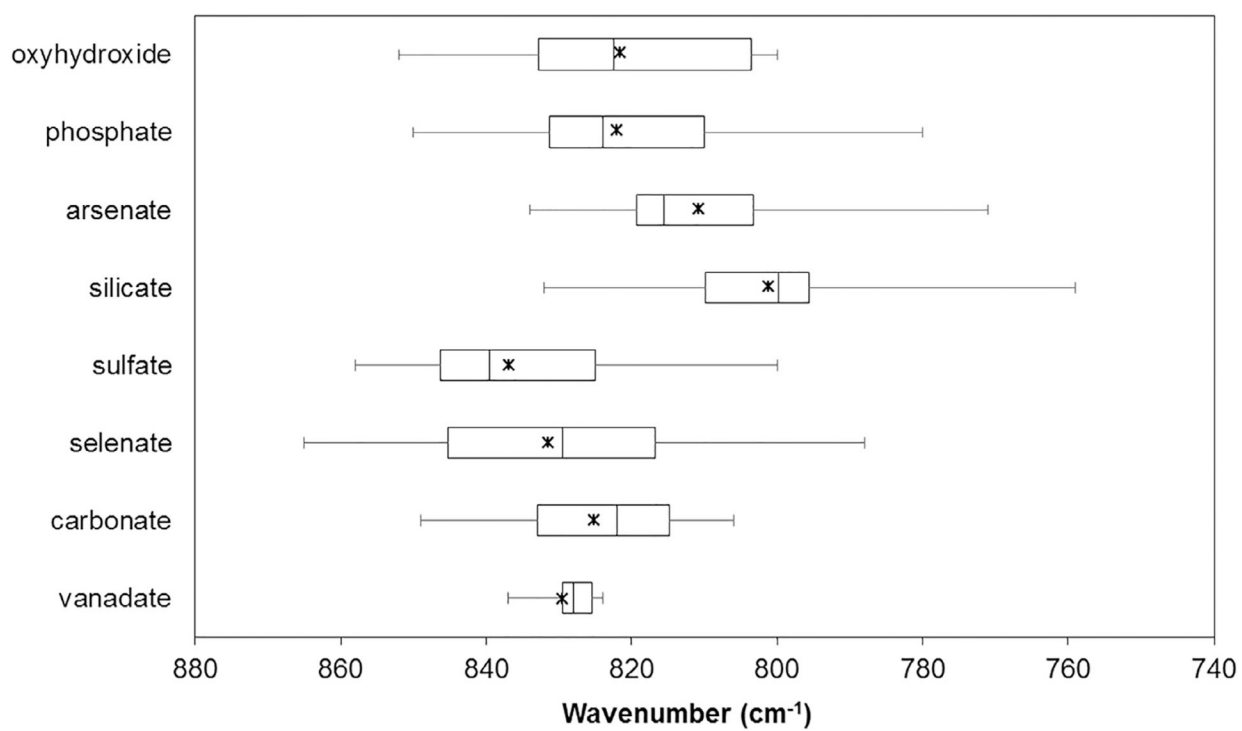


Fig. 3. Box and whisker plot that describes the median (solid vertical line within box), range (whiskers), and mean (x) values of symmetric stretching frequencies for uranyl mineral phases and inorganic compounds with extended topologies. Values are from the literature as summarized in Table 2.

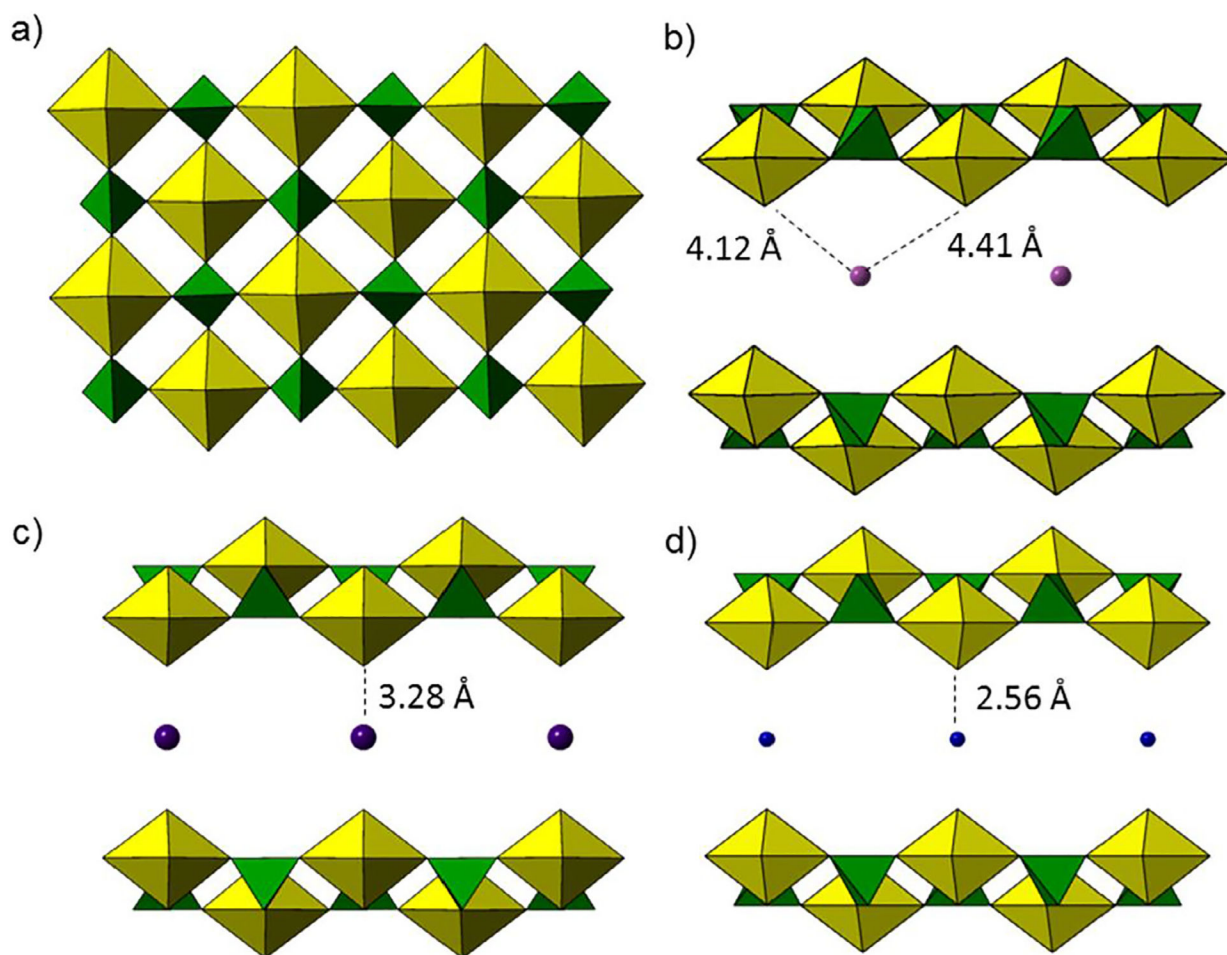


Fig. 4.

a) The autunite sheet topology contains uranyl square bipyramids (yellow polyhedra) connected to phosphate tetrahedra (green polyhedra) through shared vertices. The cation to uranyl oxo atom distance associated with (b) saleeite (Mg(II)), (c) autunite (Ca(II)), and (d) torbernite (Cu(II)) are related to the trends in the uranyl symmetric stretching mode within the Raman spectra.

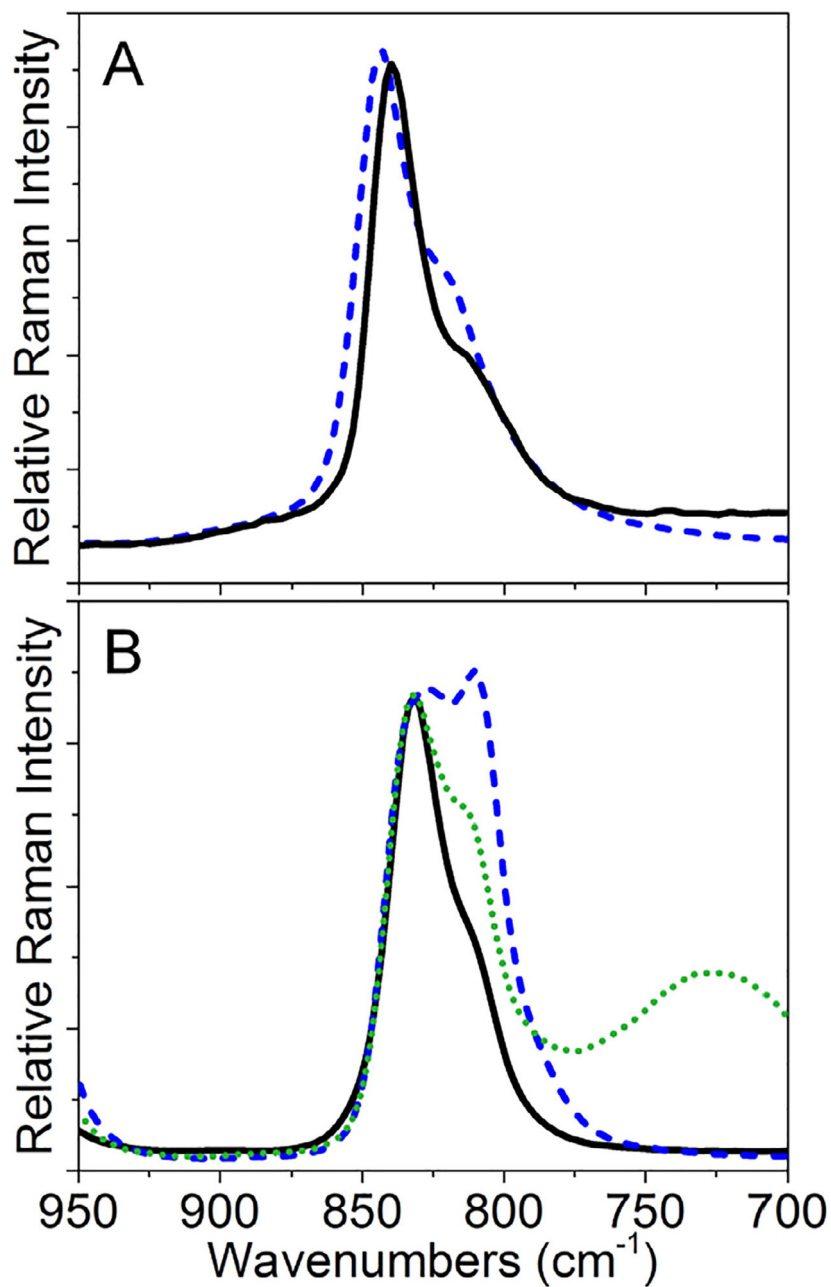


Fig. 5. Comparison of solid-state Raman spectra for (A) phosphuranylite (solid black – R130108, dashed blue – R110155) and (B) autunite (solid black – R050612, dashed blue – R060434, dotted green – R060476). Spectral intensities were normalized to the highest energy bands near 840 cm⁻¹.

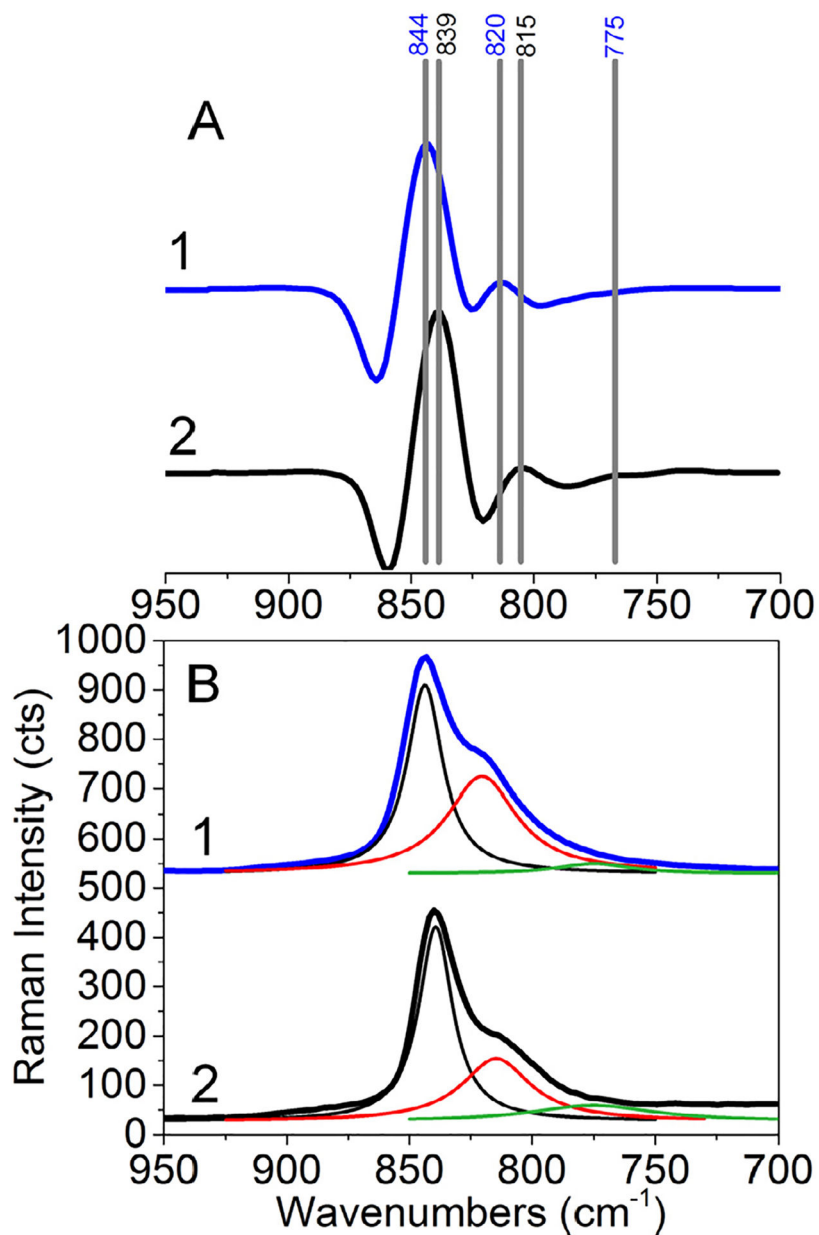


Fig. 6. Analysis of phosphuranylite spectral data in the form of Raman (A) – second derivative spectra with barcodes and (B) spectra (+ fitting) for (1) R110155 (blue) and (2) R130108 (black). Data are offset for clarity.

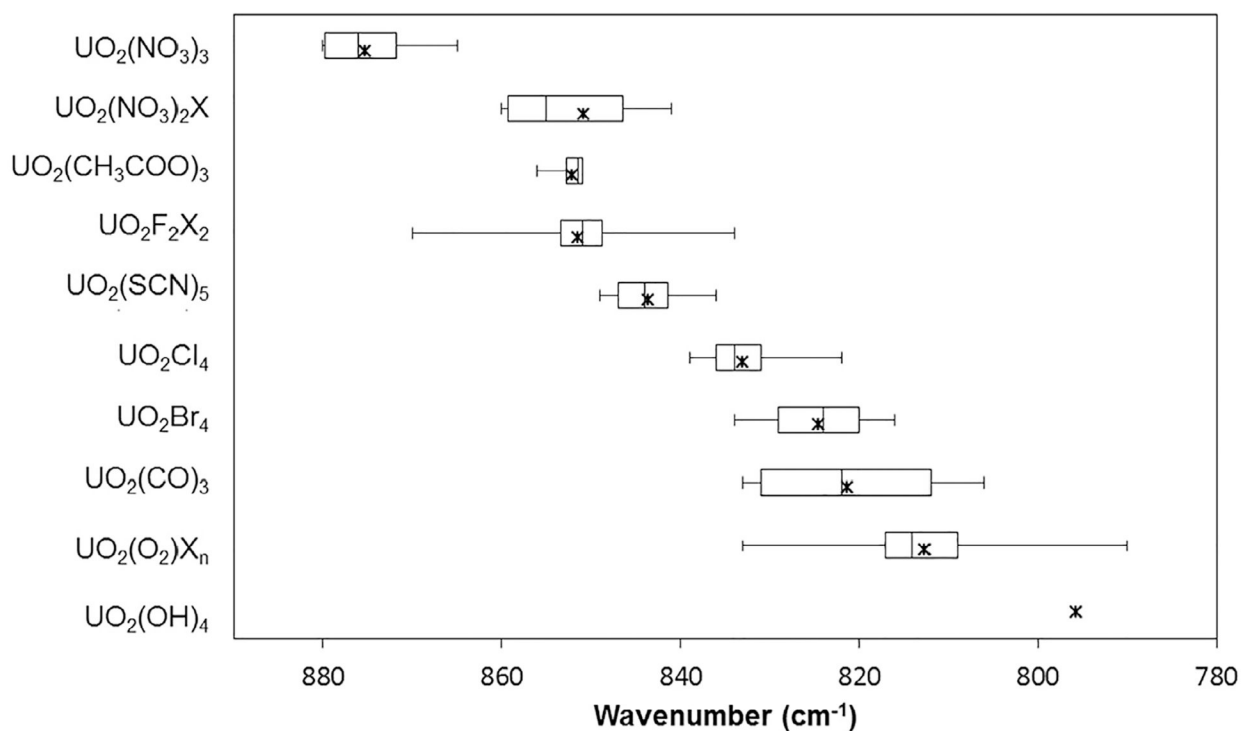


Fig. 7.

Box and whisker plot for well-defined uranyl coordination complexes that describes the median (solid vertical line within box), range (whiskers), and mean (x) values for the uranyl symmetric stretching mode (ν_1). The X in $\text{UO}_2(\text{NO}_3)_2\text{X}_2$, $\text{UO}_2\text{F}_2\text{X}_2$ and $\text{UO}_2(\text{O}_2)\text{X}_n$ represents substitution by a range of O- and N-donor ligands. Uranyl phosphonates and O donors (both isolated molecular species and coordination polymers with ligands containing carboxylate, oxalate, or ketones) were not included in this plot due to the diversity of coordination modes and ligands within these groups of compounds. Frequencies for all uranyl coordination complexes and polymers can be found in Table 2.

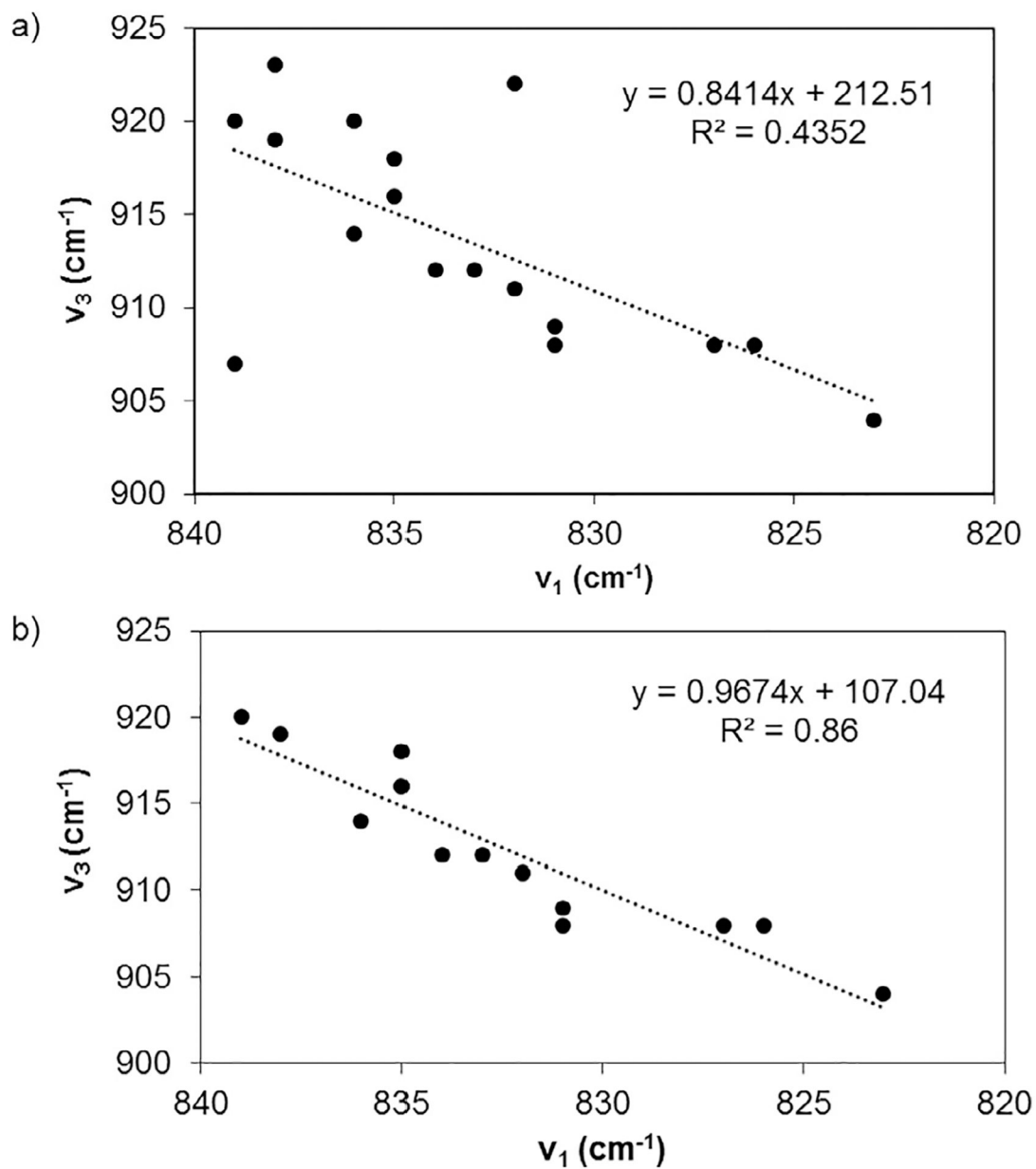


Fig. 8. The least squares regression for (a) all uranyl tetrachloro compounds and (b) excluding densely packed solids and less resolved crown-ether compounds.

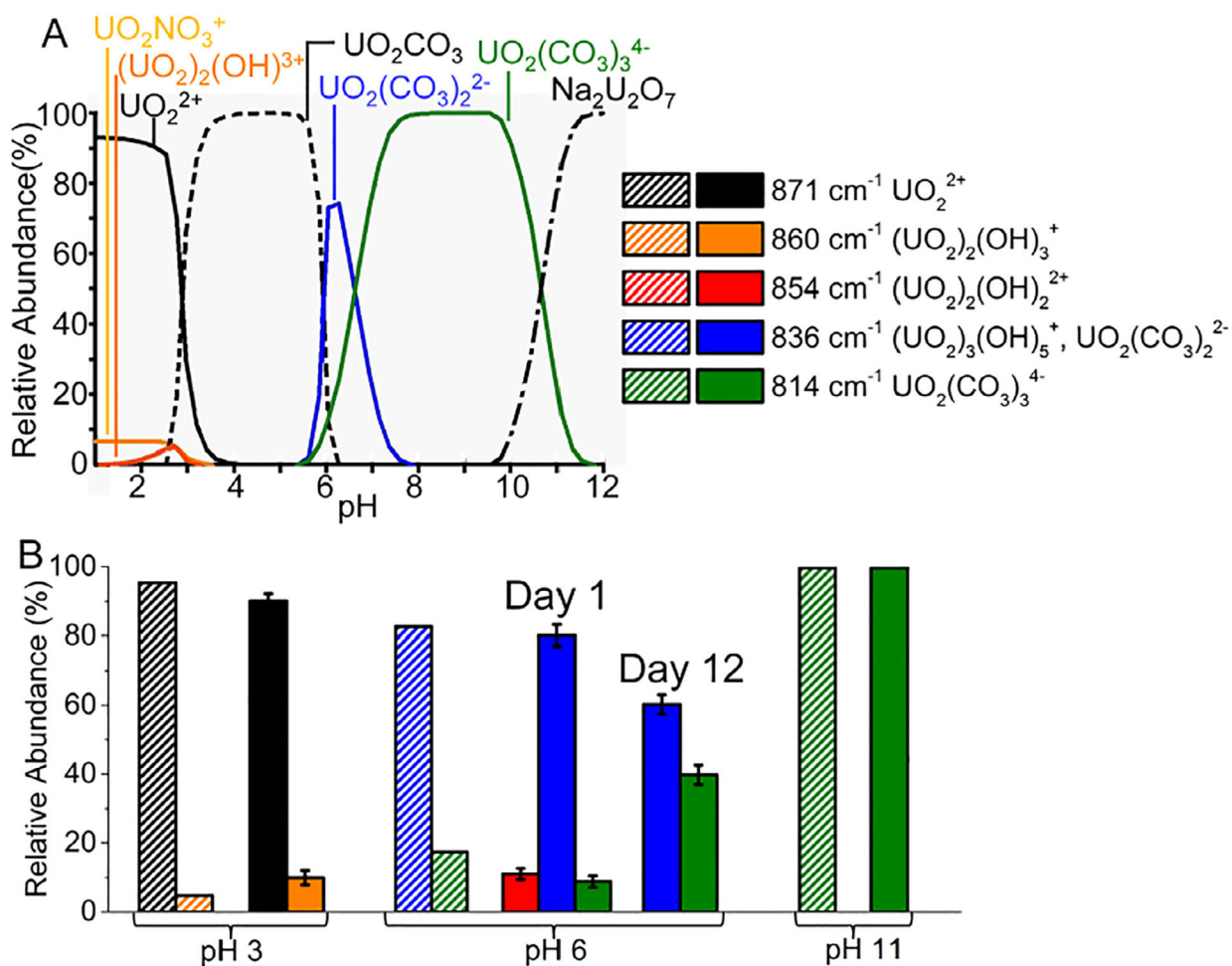


Fig. 9. Investigations by Lu et al.[48] utilized Raman spectroscopy to explore the presence of uranyl carbonate and hydroxide phases in aqueous solutions and related these values to the calculated equilibrium diagram. Slow kinetics resulted in initial differences between spectral analysis and predicted values. Reprinted with permission from Ref. [49]. Copyright 2016 American Chemical Society.

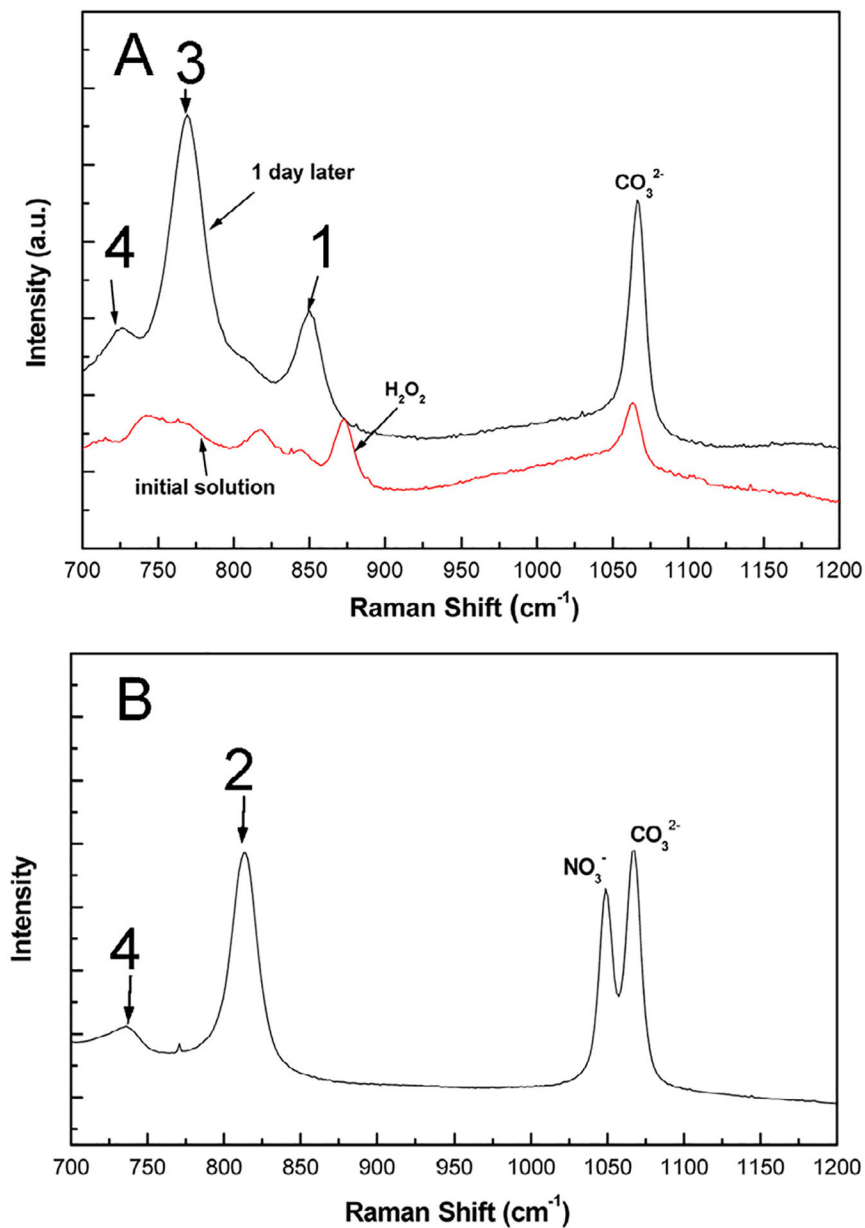


Fig. 10. Raman spectra of (A) uranyl in 0.5 M Na_2CO_3 with 1.0 M H_2O_2 at pH 11.4, and (B) uranyl in 0.5 M Na_2CO_3 at pH 10.8. Vibrational frequency of uranyl species: (1) 848 ($\text{UO}_2(\text{O}_2)_2^{2-}$), (2) 811 ($\text{UO}_2(\text{CO}_3)_3^{4-}$), (3) 769 ($\text{UO}_2(\text{O}_2)(\text{CO}_3)_2^{4-}$), and (4) 727 ($\text{UO}_2(\text{CO}_3)_x(\text{OH})_y^{2-2x-2y}$) cm^{-1} . Figure is reprinted with permission from Ref. [171]. Copyright 2012 American Chemical Society.

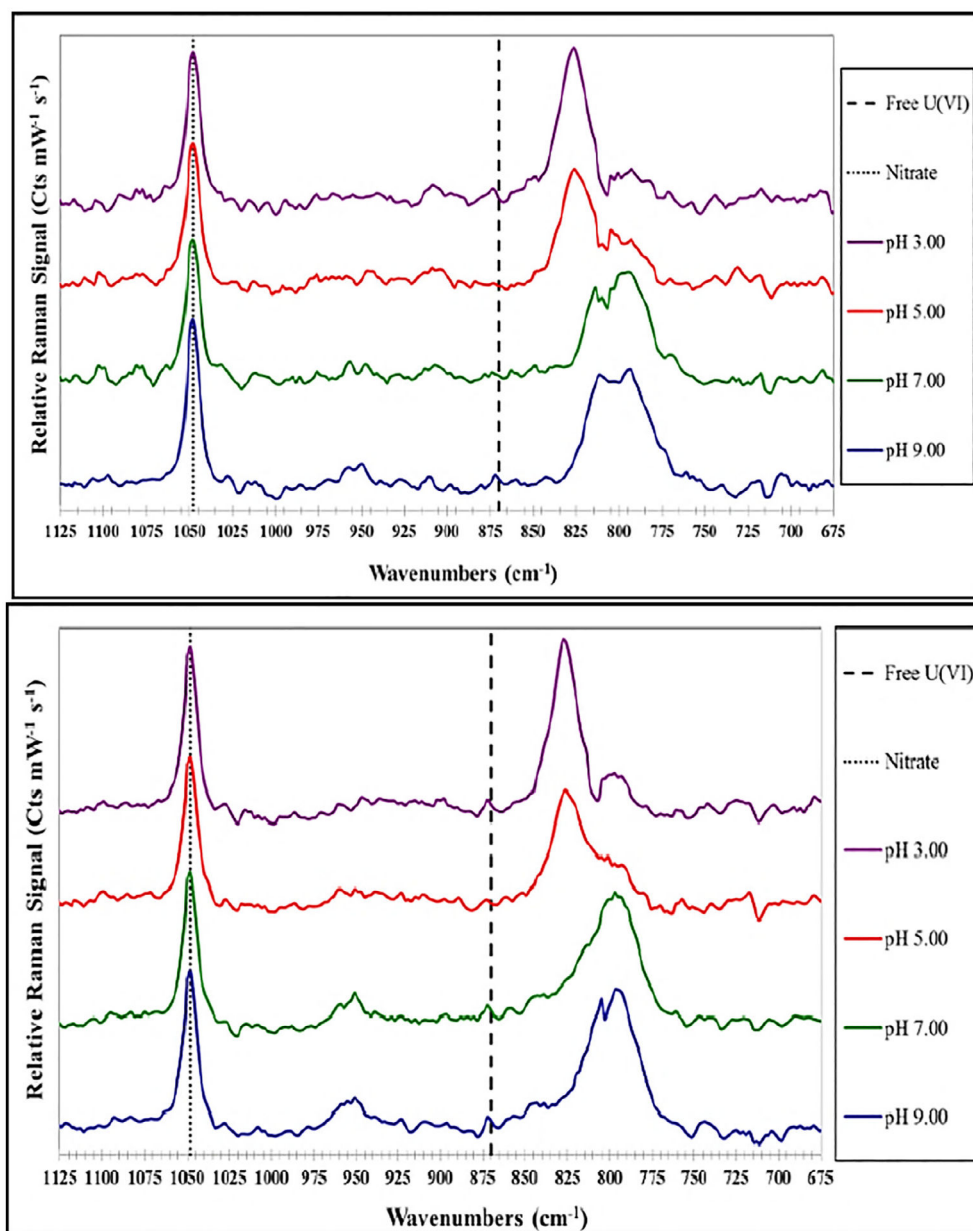


Fig. 11.

Raman spectra of aqueous solutions at pH 3, 5, 7, and 9 containing $[\text{UO}_2^{2+}]:[\text{C}_6\text{H}_5\text{O}_7^{3-}]$ in the ratio of (a) 1:1 and (b) 1:2 indicate a shift from a dominant dimeric species to a trimer with increasing pH. Peaks were normalized based upon the NO_3^- peak at 1047 cm^{-1} , and the dashed line indicates the expected vibrational frequency from $[(\text{UO}_2)(\text{H}_2\text{O})_5]^{2+}$. Vibrational frequencies of uranyl citrates are (1) 825 cm^{-1} ($(\text{UO}_2)_2(\text{C}_6\text{H}_5\text{O}_7)_2^{2-}$), (2) 800 cm^{-1} ($(\text{UO}_2)_3(\text{C}_6\text{H}_5\text{O}_7)_3^{3-}$), and 790 cm^{-1} ($(\text{UO}_2)_3(\text{C}_6\text{H}_5\text{O}_7)_2$) cm^{-1} . Reprinted from Ref. [16] with permission from The Royal Society of Chemistry.

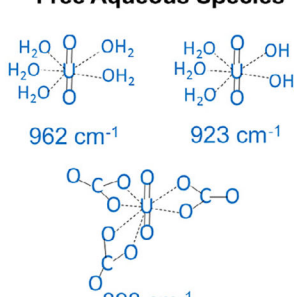
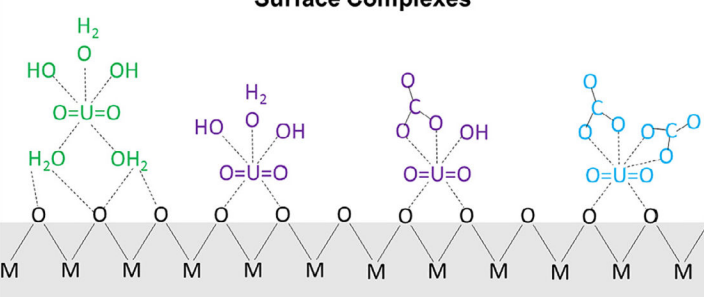
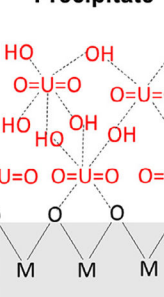
Free Aqueous Species	Surface Complexes		Precipitate
			
Ferrihydrite ($\text{Fe}_2\text{O}_3 \cdot 0.5 \text{H}_2\text{O}$) Hematite ($\alpha\text{-Fe}_2\text{O}_3$) Rutile (TiO_2) Maghemite ($\alpha\text{-Fe}_2\text{O}_3$) Silica (SiO_2) Corundum ($\gamma\text{-Al}_2\text{O}_3$) Gibbsite (Al_2O_3)	915 cm^{-1} 912 cm^{-1}	903 cm^{-1} 906 cm^{-1} 899 cm^{-1} 912 cm^{-1} 912 cm^{-1} 913 cm^{-1}	893 cm^{-1} 903 cm^{-1} 893 cm^{-1} 942 cm^{-1}

Fig. 12.

Previously reported uranyl species and asymmetric stretching frequencies (ν_3) for isolated aqueous and surface complexes and extended solid-state precipitates on metal (M) oxides (O). The pH for all reported studies range from 5 to 8 and the surface state is depicted as O atoms for simplicity. Data based upon Refs. [152,215,218,220,221,224–227].

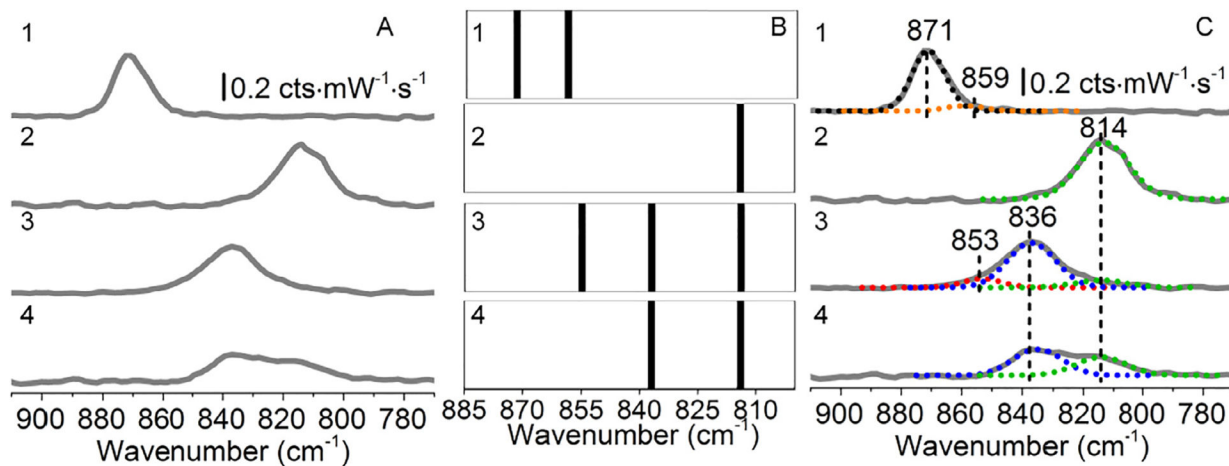


Fig. 13.

Detect and identify uranium species in aqueous solution including 30 mM $\text{UO}_2(\text{NO}_3)_2$ and 105 mM Na_2CO_3 at pH (1) 3, (2) 11, (3) 6 (24 h), and (4) 6 (12 days). (A) Collected normal Raman spectra, (B) barcode, and (C) spectral peak fitting analyses and experiment conditions: excitation wavelength $\lambda_{\text{ex}} = 785 \text{ nm}$; $t_{\text{int}} = 20 \text{ s}$; $P = 80 \text{ mW}$, and 10 averages. Uranium vibrational frequencies: 871 (UO_2^{2+}), 859 ($\text{UO}_2)_2\text{OH}^{3+}$), 853 ($(\text{UO}_2)_2(\text{OH})_2^{2+}$), 836 ($\text{UO}_2(\text{CO}_3)_2^{2-}$), and 814 ($\text{UO}_2(\text{CO}_3)_3^{4-}$). cm^{-1} . Reprinted with permission from Ref. [49].

Copyright 2016 American Chemical Society.

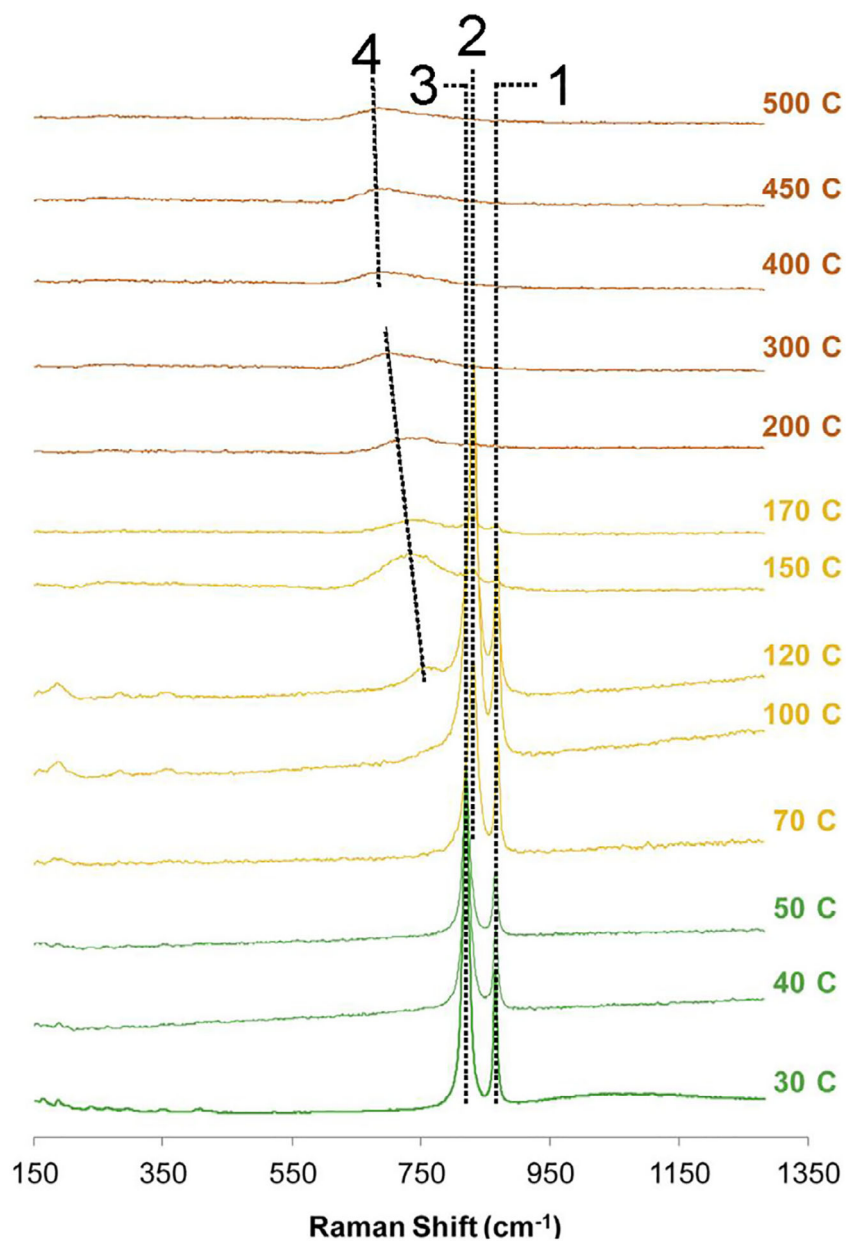


Fig. 14. Thermal decomposition of uranyl peroxide, $\text{UO}_4 \cdot 4\text{H}_2\text{O}$, is monitored by Raman spectroscopy from 30 to 500 °C. The vibrational frequencies of symmetric stretching of $\text{U}-\text{O}$ are (1) 863, (2) 828, and (3) 818 cm^{-1} . Vibrational frequency of peroxide anion is centered at 748 cm^{-1} at 120 °C and (4) 675 cm^{-1} at 400 °C. Figure is reproduced with permission from Ref. [254]. Copyright 2017 Elsevier.

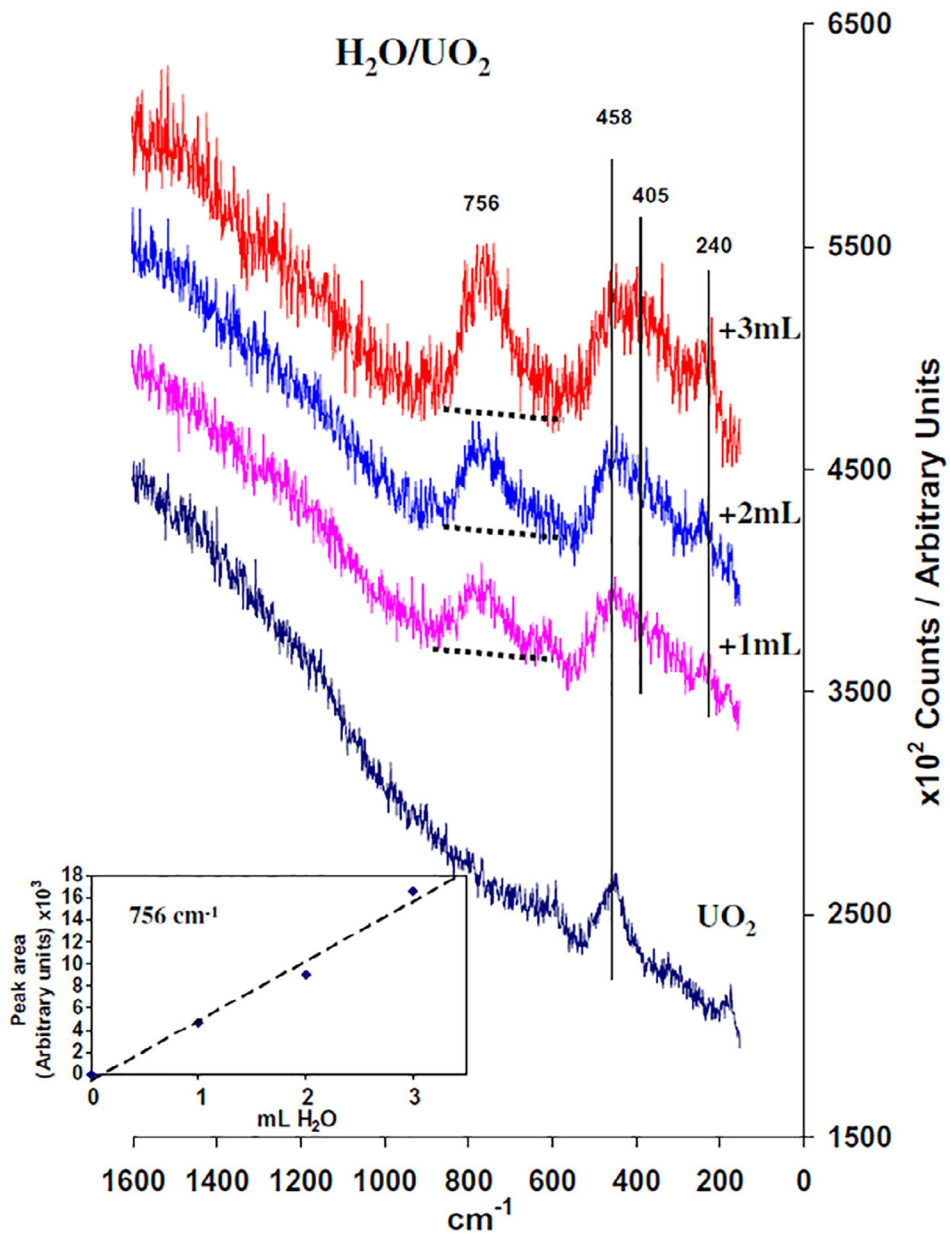


Fig. 15. *In situ* Raman spectra of the oxidation of UO₂ (458 cm⁻¹) to U₃O₈ (756 cm⁻¹) by injecting H₂O vapor ranging from 0, 1, 2, and 3 mL. Inset shows the increase of 756 cm⁻¹ (U₃O₈) band increases with the volume of H₂O. Experiment condition: excitation wavelength $\lambda_{\text{ex}} = 488$ nm; integration time: 20 s. Figure is reproduced with permission from Ref. [67]. Copyright 2005 Elsevier.

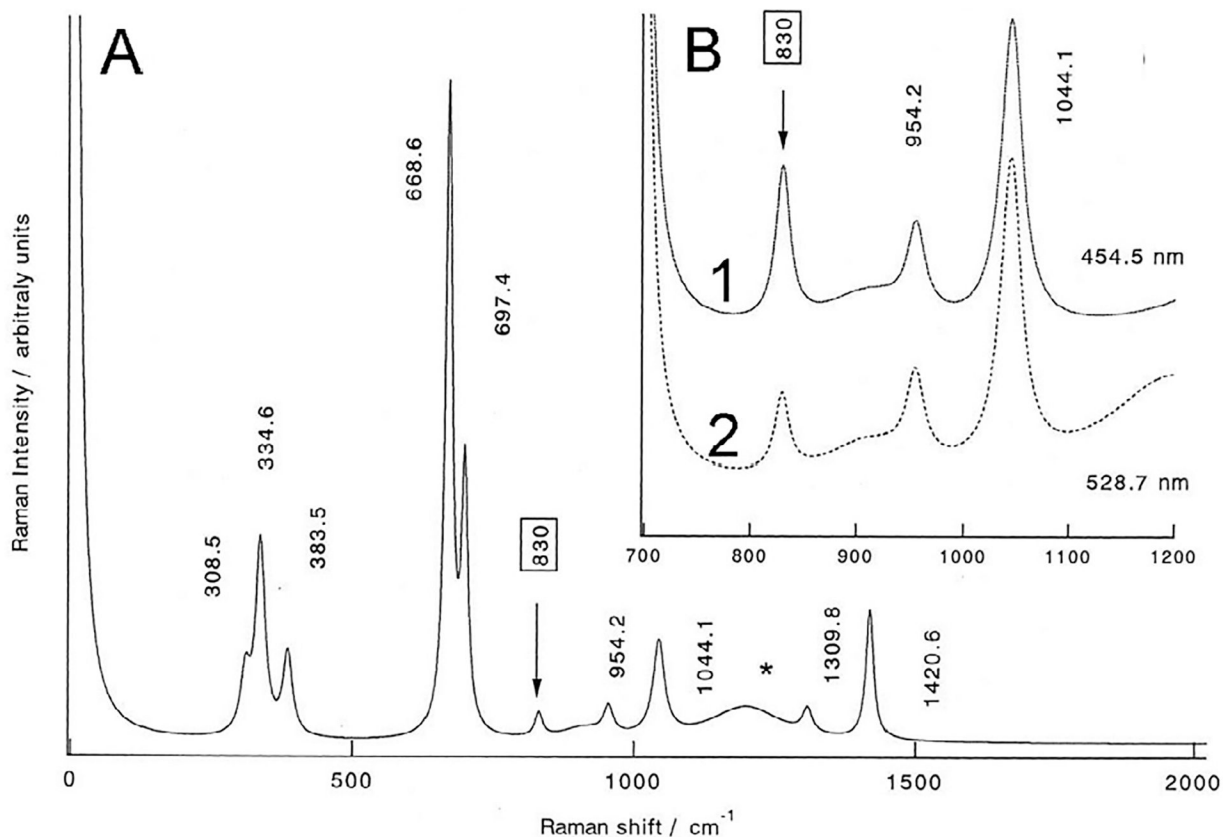


Fig. 16.

(A) Resonance Raman spectrum of $\text{Cs}_2\text{UO}_2\text{Cl}_4$ in DMSO. Experiment condition: excitation wavelength $\lambda_{\text{ex}} = 528.7$ nm. Vibrational frequencies: 830 cm^{-1} ($\text{UO}_2\text{Cl}_4^{2-}$) and 1044.1 cm^{-1} (DMSO). (B) Magnified spectra of Fig. 5A from 1200 to 700 cm^{-1} . Experiment condition: excitation wavelength $\lambda_{\text{ex}} =$ (1) 484.5 and (2) 528.7 nm. Figure is reproduced with permission from Ref. [264]. Copyright 2001 Elsevier.

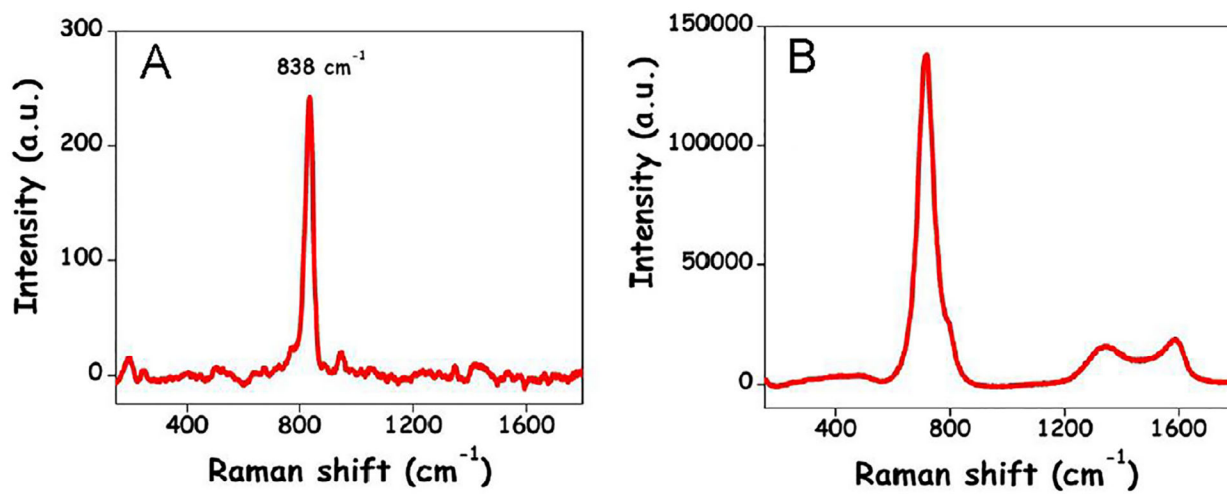


Fig. 17.

(A) Normal Raman spectrum of 5 mM uranyl acetate and (B) SERS spectra of 10 μ M of uranyl acetate on silver doped reduced graphene oxide nanosheets. Figure is reprinted with permission from Ref. [272] Copyright 2013 American Chemical Society.

Table 1

Instrumentation to assess the chemistry of uranium in solution and solid-state samples.

	Phase	Chemical Speciation/Coordination	Isotopic Ratios	Detection Limit/Dynamic Range	Complex Matrix Compatibility
Alpha Spectrometry	Solution	Poor	Excellent	0.05 pCi/-	Poor
Liquid Scintillation Counter	Solution	Poor	Poor/Good	50 pCi/-	Poor
X-ray Diffraction	Solid	Excellent	Poor	1%/-	Poor
X-ray Photoelectron Spectroscopy	Solid	Good	Poor	0.1–1%/-	Poor
X-ray Absorption Spectroscopy	Solution/solid	Excellent	Poor	1×10^{-6} M/-	Good
X-ray Scattering	Solution	Excellent	Poor	1×10^{-3} M/-	Fair
Mass Spectrometry	Solution	Good	Excellent	1×10^{-11} M/-	Poor
Fluorescence	Solution/solid	Excellent	Poor	5×10^{-6} M/5+	Good
Time-Resolved Fluorescence Spectroscopy	Solution	Excellent	Poor	1×10^{-7} M/5+	Good
UV-Vis Absorption	Solution/solid	Poor	Poor	1×10^{-6} M/3+	Good
Infrared Absorption	Solution/solid	Good	Poor	1×10^{-7} M/3+	Good
Raman Scattering	Solution/solid	Excellent	Poor	1×10^{-5} M/2+	Excellent

Table 2
Vibrational modes for solid state inorganic compounds and mineral phases for hexavalent uranium compounds.

Compound (Mineral Name)	ν_1 (cm ⁻¹)	ν_3 (cm ⁻¹)	Refs.
<i>Oxides, Oxyhydroxides, Peroxides, Halides</i>			
(Ca,U(VI))O ₄ (Vorlanite)	683		[84]
[(UO ₂) ₈ O ₂ (OH) ₁₂]·12H ₂ O (schoepite)	838		[86]
K ₂ [(UO ₂) ₂ O ₂ (OH) ₃] ₂ ·7H ₂ O (compreignacite)	848, 824		[273]
	831		[87]
Ca[(UO ₂) ₆ O ₄ (OH) ₆]·8H ₂ O (becquerelite)	838, 813		[86]
	829, 796	948, 872	[87]
Ba[(UO ₂) ₆ O ₄ (OH) ₆](billietite)	830		[86]
Pb[(UO ₂) ₁₀ O ₆ (OH) ₁₁](vandriesscheite)	852, 840		[86]
Pb _{3+x} (H ₂ O)[(UO ₂) ₄ O _{4+x} (OH) _{3x}] ₂ (curite)	803, 791	912, 876	[86,88]
Cu[UO ₂ (OH) ₄] (vandenbrandeite)	805	897	[89]
K ₂ Ca[(UO ₂) ₆ O ₆ (OH) ₄]·6H ₂ O (rameauite)	813		[274]
KPb[(UO ₂) ₇ O ₅ (OH) ₇]·8H ₂ O (gauthierite)	833	915	[275]
[N(C ₂ H ₅) ₄] ₂ [(UO ₂) ₄ (OH) ₃ F ₁₀]	845	927	[276]
[(UO ₂)(O ₂)(H ₂ O) ₂]·2H ₂ O (studtite)	831		[95]
UO ₂ F ₂	867	915	[100]
UO ₂ Cl ₂	871	960	[101]
<i>Carbonates</i>			
Ca ₂ [UO ₂ (CO ₃) ₃]·11H ₂ O (liebigite)	822		[277]
Ca ₂ [UO ₂ (CO ₃) ₃]·11H ₂ O (liebigite)	829	906	[87]
Ca ₂ [UO ₂ (CO ₃) ₃]·10H ₂ O (synthetic)	826		[278]
Mg ₂ [UO ₂ (CO ₃) ₃]·18H ₂ O (bayleyite)	822		[278]
Na ₄ [(UO ₂)(CO ₃) ₃] (cejkaite)	805		[279]
Na ₄ [(UO ₂ (CO ₃) ₃] (synthetic)	810, 816		[279]
Na ₂ Ca(UO ₂)(CO ₃) ₃ ·6H ₂ O (andersonite)	806, 832	899, 913	[87]
	832	898	[253]
K ₃ Na(UO ₂)(CO ₃) ₃ ·H ₂ O (grimselite)	815	876	[87]

Compound (Mineral Name)	ν_1 (cm ⁻¹)	ν_3 (cm ⁻¹)	Refs.
Si ₂ [UO ₂ (CO ₃) ₃]·8H ₂ O	812		[278]
B ₄ [UO ₂ (CO ₃) ₃]·6H ₂ O	818		[278]
K ₄ UO ₂ (CO ₃) ₃	806		[280]
Pb ₂ (UO ₂)(CO ₃) ₃ (Widenmannite)	849	926	[281]
(UO ₂ CO ₃) (Rutherfordine)	886	956	[282,283]
	886	932	[284]
NaCa ₃ (UO ₂)(CO ₃) ₃ (SO ₄)F·10H ₂ O (schrockingerite)	817	898	[285]
Ca[(UO ₂)(CO ₃) ₂ (H ₂ O) ₂]·3H ₂ O (zellerite)	834	899	[286]
Ca ₂ Cu[(UO ₂)(CO ₃) ₃](CO ₃)·6H ₂ O (voglite)	836	898	[287]
Y ₂ (UO ₂) ₄ (CO ₃) ₃ (OH) ₈ ·10–11H ₂ O (kamotoite-Y)	814.7	911	[288]
CaU ⁵⁺ (UO ₂) ₂ (CO ₃)O ₄ (OH)(H ₂ O) ₇ (Wyarite)	853, 837		[124]
<i>Sulfate and Selenate</i>			
UO ₂ SO ₄ ·2.5H ₂ O	863,853	952, 938	[289]
UO ₂ SO ₄ ·3.5H ₂ O	865		[290]
(H ₃ O) ₂ [(UO ₂) ₂ (SO ₄) ₃ (H ₂ O)]·7H ₂ O		930	[291]
(H ₃ O) ₂ [(UO ₂) ₂ (SO ₄) ₃ (H ₂ O)]·4H ₂ O		918, 928, 935	[291]
[(UO ₂) ₆ (SO ₄)O ₂ (OH) ₆ (H ₂ O) ₆](H ₂ O) ₈ (uranopilite)	843, 835, 819	941, 929, 910	[292,293]
(UO ₂) ₈ (SO ₄)(OH) _{1,4} ·13H ₂ O (jachymovite)	839, 828, 807, 800	902, 923	[294]
K _{0,6} (H ₃ O) _{0,4} [(UO ₂) ₆ (SO ₄) ₃ (OH) ₇]·8H ₂ O (zippeite)	849, 838, 826, 814	911, 873	[295]
Na ₄ [(UO ₂) ₆ (SO ₄) ₃ (OH) ₁₀]·4H ₂ O (Na zippeite)	840, 841, 833, 823	880, 912	[296]
Na ₅ (UO ₂) ₈ (SO ₄) ₄ O ₅ (OH) ₃ ·8H ₂ O (natrozippeite)	840		[109]
Cu(UO ₂) ₂ (OH) ₂ (SO ₄) ₂ ·8H ₂ O(johannite)	811		[297]
	836		[109]
Cu ₆ [(UO ₂) ₄ O ₄ (SO ₄) ₂] ₂ (OH) ₅ ·25H ₂ O (pseudojohannite)	810,805		[298]
Fe(UO ₂)(SO ₄) ₂ (H ₂ O) ₁₁ (leydetite)	858, 851, 846, 843, 836, 828	937, 930	[299]
Fe[(UO ₂) ₂ (SO ₄) ₂ (OH) ₂](H ₂ O) ₇ (deliensite)	838	933	[300]
(UO ₂) ₈ (SO ₄)(OH) _{1,4} ·13H ₂ O (jachymovite)	839, 828, 807, 800	902, 923	[294]
Na ₅ (UO ₂)(SO ₄) ₃ (SO ₃ OH)(H ₂ O)(meisserite)	847		[301]
Na ₇ (UO ₂)(SO ₄)Cl(H ₂ O) ₂ (bluelizardite)	854,848		[302]

Compound (Mineral Name)	ν_1 (cm ⁻¹)	ν_3 (cm ⁻¹)	Refs.
K(UO ₂)(SO ₄)(OH)(H ₂ O) (adolfpareraite)	843	890	[303]
N ₄₆ [(UO ₂)(SO ₄) ₄](H ₂ O) ₄	860, 845, 830, 805		[304]
Fe(UO ₂)(SO ₄) ₂ ·5H ₂ O (rietveldite)	862	924	[305]
[(UO ₂)(SO ₄)(H ₂ O) ₂] ₂ ·H ₂ O (shumwayite)	865, 850	951, 927	[306]
(UO ₂) ₃ (SeO ₃) ₂ (OH) ₂ ·5H ₂ O (haynesite)	811, 800	905, 862	[307, 308]
Cu[(UO ₂) ₃ (SeO ₃) ₂ O ₂]·8H ₂ O (marthozite)	812	863	[309]
Cu ₄ UO ₂ (SeO ₃) ₂ (OH) ₆ H ₂ O (derricksite)	788	859	[310]
Pb ₂ Cu ₅ (UO ₂) ₂ (SeO ₃) ₆ (OH) ₆ ·2H ₂ O (demesmaekerite)	822	878	[311]
Ba[(UO ₂) ₃ O ₂ (SeO ₃) ₂](H ₂ O) ₃ (guilleminite)	831	912	[312]
(Y _{1.98} Dy _{0.24}) ₂ H _{0.34} [(UO ₂) ₈ O ₈₈ O ₇ (OH)(H ₂ O) ₂₆ (sejkoraites-Y)]	829	911	[313]
<i>Phosphate and Arsenate</i>			
UO ₂ (H ₂ PO ₂) ₂ ·H ₂ O	830	909	[314]
UO ₂ (H ₂ PO ₂) ₂ ·H ₃ PO ₂	830	912	[314]
(H ₃ O)(UO ₂)PO ₄ ·4.5H ₂ O	842		[315]
K _{0.9} (H ₃ O) _{0.1} (UO ₂)PO ₄ ·2.5H ₂ O	826		[315]
K _{0.4} (H ₃ O) _{0.6} (UO ₂)PO ₄ ·3H ₂ O	840		[315]
Cs ₃ (UO ₂) ₂ (PO ₄) ₂ O ₂		885, 855, 838, 805	[316]
Ca(UO ₂) ₂ (PO ₄) ₂ ·11H ₂ O (autinite)	830		[108]
KCa(H ₃ O) ₃ (UO ₂) ₇ (PO ₄) ₄ O ₄ ·8H ₂ O (phosphuranylite)	827		[108]
	832	894	[115]
Ca(UO ₂) ₃ (PO ₄) ₂ (OH) ₂ ·6H ₂ O (phosphuranylite)	801		[109]
Ca ₂ (UO ₂) ₃ O ₂ (PO ₄) ₂ ·7H ₂ O (phurcalite)	810	874	[317]
[Mg(UO ₂ PO ₄) ₂ ·10H ₂ O] (salecite)	837	901	[108]
[CaCu(UO ₂)(PO ₄) ₂ ·4H ₂ O] (ulrichite)	812	880	[108]
[Cu(UO ₂ PO ₄) ₂ ·8H ₂ O] (metatorbernite)	826	906	[108]
	813	876–902	
	840		
(H ₃ O) _{0.4} Cu _{0.8} (UO ₂) ₂ (PO ₄) ₂ ·7.6H ₂ O (metatorbernite)	822	895	[318]
Cu(UO ₂) ₂ (PO ₄) ₂ ·12H ₂ O (torbernite)	825		[109]

Compound (Mineral Name)	ν_1 (cm ⁻¹)	ν_3 (cm ⁻¹)	Refs.
[(Ba) ₂ (UO ₂) ₃ (PO ₄) ₂ (OH) ₄ ·8H ₂ O] (bergenite)	810, 798		[319]
(H ₃ O)Al(UO ₂) ₄ (PO ₄) ₄ ·15H ₂ O (sabugalite)	850, 836, 826, 810		[110]
Al[(UO ₂) ₂ (PO ₄) ₂](OH)·8H ₂ O (hreadgoldite)	827		[320]
Pb ₂ (UO ₂)(PO ₄) ₂ ·n H ₂ O (parsonsite)	807, 796		[321]
Pb ₃ [H(UO ₂) ₃ O ₂ (PO ₄) ₂] ₂ ·12H ₂ O (dewindtite)	831, 823, 818, 808, 795		[322]
Pb ₂ [(UO ₂) ₃ O ₂ (PO ₄) ₂] ₂ ·5H ₂ O (dumontite)	815, 800, 780		[323]
(UO ₂)Bi ₄ O ₄ (PO ₄) ₂ ·2H ₂ O (phosphowalpurkite)	885		[324]
Nd[(UO ₂) ₃ O(OH)(PO ₄) ₂] ₂ ·6H ₂ O (francoisite-Nd)	830		[325]
U(OH) ₄ [(UO ₂) ₃ (PO ₄) ₂ (OH) ₂] ₄ ·4H ₂ O (vanmeersscheite)	860		[326]
(Na ₂ , Ca) ₄ [(UO ₂)(AsO ₄) ₂] ₂ ·5H ₂ O (natrouranospinitite)	816, 810		[327]
Ca[(UO ₂)(AsO ₄) ₂] ₂ ·8H ₂ O (metauranospinitite)	815, 806	904, 893	[328]
Ca(UO ₂)[(UO ₂) ₃ (AsO ₄) ₂ (OH) ₂] ₂ ·6H ₂ O (arsenouranlyite)	795, 787		[326]
Mg(UO ₂) ₂ (AsO ₄) ₂ ·10H ₂ O (novacekite)	817		[109]
Cu(UO ₂) ₂ (AsO ₄) ₂ ·12H ₂ O (zeunerite)	821		[109]
Cs ₂ [(UO ₂)(As ₂ O ₇)]	832		[329]
α-Cs[(UO ₂)(HAs ₂ O ₇)]	834		[329]
β-Cs[(UO ₂)(HAs ₂ O ₇)]	820		[329]
Cs[(UO ₂)(HAs ₂ O ₇)]·0.17H ₂ O	809	896	[329]
Ni(UO ₂) ₂ (AsO ₄) ₂ ·8H ₂ O (metaaichite)	817	947	[330]
(UO ₂)Bi ₄ O ₄ (AsO ₄) ₂ ·2H ₂ O (walpurkite)	790, 770	888	[331]
(zn _{0.72} Fe _{0.10} Mg _{0.06} Al _{0.05})(UO ₂) ₂ [(AsO ₄) _{1.5} (PO ₄) _{0.5}] ₂ ·8.43H ₂ O (metalodovite)	819	891	[331]
<i>Silicates</i>			
(UO ₂) ₂ SiO ₄ ·2H ₂ O (soddyite)	832, 828		[233]
	830	897	[332]
	828, 809, 802	904, 910, 900	[333, 334]
		848	[335]
Na ₄ [UO ₂ SiO ₃ (OH)]·0.5H ₂ O (sodium boltwoodite)		841	[335]
K[UO ₂ SiO ₃ (OH)]·H ₂ O (boltwoodite)		853	[336]
(K, Na)[(UO ₂)(SiO ₃ OH)]·1.5H ₂ O (boltwoodite)	799, 796, 786		
K ₂ [(UO ₂) ₂ (Si ₅ O ₁₃)]·H ₂ O (weeksite)	814, 810, 800	916, 903	[333, 334]

Compound (Mineral Name)	ν_1 (cm ⁻¹)	ν_3 (cm ⁻¹)	Refs.
Ca(UO ₂) ₂ (SiO ₃ OH) ₂ ·5H ₂ O (uranophane)	799, 796, 799	856, 878, 852	[337]
		855	[335]
	800		[338]
	800		[109]
	798		[233]
Mg(UO ₂) ₂ (SiO ₃ OH) ₂ ·5H ₂ O (sklodowskite)	827, 801, 777	854, 821	[336]
Cu(UO ₂) ₂ (SiO ₃ OH) ₂ ·6H ₂ O (cuprosklodowskite)	787	871	[336]
	792		[109]
PbUO ₂ SiO ₄ ·H ₂ O (kasolite)	759	904	[336]
	768		[109]
Ca[(UO ₂) ₂ (Si ₅ O ₁₂ (OH) ₂)(H ₂ O) ₃ (hairweeite)	808, 800	909, 877	[333,334]
<i>Iodates and Tellurates</i>			
UO ₂ (IO ₃) ₂ (H ₂ O)·2HIO ₃		902	[339]
Na ₂ [UO ₂ (IO ₃) ₄ (H ₂ O)]		903	[340]
K ₂ [(UO ₂) ₂ (VO) ₂ (IO ₆) ₂ O]·H ₂ O	862	982	[341]
K ₂ [UO ₂ (MoO ₄)(IO ₃) ₂]		909	[342]
K[UO ₂ Te ₂ O ₅ (OH)]		860	[343]
Tl ₃ (UO ₂) ₂ [Te ₂ O ₅ (OH)](Te ₂ O ₆)·2H ₂ O		863	[343]
α-Tl ₂ [UO ₂ (TeO ₃) ₂]		843	[343]
Si ₃ [UO ₂ (TeO ₃) ₂](TeO ₃) ₂		847	[343]
[UO ₂ TeO ₃] (schmitterite)	823	937, 882	[344]
PbUO ₂ (TeO ₃) ₂ (moctezumite)	826	837	[345]
<i>Tungstates, Vanadates, and Chromates</i>			
Cs ₄ [(UO ₂) ₄ (WO ₃)(W ₂ O ₈)O ₂]	765, 782		[118]
Cs ₄ [(UO ₂) ₇ (WO ₃) ₃ O ₃]	871, 828, 786, 766		[118]
Na ₈ [TeW ₉ O ₃₃]·19·5H ₂ O	796		[346]
(NH ₄) ₁₄ [(UO ₂) ₂ (H ₂ O) ₂ (SbW ₉ O ₃₃) ₂]·24H ₂ O	804		[346]
Pb ₂ (UO ₂)(V ₂ O ₈)·5H ₂ O (camotite)	837, 826	900, 860	[347]
K ₂ (UO ₂)(V ₂ O ₈)·3H ₂ O (curientite)	825		[347]

Compound (Mineral Name)	ν_1 (cm ⁻¹)	ν_3 (cm ⁻¹)	Refs.
Ba ₂ Pb(UO ₂) ₂ (V ₂ O ₈) ₂ ·5H ₂ O (francevillite)	828		[347]
Ca(UO ₂) ₂ (V ₂ O ₈) ₂ ·9H ₂ O (Tyuyamunite)	829		[347]
Ca(UO ₂) ₂ (V ₂ O ₈) ₂ ·3H ₂ O (metatyuyamunite)	824, 793		[347]
K ₅ (UO ₂) ₄ (SO ₄) ₄ (VO ₃) ₄ ·4H ₂ O (mathesiusite)	830	888, 896	[348]
Rb[UO ₂ (CrO ₄)(IO ₃)(H ₂ O)]		914	[342]
K ₂ [UO ₂ (CrO ₄)(IO ₃) ₂]		902	[342]
Rb ₂ [UO ₂ (CrO ₄)(IO ₃) ₂]		903	[342]
Cs ₂ [UO ₂ (CrO ₄)(IO ₃) ₂]		880	[342]

Table 3
Vibrational modes for uranyl coordination compounds and metal organic materials.

Compound	ν_1 (cm ⁻¹)	ν_3 (cm ⁻¹)	Refs.
<i>Peroxides</i>			
[Na ₄ K ₂ (UO ₂) ₂ (O ₂)(C ₂ O ₄) ₄]·6H ₂ O	822		[349]
(NH ₄) ₃ [(UO ₂) ₂ (O ₂) ₃ His(H ₂ O) ₂]		890	[350]
(NH ₄) ₃ [(UO ₂) ₂ (O ₂) ₃ salcy(H ₂ O) ₂]		895	[350]
K ₄ [(UO ₂) ₄ (O ₂) ₂ (C ₁₀ H ₁₃ O ₈ N ₂) ₂ (IO ₃) ₂]·16H ₂ O	790	890	[351]
LiK ₃ [(UO ₂) ₄ (O ₂) ₂ (C ₁₀ H ₁₂ O ₈ N ₂) ₂ (H ₂ O) ₂]·18H ₂ O	833	890	[351]
Na ₁₀ [(UO ₂ (O ₂ (C ₃ H ₂ O ₄)) ₅ ·20H ₂ O	806		[349]
NaK ₁₅ [(UO ₂) ₈ (O ₂) ₈ (C ₁₀ H ₁₂ O ₁₀ N ₂) ₂ (C ₂ O ₄) ₄]·14H ₂ O	819	871	[351]
Li ₄ K ₆ [(UO ₂) ₈ (O ₂) ₆ (C ₁₀ H ₁₂ O ₁₀ N ₂) ₂ (NO ₃) ₆]·26H ₂ O	817	890	[351]
LiU ₂₄	813		[352]
BiU ₂₄	814		[352]
PbU ₂₄	814		[352]
LiU ₂₄	814		[140]
LiU ₂₈	809		[140]
U ₂₄ Fe ₂₄ P	803	873	[176]
Na ₄ [(UO ₂)(S ₂) ₃](CH ₃ OH) ₈			[353]
<i>Halides and Hydroxides</i>			
CS ₂ UO ₂ Br ₄	836	920	[101]
[Li(12-crown-4)] ₂ [UO ₂ Br ₄]	822	913	[354]
[Na(15-crown-5)] ₂ [UO ₂ Br ₄]	824	904	[354]
[K(18-crown-6)] ₂ [UO ₂ Br ₄]	816	916	[354]
Rb ₂ [UO ₂ Cl ₄]·2H ₂ O	839	907	[146]
CS ₂ [UO ₂ Cl ₄]	832	922	[125]
	834	922	[101]
[Me ₄ N] ₂ [UO ₂ Cl ₄]	831	909	[125]
[Bmim] ₂ [UO ₂ Cl ₄]	839	920	[126]

Compound	ν_1 (cm ⁻¹)	ν_2 (cm ⁻¹)	Refs.
[Bmmim] ₂ [UO ₂ Cl ₄]	835	918	[126]
[Emim] ₂ [UO ₂ Cl ₄]	827	908	[126]
[Emmim] ₂ [UO ₂ Cl ₄]	835	916	[126]
[Bmmim] ₂ [UO ₂ Cl ₄]	831	908	[126]
[PPPh ₄] ₂ UO ₂ Cl ₄ (PI ⁻)	838	919	[125]
[PPPh ₄] ₂ UO ₂ Cl ₄ (P ₂ /c)	823	904	[125]
[PPPh ₄] ₂ UO ₂ Cl ₄ ·2CH ₂ Cl ₂	833	912	[125]
[PPPh ₄] ₂ UO ₂ Cl ₄ ·MeCN	832	911	[125]
[PPPh ₄] ₂ UO ₂ Cl ₄ ·MeOH	836	914	[125]
[AsPh ₄] ₂ UO ₂ Cl ₄ ·2CH ₂ Cl ₂	834	912	[125]
[K(18-crown-6)] ₂ [UO ₂ Cl ₄] ₂ [UO ₂ Cl ₄]	826	923	[354]
[Na(15-crown-5)] ₂ [UO ₂ Cl ₄] ₂ [UO ₂ Cl ₄]	838, 843	910	[354]
[Li(12-crown-4)] ₂ [UO ₂ Cl ₄] ₂ [UO ₂ Cl ₄]	822	913	[354]
UO ₂ Cl ₂ (N(CH ₃) ₂) ₃ PO ₂	831	920	[355]
UO ₂ F ₂ (CH ₃ NH ₂ CO)	854	955	[356]
UO ₂ F ₂ DMA	852	941	[356]
UO ₂ F ₂ DMF	857	930	[356]
UO ₂ F ₂ DMSO	851	938	[356]
UO ₂ F ₂ (H ₂ N) ₂ CO	834	915	[356]
UO ₂ F ₂ (H ₂ O) ₂	870	940	[356]
UO ₂ F ₂ (C ₁₁ H ₁₂ N ₂ O)	848	935	[356]
UO ₂ F ₂ (CH ₃ NH) ₂ CO	851	940	[356]
UO ₂ F ₂ ((CH ₃) ₂ N) ₂ CO	848	930	[356]
UO ₂ F ₂ (N(CH ₃) ₂) ₃ PO ₂	831	933	[355]
[Co(NH ₃) ₆] ₂ [UO ₂ (OH) ₄] ₃ ·H ₂ O	796		[357]
<i>Nitrates</i>			
UO ₂ (NO ₃) ₂ ·6H ₂ O	871	939	[101]
	865		[58]
UO ₂ (NO ₃) ₂ ·2H ₂ O	876		[57]

Compound	ν_1 (cm ⁻¹)	ν_3 (cm ⁻¹)	Refs.
UO ₂ (NO ₃) ₂ ·2H ₂ O	876		[57]
KUO ₂ (NO ₃) ₃	870	950	[101]
	874		[127]
C ₈ SUO ₂ (NO ₃) ₃	874		[127]
	879	956	[101]
RbUO ₂ (NO ₃) ₃	880		[127]
	879	956	[101]
NH ₄ UO ₂ (NO ₃) ₃	880		[127]
	880		[128]
	880		[101]
	871	936	[101]
E ₄ N(UO ₂ (NO ₃) ₃) ₃	853		[58]
(C ₃ H ₅ N ₂) ₂ [(UO ₂) ₂ (μ-OH) ₂ (NO ₃) ₄]			
[Bmim] ₂ [(UO ₂) ₂ (μ-OH) ₂ (NO ₃) ₄]	839	922	[126]
(CH ₃ NH ₂ CO) ₂ UO ₂ (NO ₃) ₂	860	938	[101]
(phen)(UO ₂ (NO ₃) ₂)	862	942	[101]
(NO)UO ₂ (NO ₃) ₃	869	949	[358]
(Ph ₃ PO) ₂ UO ₂ (NO ₃) ₂	848	920, 932	[101]
(Ph ₃ AsO) ₂ UO ₂ (NO ₃) ₂	818	920, 930	[101]
((EtO) ₃ PO) ₂ UO ₂ (NO ₃) ₂	860	935	[101]
[UO ₂ (NO ₃) ₂ (TEM ₃) ₂][OTf] ₂	841	919	[130]
[UO ₂ (NO ₃) ₂ (TEGA) ₂][OTf] ₂	860	932	[130]
[UO ₂ (NO ₃) ₂ (TEAA) ₂][OTf] ₂	857	929	[130]
[UO ₂ (NO ₃) ₂ (TEPA) ₂][OTf] ₂	854	929	[130]
[UO ₂ (NO ₃) ₂ (TESUA) ₂][OTf] ₂	846	923	[130]
UO ₂ (NO ₃) ₂ (NBP) ₂	856	934	[359]
UO ₂ (NO ₃) ₂ (NCMeP) ₂	856	933	[359]
UO ₂ (NO ₃) ₂ (DMI) ₂	850	931	[359]
UO ₂ (NO ₃) ₂ (N(CH ₃) ₂) ₃ PO) ₂	845	932	[355]

Isothiocyanate

Compound	ν_1 (cm ⁻¹)	ν_2 (cm ⁻¹)	Refs.
(C ₁₀ H ₁₀ N ₃) ₃ [UO ₂ (NCS) ₅]·3H ₂ O	849	906	[360]
(C ₁₀ H ₁₀ N ₃) ₃ [UO ₂ (NCS) ₅]	849.5	908	[360]
(C ₁₀ H ₉ N ₂) ₃ [UO ₂ (NCS) ₅]	836	897	[360]
(C ₁₀ H ₁₀ N ₂) ₃ [UO ₂ (NCS) ₅]·2H ₂ O	837.5	908	[360]
(C ₁₀ H ₁₀ N ₂) ₂ [UO ₂ (NCS) ₅]·NO ₃	844	901,914	[360]
[Brimim] ₃ [UO ₂ (NCS) ₅]	847	920	[126]
[(CH ₃) ₄ N] ₃ [UO ₂ (NCS) ₅]	841		[361]
[(C ₂ H ₅) ₄ N] ₃ [UO ₂ (NCS) ₅]	847		[361]
[(C ₃ H ₇) ₄ N] ₃ [UO ₂ (NCS) ₅]	846		[361]
(C ₁₀ H ₁₀ N ₂) ₂ [UO ₂ (NCS) ₄ (NCS) _{0.75} (Cl) _{0.25}]·(SCN)	842	901	[360]
(C ₁₀ H ₁₀ N ₂) ₂ [UO ₂ (NCS) ₄ (Cl)·Cl·2H ₂ O	842	908	[360]
UO ₂ (NCS) ₂ ((CH ₃ NH ₂ CO)) ₃	854	939	[356]
UO ₂ (NCS) ₂ ((H ₂ N) ₂ CO) ₃	837	910	[356]
UO ₂ (NCS) ₂ (N(CH ₃) ₂) ₃ PO ₂	840	928	[355]
[nBu ₄ N] ₃ [UO ₂ (NCS) ₅]	850	919	[362]
[Me ₃ NBz] ₃ [UO ₂ (NCS) ₅]	845	916	[362]
[Et ₃ NBz] ₃ [UO ₂ (NCS) ₅]	842	910	[362]
[Ph ₄ P] ₂ [UO ₂ (NCS) ₃ (NO ₃) ₂]	860	928	[362]
[Me ₄ N] ₃ [UO ₂ (NCS) ₅]·H ₂ O	848	920	[362]
[n Pr ₄ N] ₃ [UO ₂ (NCS) ₅]	852	926	[362]
[Et ₃ NBz] ₃ [UO ₂ (NCS) ₅]	842	920	[362]
<i>Oxygen Donors (Carboxylates, Oxalate, Ketones)</i>			
Coordination Complexes			
[HNEt ₃] ₂ [UO ₂ PDC ₂]·2H ₂ O	825		[363,364]
[C ₄ H ₁₂ N ₂][(UO ₂) ₂ (C ₆ H ₅ O ₇) ₂](H ₂ O) ₆	825	917	[16]
[Na ₄ (C ₄ H ₁₂ N ₂) ₆][(UO ₂) ₆ O ₂ (C ₆ H ₄ O ₇) ₆](H ₂ O) ₃₈	800	890	[16]
[Na ₉ (Mg(H ₂ O) ₄) ₃][(UO ₂) ₆ (OH) ₃ O ₃ (C ₆ H ₄ O ₇) ₆](H ₂ O) ₁₃	790	880	[16]
(Na ₃ [(UO ₂) ₃ (OH) ₃ (ida) ₃]·8H ₂ O	816	890	[133]
(pip) ₂ [(UO ₂) ₃ O(mal) ₃]·6H ₂ O	816	890	[133]

Compound	ν_1 (cm ⁻¹)	ν_2 (cm ⁻¹)	Refs.
$[\text{UO}_2]_{11}(\text{O})_4(\text{OH})_4(\text{mal})_6(\text{CO}_3)_2 \cdot 23\text{H}_2\text{O}$	816	890	[133]
$\text{Na}[\text{Mg}(\text{H}_2\text{O})_6][\text{UO}_2(\text{CH}_3\text{COO})_3]_2$	852	929	[365]
$\text{Na}[\text{Co}(\text{H}_2\text{O})_6][\text{UO}_2(\text{CH}_3\text{COO})_3]_2$	851	927	[365]
$\text{Na}[\text{Ni}(\text{H}_2\text{O})_6][\text{UO}_2(\text{CH}_3\text{COO})_3]_2$	851	928	[365]
$\text{Na}[\text{Zn}(\text{H}_2\text{O})_6][\text{UO}_2(\text{CH}_3\text{COO})_3]_2$	851	928	[365]
$[\text{UO}_2(\text{C}_{10}\text{H}_{10}\text{N}_2)(\text{C}_7\text{H}_3\text{Cl}_2\text{O}_2)_2]$	850	928	[366]
$[\text{UO}_2(\text{OH})(\text{C}_{15}\text{H}_{11}\text{N}_3)(\text{C}_7\text{H}_3\text{Cl}_2\text{O}_2)_3]$	836	930	[366]
$[\text{UO}_2(\text{OH})(\text{C}_{15}\text{H}_{10}\text{N}_3\text{Cl})(\text{C}_7\text{H}_3\text{Cl}_2\text{O}_2)_3]$	841	926	[366]
$[(\text{UO}_2)(\text{NO}_3)_2(\text{HINT})_2]$	828		[367]
$[\text{C}_4\text{H}_{12}\text{N}_2]_2[(\text{UO}_2)(\text{C}_5\text{O}_3)(\text{H}_2\text{O})] \cdot 3\text{H}_2\text{O}$	848		[368]
$[\text{C}_4\text{H}_{12}\text{N}_2]_2[(\text{UO}_2)(\text{C}_5\text{O}_3)(\text{H}_2\text{O})] \cdot 3\text{H}_2\text{O}$	833		[368]
$[\text{dabcoH}_2][\text{UO}_2(\text{C}_2\text{O}_4)_2(\text{H}_2\text{O})] \cdot 2\text{H}_2\text{O}$	834	912	[369]
$[\text{dabcoH}_2][(\text{UO}_2)_2(\text{C}_2\text{O}_4)_3(\text{H}_2\text{O})_2] \cdot 2\text{H}_2\text{O}$	848	928	[369]
$[\text{pipH}] [\text{UO}_2(\text{C}_2\text{O}_4)_2(\text{H}_2\text{O})] \cdot 4\text{H}_2\text{O}$	839	924	[369]
$[\text{pipH}][(\text{UO}_2)_2(\text{C}_2\text{O}_4)_3(\text{H}_2\text{O})_2] \cdot 2\text{H}_2\text{O}$	852	939	[369]
$(\text{UO}_2)_4(\text{pdzdc})_3(\text{OH})_2(\text{H}_2\text{O})_5 \cdot 11\text{H}_2\text{O}$	830, 845, 854, 865	928	[370]
$[\text{UO}_2(\text{C}_7\text{H}_3\text{BrF}_3\text{IO}_2)_2]_n$	854	946	[371]
$[\text{UO}_2(\text{C}_{12}\text{H}_8\text{N}_2)(\text{C}_7\text{H}_4\text{ClO}_2)_2]_2$	839	912	[371]
$[\text{UO}_2(\text{C}_{12}\text{H}_8\text{N}_2)(\text{C}_7\text{H}_4\text{BrO}_2)_2]$	834.5	908	[371]
$[\text{UO}_2(\text{C}_{12}\text{H}_8\text{N}_2)(\text{C}_7\text{H}_4\text{O}_2)_2]$	840	912	[371]
$[\text{UO}_2(\text{C}_{12}\text{H}_8\text{N}_2)(\text{C}_7\text{H}_4\text{ClO}_2)_2]$	841	922	[371]
$[\text{UO}_2(\text{C}_{12}\text{H}_8\text{N}_2)(\text{C}_7\text{H}_4\text{BrO}_2)_2]$	839.5	922	[371]
$[\text{UO}_2(\text{C}_{12}\text{H}_8\text{N}_2)(\text{C}_7\text{H}_4\text{IO}_2)_2]$	838	920	[371]
$[\text{UO}_2(\text{C}_{15}\text{H}_{11}\text{N}_3)(\text{C}_7\text{H}_4\text{ClO}_2)_2]$	826	916	[371]
$[\text{UO}_2(\text{C}_{15}\text{H}_{11}\text{N}_3)(\text{C}_7\text{H}_4\text{BrO}_2)_2]$	826	916	[371]
$[\text{UO}_2(\text{C}_{15}\text{H}_{11}\text{N}_3)(\text{C}_7\text{H}_4\text{IO}_2)_2]$	821.5	910	[371]
$[\text{UO}_2(\text{C}_{12}\text{H}_8\text{N}_2)(\text{C}_7\text{H}_2\text{F}_3\text{O}_2)_2] \cdot (\text{C}_{12}\text{H}_8\text{N}_2)$	816	900	[372]
$[\text{UO}_2(\text{OH})(\text{C}_{12}\text{H}_8\text{N}_2)(\text{C}_7\text{H}_2\text{F}_3\text{O}_2)_2]$	843.5	918.5	[372]

Compound	ν_1 (cm ⁻¹)	ν_3 (cm ⁻¹)	Refs.
[UO ₂ (C ₁₂ H ₁₈ N ₂) ₂ (C ₇ H ₅ Cl ₃ O ₂) ₂].2H ₂ O	844	888.5	[372]
[UO ₂ (C ₁₂ H ₁₈ N ₂)(C ₇ H ₂ Cl ₃ O ₂) ₂]	847	924	[372]
[UO ₂ (C ₁₂ H ₁₈ N ₂) ₂ (C ₇ H ₅ Br ₃ O ₂) ₂]	839	886.5	[372]
[UO ₂ (OH)(C ₁₂ H ₁₈ N ₂)(C ₇ H ₅ Br ₃ O ₂) ₂]	841	909	[372]
[UO ₂ (C ₁₂ H ₁₈ N ₂)(C ₇ H ₂ Br ₃ O ₂) ₂]	874.5	937	[372]
[UO ₂ (C ₁₂ H ₁₈ N ₂)(C ₇ H ₅ O ₂) ₂]	833	913	[372]
[UO ₂ (C ₁₅ H ₁₁ N ₃)(C ₇ H ₅ Cl ₂ O ₂) ₂]	833	919	[373]
[UO ₂ (C ₁₅ H ₁₁ N ₃)(C ₇ H ₃ Br ₂ O ₂) ₂]	834	920	[373]
[UO ₂ (C ₁₅ H ₁₀ ClN ₃)(C ₇ H ₃ Cl ₂ O ₂) ₂]	836	921	[373]
[UO ₂ (C ₁₅ H ₁₀ ClN ₃)(C ₇ H ₃ Br ₂ O ₂) ₂]	826	910	[373]
UO ₂ (baa) ₂ TPPO	830	938	[374]
UO ₂ (baa) ₂ ADA	816	941	[374]
UO ₂ (baa) ₂ AZA	814	941	[374]
UO ₂ (sal) ₂	834	924	[375]
UO ₂ (2HIN) ₂	841	920	[376]
UO ₂ (HBDM) ₂	836		[377]
UO ₂ (HBTf) ₂	830		[377]
UO ₂ (aacac) ₂	836	921	[378,379]
K ₂ (UO ₂)(H ₂ O)(C ₅ O ₃) ₂	831	895	[380]
UO ₂ (SO ₄)(HMPA) ₂	834	927	[355]
α-UO ₂ SO ₄ (CO(NH ₂) ₂) ₂	845		[290]
β-UO ₂ SO ₄ (CO(NH ₂) ₂) ₂	859		[290]
UO ₂ Cl ₂ (THF) ₂	835		[381]
UO ₂ (OH) ₂ (THF) ₃	842		[381]
Coordination Polymers			
Ni(UO ₂)(PDC) ₂ (H ₂ O) ₄ .4(H ₂ O)	859		[364]
Co(UO ₂)(PDC) ₂ (H ₂ O) ₄ .4(H ₂ O)	864		[364]
Fe(UO ₂)(PDC) ₂ (H ₂ O) ₄ .4(H ₂ O)	857		[364]
Zn(UO ₂)(PDC) ₂ (H ₂ O) ₄ .4(H ₂ O)	858		[364]

Compound	ν_1 (cm ⁻¹)	ν_2 (cm ⁻¹)	Refs.
Co(UO ₂)(PDC) ₂ (H ₂ O) ₄]·4(H ₂ O)	860		[364]
[C ₄ H ₁₂ N ₂][(UO ₂)(C ₄ O ₄) ₂ (H ₂ O)]·H ₂ O	829		[368]
[C ₅ H ₆ N][(UO ₂)(C ₄ O ₄)(OH)]·(H ₂ O) ₂	834		[368]
[C ₂ H ₁₀ N ₂] ₂ [(UO ₂) ₆ (C ₄ O ₄) ₃ (O) ₂ (OH) ₆]	847		[368]
[C ₂ H ₁₀ N ₂] ₅ [(UO ₂) ₆ (C ₅ O ₅) ₆ (O) ₂ (OH) ₆ (H ₂ O) ₄]	829		[368]
(UO ₂) ₃ (C ₂ H ₅ NO ₂) ₂ (O) ₂ (OH) ₂ [(H ₂ O) ₆]	819	904	[147]
[(UO ₂) ₃ (C ₂ H ₅ NO ₂) ₂ (O) ₂ (OH) ₂](H ₂ O) _{1.5}	809	903	[147]
[(UO ₂) ₃ (C ₃ H ₆ NO ₂) ₂ O(OH) ₃](NO ₃)(H ₂ O) ₃	840	930	[147]
[C ₆ H ₁₃ N ₂][(UO ₂) ₃ (HCOO) ₂ O(OH) ₃]4H ₂ O	844	925	[147]
(C ₄ H ₁₂ N ₂)[(UO ₂) ₂ (C ₄ H ₃ O ₅) ₂]·4H ₂ O	826		[257]
[(UO ₂)(C ₄ H ₅ O ₃ Cu(C ₁₀ H ₈ N ₂ Cl)(H ₂ O))]·2H ₂ O	841		[257]
[(UO ₂) ₂ (C ₄ H ₃ O ₅) ₂ Cu(C ₅ H ₅ N) ₂ (H ₂ O) ₂]·2H ₂ O	833		[257]
[(UO ₂) ₂ (C ₇ O ₃ H ₆) ₂ (C ₇ O ₃ H ₅)(DMF)(H ₂ O) ₃]·4H ₂ O	854		[136]
[(UO ₂)(C ₈ O ₄ H ₆)(DMF)]	841		[136]
[(UO ₂)(OH)(INT)]	833		[367]
[(UO ₂) ₃ CuO ₂ (C ₆ NO ₂) ₅]	809, 839	909	[382]
[(UO ₂)Cu(C ₆ NO ₂) ₅]	840, 865	909	[382]
(UO ₂)(C ₁₄ O ₄ H ₈)	848	932	[383]
[(UO ₂) ₂ (C ₁₄ O ₄ H ₈) ₂ (OH)]·(NH ₄)(H ₂ O)	873?		[383]
(UO ₂) ₂ (C ₁₄ O ₄ H ₈)(OH) ₂	829, 855		[383]
(UO ₂) ₂ [UO ₄ (trz) ₂](OH) ₂	837	904	[384]
	769	880	
(UO ₂) ₈ O ₂ (OH) ₄ (H ₂ O) ₄ (1,3-bdc) ₄ ·3·4H ₂ O	810	880	[385]
	834	901	
	846	923	
	852	942	
(UO ₂)(OH)(Pic) (HPic = picolinic acid)	845		[255]
(NH ₄) ₂ [(UO ₂) ₃ (O) ₂ (OH)(Pic) ₂]	820		[255]
Sr _{1.5} [(UO ₂) ₁₂ (O) ₂₅ (OH) ₁₃ (bdc) ₄]·6H ₂ O	851, 837, 816?		[135]

Compound	ν_1 (cm ⁻¹)	ν_3 (cm ⁻¹)	Refs.
K ₃ [(UO ₂) ₂ (O) ₃ (OH) ₃ (bdo) ₄]·8H ₂ O	855, 836, 818?		[136]
(ED)[(UO ₂)(btca)]·(DMSO)·3H ₂ O	838, 818	945, 868	[134]
(NH ₄) ₂ [(UO ₂) ₂ (OH) ₆ (btca)]·~6H ₂ O	851		[134]
[(UO ₂) ₂ (H ₂ O)(btca)]·4H ₂ O		946–920, 871	[134]
<i>Nitrogen Donor Ligands</i>			
[UO ₂ (dapdoH ₂)Cl] ₂ ·2,6-diacetylpyridine dioxime (dapdoH ₂)	850	901	[386]
(1,8-naphthalimide dioxime)(UO ₂ (NO ₃)(CH ₃ OH))	867	935	[387]
(UO ₂ (ZT)) ₃ ·H ₂ O	859	945, 821	[388]
<i>Non-Aqueous Systems</i>			
UO ₂ Cl ₂ (C ₁₄ N ₄ H ₁₆)	813		[381]
UO ₂ Cl ₂ (C ₁₆ N ₄ H ₂₁)	815		[381]
UO ₂ (OH)THF(C ₁₆ N ₄ H ₂₁)(OTf)	833		[381]
UO ₂ (OH) ₂ (C ₁₄ N ₄ H ₁₆)	831		[381]
[UO ₂ (salmnt(Et ₂ N) ₂)(H ₂ O)]	826	898	[389]
[UO ₂ (salmnt(Et ₂ N) ₂)(pyd)]	823	893	[389]
[UO ₂ (salmnt(Et ₂ N) ₂)(DMSO)]	828	885	[389]
[UO ₂ (salmnt(Et ₂ N) ₂)(DMF)]	819	899	[389]
[UO ₂ (salmnt(Et ₂ N) ₂)(TPPO)]	820	888	[389]
UO ₂ (sal-p-phdn)	842, 829	930, 915	[390]
[UO ₂ Cl(<i>q</i> ₇ -CH(Ph ₂ PNSiMe ₃) ₂)(THF)]	825	908	[391]
[UO ₂ Cl(<i>q</i> ₇ -N(Ph ₂ PNSiMe ₃) ₂)(THF)]	829	909	[391]
[UO ₂ Cl(<i>q</i> ₇ -N(Ph ₂ PNSiMe ₃) ₂) ₂]	846	924	[391]
[UO ₂ (N(SiMe ₃) ₂)(<i>q</i> ₇ -CH(Ph ₂ PNSiMe ₃) ₂)]	823	918	[391]
[Na(THF) ₂][UO ₂ (N(SiMe ₃) ₂) ₃]	805	928	[392]
<i>Phosphorus Containing Ligands</i>			
AgUO ₂ [CH ₂ (PO ₃)(PO ₃ H)]	816, 829		[393]
[Ag ₂ (H ₂ O) _{1.5}][(UO ₂) ₂ [CH ₂ (PO ₃) ₂] ₂ ·(H ₂ O) _{0.5}]	822		[393]
Ag ₂ UO ₂ [CH ₂ (PO ₃) ₂]	802		[393]

Compound	ν_1 (cm ⁻¹)	ν_3 (cm ⁻¹)	Refs.
K ₂ (UO ₂) ₂ [B ₂ P ₂ O ₇ (OH)] ₂ (OH)(H ₂ O) ₂	822		[394]
K ₂ (UO ₂) ₂ B(H ₂ PO ₄) ₄ (PO ₄) ₈ (OH)(H ₂ O) ₆	808, 839, 868		[394]
[EMim][UO ₂ (pmbH ₂) _{0.5} (ox) _{0.5}]	831	918	[395]
[BMMim][UO ₂ (pmbH ₂) ₂ (pmb)]	824	910	[395]
[C ₄ mim][UO ₂ (1,3-pbph)(1,3-pbph)·Hmim]	820	909	[396]
[UO ₂ (1,3-pbPh ₂)H ₂ O·mpr]	847	918	[396]
[Etpy][UO ₂ (1,3-pbPh ₂)F]	824	908	[396]
[H ₂ bipy] ₂ [(UO ₂) ₆ Zn ₂ (PO ₃ OH) ₄ (PO ₄) ₄]·H ₂ O	833		[397]
<i>trans</i> -UO ₂ (N(NO ₂) ₂ (OP(NMe ₂) ₃) ₂) ₂	833	888	[398]
[UO ₂ (OP(NMe ₂) ₃) ₄][N(NO ₂) ₂] ₂	833	918	[398]
[UO ₂ (N(CN) ₂ (OP(NMe ₂) ₃) ₂) ₂] ₂	849	928	[398]
UO ₂ (NC) ₂ C ₂ N ₃ ₂ (OPPh ₃) ₃	854	933	[398]
[UO ₂ (ReO ₄) ₂ (TPPO) ₃]	823	933	[399]
[(UO ₂)(TPPO) ₃] ₂ (μ ₂ -O ₂)][ReO ₄] ₂	826	931	[399]

Table 4

Vibrational modes and formation constants for uranyl species in aqueous solution.

Uranyl Species	ν_1 (cm ⁻¹)	ν_2 (cm ⁻¹)	log K ^d	Refs.	ν_3
UO ₂ (H ₂ O) ₅ ²⁺	870	959		[149]	[149]
UO ₂ (CO ₃) ₂ ⁻	832		16.610 ± 0.090	[48,152,166,167]	
UO ₂ (CO ₃) ₃ ⁴⁻	812	885	21.840 ± 0.040	[48,152,166,167]	[168]
UO ₂ (O ₂)(CO ₃) ₂ ⁴⁻	769			[171]	
UO ₂ (CH ₃ COO) ⁺	861	949		[152,153]	
UO ₂ (CH ₃ COO) ₂	852, 841	939		[152,153]	
UO ₂ (CH ₃ COO) ₃ ⁻	843, 823	924		[152,153]	
(UO ₂) ₂ (C ₆ H ₅ O ₇) ₂ ²⁻	825	919, 921		[188]	[186,187]
(UO ₂) ₃ (C ₆ H ₅ O ₇) ₃ ³⁻	800	891		[188]	[186]
(UO ₂) ₃ (C ₆ H ₅ O ₇) ₂ ⁻	790	888		[188]	[186]
UO ₂ (C ₂ H ₄ O ₃) ⁻	(849)	932.8			[187]
UO ₂ (C ₃ H ₅ O ₃) ⁻	(847)	930.2			[187]
UO ₂ (C ₄ H ₆ O ₃) ⁻	(835)	916.2			[187]
(UO ₂) _m (C ₄ H ₄ O ₆) _n	(837)	918.4			[187]
UO ₂ F ⁺	858	908	5.160 ± 0.060	[14]	[149]
UO ₂ F ₂	846		8.830 ± 0.080	[14]	
UO ₂ F ₃ ⁻	834		10.900 ± 0.100	[14]	
UO ₂ F ₄ ²⁻	822		11.840 ± 0.110	[14]	
UO ₂ Cl ⁺	866	962.5	0.170 ± 0.020	[152,172]	[149]

Uranyl Species	ν_1 (cm ⁻¹)	ν_3 (cm ⁻¹)	log K ^a	Refs.	ν_1	ν_3
UO ₂ Cl ₂	862	956	-1.100 ± 0.400	[152,172]	[152,172]	[149]
UO ₂ Cl ₃ ⁻	858			[152,172]	[152,172]	
UO ₂ Cl ₂ ²⁻	854			[152,172]	[152,172]	
UO ₂ Cl ₃ ⁵⁻	850			[152,172]	[152,172]	
UO ₂ Br ⁺	870		0.220 ± 0.020	[14]	[14]	
UO ₂ OH ⁺	848.5		-5.25 ± 0.240	[14,132]	[14,132]	
(UO ₂) ₂ (OH) ₂ ²⁺	851/853	943	-5.620 ± 0.040	[14,132]	[14,132]	[164]
(UO ₂) ₃ (OH) ₅ ⁺	836	923	-15.550 ± 0.120	[14,132]	[14,132]	[164]
UO ₂ (OH) _(2aq) ⁰	837		-12.150 ± 0.070	[14,132]	[14,132]	
UO ₂ (OH) ₃ ⁻	805.5		-20.250 ± 0.240	[14,132]	[14,132]	
((UO ₂) ₃ (OH) ₈) ²⁻	812 ± 2		-32.400 ± 0.680	[14,132]	[14,132]	
(UO) ₃ (OH) ₁₀ ⁴⁻	800 ± 2			[14,132]	[14,132]	
(UO ₂) ₃ (OH) ₁₁ ⁵⁻	791 ± 2			[14,132]	[14,132]	
UO ₂ (OH) ₄ ²⁻	782 ± 2			[14,132]	[14,132]	
UO ₂ (NO ₃) ⁺	870	961	0.300 ± 0.680	[152]	[152]	[149]
UO ₂ ClO ₄ ⁺	870	962.5		[152,162]	[152,162]	[149]
≡ SiO ₂ -UO ₂ PO ₄ ³⁻	840, (837)	919		[231]	[231]	4
UO ₂ SO ₄ ⁰	961	956	3.150 ± 0.020	[152,181,182]	[152,181,182]	[149,183]
UO ₂ (SO ₄) ₂ ²⁻	852	950	4.140 ± 0.070	[152,181,182]	[152,181,182]	[183]

Uranyl Species	ν_1 (cm ⁻¹)	ν_3 (cm ⁻¹)	log K ^a	Refs.	ν_1	ν_3
UO ₂ (SO ₄) ₃ ⁴⁻	841	945	3.020 ± 0.380	[152,181,182]	[152,181,182]	[183]

^aFrom Ref. [248].

Author Manuscript

Author Manuscript

Author Manuscript

Author Manuscript